ABSTRACT

BLISS, KAREN M. Modeling of Red Blood Cell Dynamics in Patients with Chronic Kidney Disease. (Under the direction of H.T. Banks and H.T. Tran.)

Kidneys are the main site of production of the hormone erythropoietin (EPO) that is the major regulator of erythropoiesis, or red blood cell production. EPO level is normally controlled by a negative feedback mechanism in the kidneys, but patients with chronic kidney disease (CKD) do not produce sufficient levels of EPO to maintain blood hemoglobin concentration.

In order to prevent anemia, patients typically receive recombinant human EPO (rHuEPO) intravenously to stimulate red blood cell production. Iron is required to produce hemoglobin, and iron deficiency can be an issue among patients receiving rHuEPO therapy, so intravenous iron supplementation is common among patients undergoing rHuEPO therapy. Iron availability is negatively affected by inflammation level in the body.

An age-structured model is developed for erythropoiesis in patients with CKD. Both rHuEPO therapy and iron therapy are taken into consideration, as is the overall inflammation level in the body. Hemoglobin concentration is the output of the model. The result is a nonlinear coupled system of ordinary and partial differential equations with nontrivial boundary coupling.

This system is solved numerically in Matlab, using the finite element method with upwinding for the partial differential equations. The code is validated using a forcing function strategy. Simulations are performed for various treatment protocols and patient inflammation levels and results are discussed.

The model assumptions are then revisited in order to assimilate iron into the erythrocytes in a more biologically reasonable fashion. Significant changes, including the inclusion of a second structure variable to account for the iron content of erythrocytes, are made to the model, which will make its numerical solution more difficult.

Modeling of Red Blood Cell Dynamics in Patients with Chronic Kidney Disease

by
Karen M. Bliss

A dissertation submitted to the Graduate Faculty of
North Carolina State University
in partial fulfillment of the
requirements for the Degree of
Doctor of Philosophy

Applied Mathematics

Raleigh, North Carolina

2011

APPROVED BY:

Stephen Campbell	James Selgrade
Helen Kraus	
H. T. Banks Co-chair of Advisory Committee	H. T. Tran Co-chair of Advisory Committee

BIOGRAPHY

Karen M. Bliss was born in Rochester, New York, in 1976. She grew up in New York, Massachusetts and Connecticut before landing in Missouri during high school. Karen attended Missouri University of Science and Technology (then University of Missouri-Rolla) and graduated Summa cum Laude in 1998 with a Bachelor of Science in Applied Mathematics. She attended graduate school at North Carolina State University, earning a Master of Science in Applied Mathematics in 2000. Karen then began her career as an officer in the United States Navy.

Karen spent four years at Naval Nuclear Power Training Command in Charleston, South Carolina. She taught mathematics, electrical theory, and mechanical theory at Enlisted Nuclear Power School before accepting the position of Director of Nuclear Field 'A' School Mathematics. Then Karen joined the mathematics department at the United States Naval Academy in Annapolis, Maryland, where she served for three years.

Karen separated from the Navy at the rank of Lieutenant in August of 2004 and decided to return to North Carolina State to earn a Ph.D. She has accepted a Davies Fellowship at the United States Military Academy at West Point where she will teach cadets and do research with collaborators at the Army Research Laboratories in Aberdeen Proving Ground, MD. She is passionate about teaching and is committed to a career in academia.

ACKNOWLEDGEMENTS

I would like to thank my committee and my advisers. No words here could ever express enough gratitude for your support and guidance throughout this process.

My family and especially my parents have also been so supportive of me. You helped foster my intellectual curiosity when I was younger, and you've helped foster my cats recently! Knowing that I have people in my life who want nothing more than happiness for me is something for which I will be eternally grateful.

I want to extend a heartfelt thank-you to my "extended" family–the friends who've become family over the years. Vicky, Katie, Emily, and Christine: I cherish the times we have together and appreciate all you have done for me.

I want to thank all of my fellow grad students with whom I have commiserated these past years. Susan, Kristen, and Sarah: I look forward to lasting friendships that become only richer in time. Adam: Once in a lifetime you meet someone with whom you can hope to connect as we have. I know that when our paths cross again and again, each time will be the same as it ever was.

TABLE OF CONTENTS

LIST OF TABLES

LIST OF FIGURES

Chapter 1

Introduction

It is estimated that 31 million Americans have chronic kidney disease (CKD). Among those, approximately 330 thousand were classified as being in End-Stage Renal Disease (ESRD) and required dialysis [52]. Dialysis is the bidirectional exchange of materials across a semipermeable membrane [2]. For the purposes of this study, we consider only hemodialysis, where a patient's blood is exposed to a semipermeable membrane outside of the body.

In addition to regulating blood pressure and filtering waste products from blood, kidneys produce a hormone called erythropoietin (EPO) that is the major regulator of erythropoiesis, or red blood cell production. EPO level is normally controlled by a negative feedback mechanism in the kidneys, but patients in ESRD do not produce sufficient levels of EPO to maintain blood hemoglobin concentration. Hemoglobin is the protein that gives red blood cells the ability to carry oxygen. Patients with low hemoglobin concentration may present symptoms of anemia, such as decreased cardiac function, fatigue, and decreased cognitive function.

In order to prevent anemia, patients typically receive recombinant human EPO (rHuEPO) intravenously to stimulate red blood cell production. However, treatment is far from perfect. In 2006, only half of dialysis patients had a mean monthly hemoglobin greater than 11 grams per deciliter [52], the desired minimum level set by the National Kidney Foundation [35].

Iron is required to produce hemoglobin, and iron deficiency can be an issue among patients receiving rHuEPO therapy. Oral iron supplementation is often ineffective, so intravenous iron supplementation has become a mainstay in many patients undergoing

rHuEPO therapy [30].

Iron availability is negatively affected by inflammation level in the body. Most patients with CKD have elevated levels of inflammation due to CKD and the presence of other medical issues (e.g., diabetes, hypertension, etc.) [31].

We develop an initial age-structured mathematical model for red blood cell dynamics in patients in ESRD undergoing hemodialysis. We use finite element method with upwinding to implement the model numerically. We discuss the validation of our code and the results of simulations under various treatment protocols and patient conditions. Finally, we revisit the model assumptions and develop an improved model which incorporates iron into erythrocytes in a more biologically reasonable fashion. The revised model requires the use of a second structure variable to account for cellular iron content. Implementation of the revised model will be significantly more challenging, and is the subject of future work in this area.

1.1 Erythropoiesis

Erythropoiesis is the process by which red blood cells (erythrocytes) are formed. Erythrocytes transport oxygen and carbon dioxide between the lungs and all of the tissues of the body and can be thought of as a container for hemoglobin [48], the protein that carries oxygen.

Erythrocytes are produced primarily from pluripotent stem cells in bone marrow. In the presence of the cytokine named stem cell factor, hematopoietic stem cells divide asymetrically, producing a committed colony-forming-unit (CFU) while maintaining the population of stem cells. The erythrocyte lineage shares the precursor CFU-GEMM (granulocyte, erythrocyte, macrophage, megakaryocyte) with other types of blood cells (white blood cells, platelets, etc.). The exact mechanisms determining selection of lineage from this nodal point are not known [22].

Erythrocyte lineage continues as described in Figure 1.1: erythroid burst-forming unit (BFU-E), erythroid colony-forming-unit (CFU-E), proerythrocyte, basophilic erythrocyte, polychromatic erythroblast, orthochromatic erythroblast, reticulocyte, and erythrocyte. Cell division ceases with the formation of the orthochromatic erythroblast. Division rate, death rate, and maturation rate are influenced by the level of EPO [22]. This is described in more detail later.

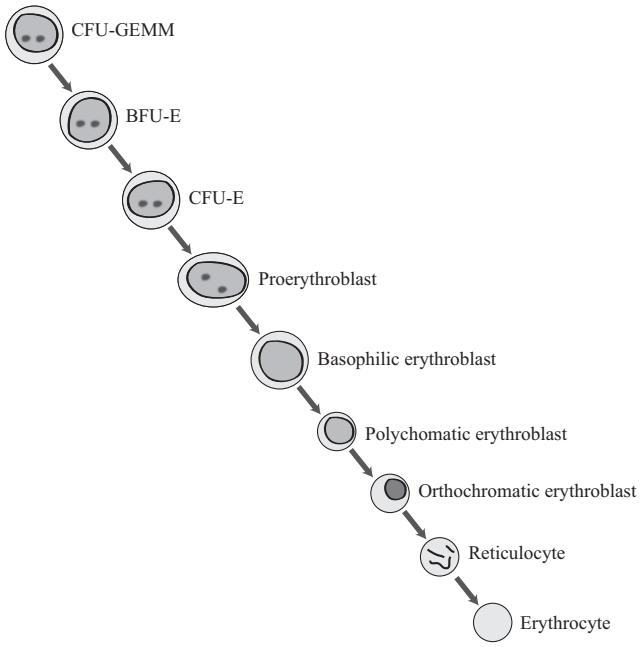

Figure 1.1: Erythropoiesis cell lineage.

Hemoglobin is synthesized beginning in the basophilic erythrocyte stage, with the majority of synthesis occurring in the polychromatic erythroblast stage. When the nucleus is extruded from the cell, the cell is named a reticulocyte. Little hemoglobin synthesis happens at the reticulocyte stage, and synthesis is completely absent in mature erythrocytes [22].

Reticulocytes begin to lose the adhesive proteins that hold them in the bone marrow. They decrease in size and begin to circulate in the blood. In healthy individuals, the time from proerythroblast to mature erythrocyte is approximately 7 days. Normal erythrocyte life span is approximately 120 days, at which time aging erythrocytes are enveloped by macrophages in the spleen.

1.2 Previous models

The process of erythropoiesis has been modeled in several physiological scenarios. In [38], rHuEPO therapy is considered in healthy volunteers. This model incorporates the negative feedback to endogenous EPO production. EPO is assumed to be cleared using Michaelis-Menten dynamics. A similar model was used to fit data in rats [56]. Both of these models use delay instead of age-structured modeling.

Both [7] and [8] use age-structured models, as does the model described in [32], which assumes that the oldest mature erythrocytes will be destroyed, yielding a moving boundary condition. In [1], EPO is assumed to accelerate maturation of cells undergoing erythropoiesis. Additionally, EPO is assumed to be consumed during the process of erythropoiesis.

The model presented here is a significant departure from these models in that it incorporates the effects of both iron plasma level and inflammation.

Chapter 2

Initial Model Development

2.1 Model Overview

We use an age-structured model with three major classifications of erythroid cells in which the structure variables μ, ν, and ψ represent maturity levels, as shown in Figure 2.1.

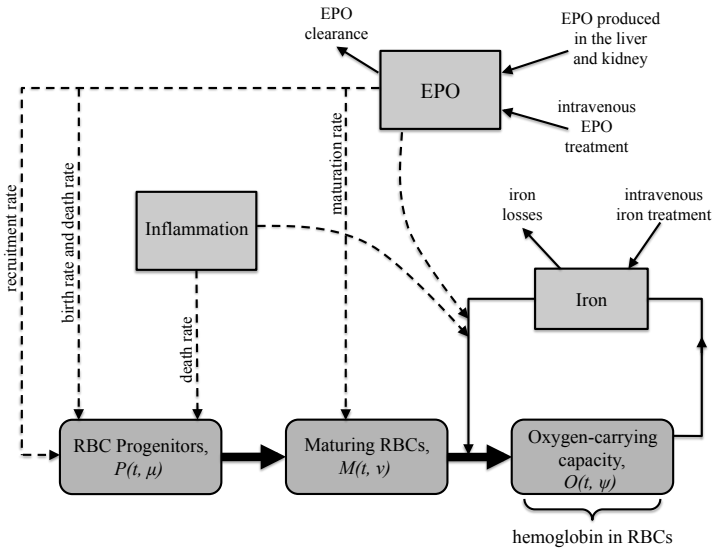

Figure 2.1: Model schematic.

$P(t,\mu)$ and $M(t,\nu)$ represent the number of progenitor cells and maturing hematopoietic cells, respectively. $O(t,\psi)$ is a measure of the oxygen carrying capacity of circulating reticulocytes and erythrocytes. For these cell classes, the second argument (e.g., μ for class P) is the structure variable, maturity level in this case. We model EPO level, E, iron level, Fe, and a measure of overall inflammation in the body, I. Time is measured in days.

Our state variables are

$$P = P(t,\mu), \quad M = M(t,\nu), \quad O = O(t,\psi), \quad E = E(t), \text{ and } Fe = Fe(t).$$

Rate of exogenous EPO treatments, $\dot{E}_{ex}$, and rate of exogenous iron treatments, $\dot{Fe}_{ex}$, are input functions, and hemoglobin concentration, $Hb(t)$, is the output of the model.

We will make use of sigmoid functions throughout the model. An increasing sigmoid function will be of the form

$$F(x) = \left(F^{min} - F^{max}\right) \cdot \frac{c^k}{c^k + x^k} + F^{max}.$$

Note that when x is small, $F(x)$ is close to F^{min}, and when x is large, $F(x)$ is close to F^{max}. The typical graph of such a function is depicted in Figure 2.2.1. The values of c and k affect the slope of the curve and the location of the area of increase.

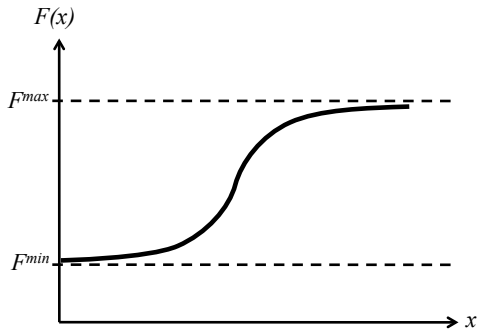

2.2.1: Generic increasing sigmoid function.

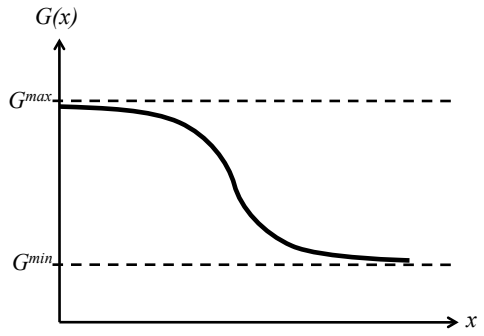

2.2.2: Generic decreasing sigmoid function.

Figure 2.2: Sigmoid function examples.

Similarly, a typical decreasing sigmoid function is depicted in Figure 2.2.2 and has the form

$$G(x) = \left(G^{max} - G^{min}\right) \cdot \frac{c^k}{c^k + x^k} + G^{min}.$$

2.2 Iron

Iron is required to make hemoglobin, the protein that gives erythrocytes the ability to carry oxygen. It is also the protein that gives erythrocytes their characteristic red color. If iron is not available during erythropoiesis, the result is lighter-colored (hypochromic) erythrocytes with reduced capacity to carry oxygen.

Control of iron in the body is a strictly regulated process, in part because there is no pathway for the excretion of excess iron (Figure 2.3).

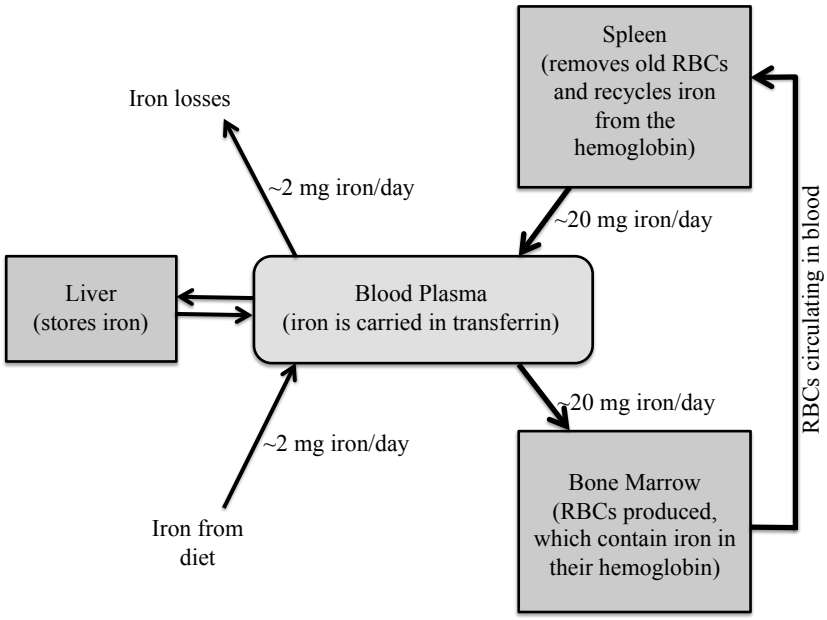

Figure 2.3: Iron cycle in healthy individuals.

When red blood cells age, they become enveloped by macrophages in the spleen. The

iron from their hemoglobin is then recaptured and sent to the bone marrow for use in making hemoglobin for new erythrocytes. This recycling process is very efficient and is the main source of iron to erythropoiesis [48]. In much smaller quantities, iron is absorbed from diet in the duodenum and can be stored in the liver. The only losses to the system are from sweating, cells being shed, blood losses, etc.

Iron is stored in the compound ferritin when it is within a cell, and in the compound transferrin when it is in the blood plasma. The protein ferroportin is required to transport iron out of a cell and into the plasma. The major regulator of this transport is the hormone hepcidin, which is produced in the liver. Hepcidin binds to ferroportin and causes the complex to be absorbed into the cell, effectively interrupting the transport of iron into the blood plasma, as depicted in Figure 2.4.

Hepcidin production is increased in the presence of certain cytokines which are released due to inflammation in the body. It is thought that this might be a defense mechanism against foreign organisms which may need iron to reproduce.

Since patients in ESRD commonly have other health problems (such as diabetes and hypertension), they often have higher than normal levels of inflammation. Thus, they may produce higher than normal levels of hepcidin. As a result, even if there is enough iron in the body, it may not be available for erythropoiesis because it cannot leave the

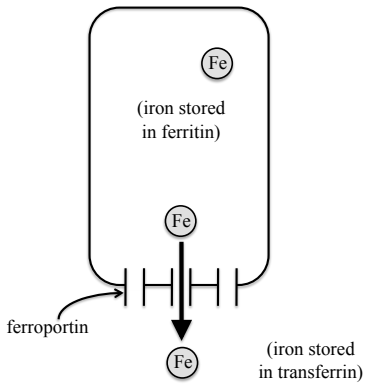

2.4.1: Ferroportin is required for the transport of iron out of cells.

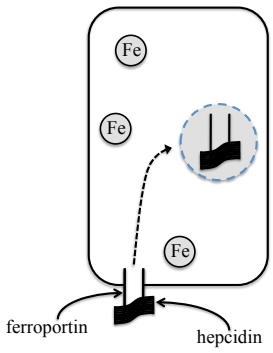

2.4.2: Hepcidin is the major regulator of iron transport out of cells.

Figure 2.4: Iron regulation at a cellular level.

cells and enter the plasma.

Current research suggests that EPO affects the interaction between cytokines and hepcidin. When EPO level is sufficiently high, the effects of inflammation cannot be seen.

We model the amount, Fe, of iron in the blood plasma, in milligrams. We formulate a mass balance involving the iron compartment (see Figure 2.5) as follows.

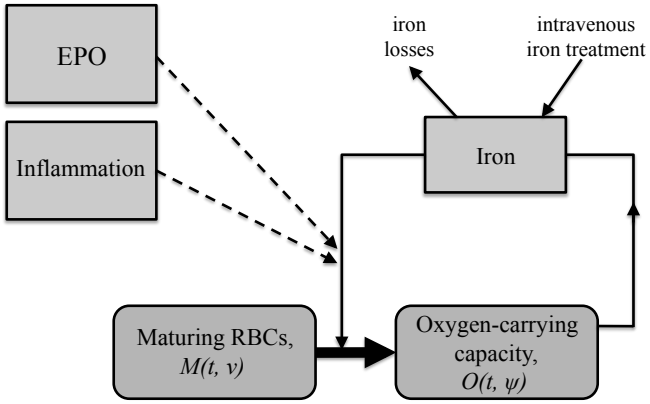

Figure 2.5: Iron compartment.

The main source of incoming iron to the compartment is recycled iron from the hemoglobin of senescent erythrocytes that are enveloped by macrophages. We will develop class O so that each member in the class is assumed to contain exactly the same amount of iron. That is, the rate of iron being recycled from class O is $k_{Fe}\int_0^{\psi_f}\delta_O(\psi)O(t,\psi)\partial\psi$, where k_{Fe} is some proportionality constant and $\delta_O(\psi)$ is the death rate of the cells in class O, explained in more detail later.

The other main source of iron to the compartment is exogenous iron supplied as part of treatment. We denote the rate of exogenous iron treatment by $\dot{Fe}_{ex}(t)$

A small amount of iron enters the system through absorption from diet and from storage in the liver, and there are also iron losses (due to sweating, blood losses during blood draws and hemodialysis, etc.). As described earlier, patients undergoing hemodialysis require iron supplements intravenously. Therefore we assume that when we sum the iron losses and the iron entering the system from diet and storage in the liver we obtain a net loss. Further, we will assume for an initial model that the loss occurs at constant rate unless the current level of iron is small, in which case a fraction of the iron is lost. That is, that rate of iron loss, $\rho_{Fe,loss}(Fe)$, is given by

$$\rho_{Fe,loss}(Fe) = \begin{cases} \rho_{Fe,const}, & Fe \geq Fe_{th} \\ \rho_{Fe,frac} \cdot Fe, & Fe < Fe_{th}. \end{cases}$$

This assumption will be revisited in future models, perhaps with greater losses when dialysis and blood draws occur.

Next we need to account for iron leaving the compartment during erythropoiesis. For our first model, we begin by making the assumption that iron enters red blood cells at the moment that a cell matures from class M to class O, which is the time that a cell leaves the bone marrow and begins circulating. Red blood cells actually collect iron over the time period that they are in class M, but the biochemistry of this process is not clearly understood. The assumption that all of the iron is collected into a cell at one moment will certainly have to be revisited in future improvements of the model.

In determining the amount of iron used during erythropoiesis, we first compute the amount of iron that would be used if every cell leaving class M were to contain the appropriate amount of hemoglobin so as to be at full oxygen-carrying capacity, i.e.,

$$Fe_{needed} = k_{Fe} M(t, \nu_f). \tag{2.1}$$

In the presence of inflammation, even if there is enough iron in the plasma, it may not be available to be used in erythropoiesis. For our initial model, we assume that there is an EPO threshold, EPO_{th}. We assume that if EPO is above the threshold, the effects of inflammation can not be seen. That is, we assume

$$Fe_{avail} = k_{Fe,eff} f(E, I) Fe, \tag{2.2}$$

where

$$f(E,I) = \begin{cases} \dfrac{(c_{Fe,av})^{k_{Fe,av}}}{(c_{Fe,av})^{k_{Fe,av}} + I^{k_{Fe,av}}}, & E < EPO_{th} \\ 1, & E \geq EPO_{th}. \end{cases}$$

Observe that in this model when EPO is greater than the threshold level, inflammation level does not impact iron availability. However, when EPO level is lower than the threshold, the amount of available iron depends on inflammation level–as $f(E,I)$ is close to one when inflammation is low and close to zero when inflammation is high. The constant $k_{Fe,eff}$, with $0 \leq k_{Fe,eff} \leq 1$, is an efficacy constant that accounts for the fact that only a fraction of the iron in the plasma will actually be available at the site of erythropoiesis at any given time.

The amount of iron actually used in erythropoiesis is therefore given by

$$\begin{aligned} Fe_{used} &= \min\left\{Fe_{needed},\ Fe_{avail}\right\}, \\ &= \min\left\{k_{Fe} M(t,\nu_f),\ k_{Fe,eff} f(E,I) Fe\right\}. \end{aligned} \tag{2.3}$$

We assume that the rate of iron leaving the iron compartment and entering class O is proportional to this quantity, Fe_{used}. That is,

$$\rho_{Fe\to O} = k_{\rho,Fe} Fe_{used}.$$

Thus, the mass balance in the iron compartment is given by

$$\begin{aligned} \dot{Fe}(t) &= (\text{rate in from class } O) + (\text{rate in intravenously}) \\ &\qquad - (\text{rate out to class } O) - (\text{rate of iron losses}) \\ &= k_{Fe} \int_0^{\psi_f} \delta_O(\psi) O(t,\psi) d\psi + \dot{Fe}_{ex}(t) - \rho_{Fe\to O} - \rho_{Fe,loss}(Fe). \end{aligned} \tag{2.4}$$

2.3 EPO

EPO is the primary regulator of erythropoiesis. It stimulates red blood cell production, differentiation and maturation, and prevents apoptosis [22]. In healthy individuals, the majority of EPO production occurs in the kidney. Sensors in the kidney monitor blood

oxygen level. EPO production is increased in response to low oxygen level and is decreased when oxygen level is high.

Patients in ESRD, whose kidneys have only minimal function, produce only a small basal level of EPO in the kidney and liver [23]. Without intervention, patients can develop anemia; therefore, patients undergoing dialysis are commonly treated with intravenous rHuEPO. Two common rHuEPOs, epoetin alfa and epoetin beta, share structural homology with endogenous EPO. Darbepoietin alfa, the other major erythropoietic agent, is designed so that it has a longer half-life *in-vivo.* In this model, we assume that darbepoietin is not the erythropoietic agent, and therefore we will not distinguish between rHuEPO and endogenous EPO with respect to their action. We assume that their effects on erythropoiesis are identical.

EPO is measured in units of EPO. We assume the rate of endogenous EPO production in the liver and kidney to be constant, and will denote it $\rho_{EPO,basal}$.

We will assume that EPO clearance is proportional to the amount present, although we could consider Michaelis-Menten dynamics in future models. Finally, we also account for the rate of EPO given via IV, denoted $\dot{E}_{ex}(t)$. So we have

$$\dot{E}(t) = \rho_{EPO,basal} + \dot{E}_{ex}(t) - \frac{1}{t_{1/2}} \ln 2 \cdot E(t),$$

where $t_{1/2}$ is the half-life of EPO.

2.4 Inflammation

Inflammation affects two aspects of erythropoiesis, as depicted in Figure 2.1.

Even in patients without CKD, chronic inflammation can cause anemia, termed the anemia of chronic disease. While the exact chemical pathways are not necessarily known, it is known that the presence of inflammation can suppress erythropoiesis and may inhibit the action of EPO [49]. Since EPO affects the birth and death rate of progenitors, we incorporate inflammation in the death rate term associated with the progenitor cell class, P.

Inflammation level also impacts iron availability for erythropoiesis, as described previously. Inflammation may cause an increase in ferritin production, which would cause iron to be retained within cells, inhibiting the use of iron to make hemoglobin. Inflammation may also impair the ability of the body to absorb dietary iron [49].

It is almost certain that inflammation affects these two aspects of erythropoiesis via completely different chemical pathways. We assume that both aspects can be sufficiently described with some overall measure of inflammation in the body. There are markers of inflammation, such as albumin and C-reactive protein, which are often measured in patients undergoing dialysis. In future work, we will investigate whether inflammation can be described as some combination of the levels of these markers.

2.5 Class $P(t, \mu)$

We group the progenitor cells (CFU-GEMM, BFU-E and CFU-E) in one class, $P(t, \mu)$. These cells are affected by EPO level and inflammation level.

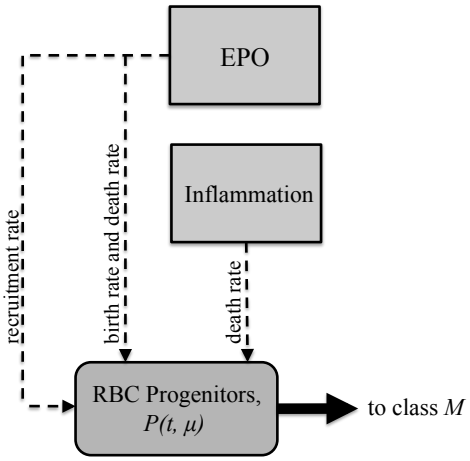

Figure 2.6: The progenitor cells, $P(t, \mu)$.

We make the following assumptions:

(i) There is a smallest maturity level, $\mu_0 = 0$, and a largest maturity level, μ_f; i.e., $0 \leq \mu \leq \mu_f$.

(ii) The maturity rate depends on the EPO concentration and the maturity level [22].

For simplification in our initial model, we assume that the maturity rate is constant:

$$\frac{d\mu}{dt} = \rho_P.$$

(iii) The birth rate depends on EPO concentration [22] and the maturity level.

Regulation of erythropoiesis by EPO is focused on the progenitor class, and probably most importantly the CFU-E. A rise in EPO level results in proliferation of CFU-E [22]. We will assume EPO affects all cells in class P equally, independent of maturity level. We will model the birth rate as an increasing sigmoid function,

$$\beta_P(E) = \left(\beta_P^{min} - \beta_P^{max}\right) \frac{(c_{\beta,P})^{k_{\beta,P}}}{(c_{\beta,P})^{k_{\beta,P}} + E^{k_{\beta,P}}} + \beta_P^{max}.$$

(iv) The number of stem cells being recruited into the precursor cell population is directly proportional to EPO level:

$$P(t,0) = R_P E(t).$$

It is reasonable to assume that recruitment is related to EPO level, as it is one of the hormones that affects whether a stem cell will become an erythrocyte. Other hormones are certainly involved as well, but the chemical pathway governing the differentiation of stem cells is still largely unknown [22].

(v) The death rate depends on the concentration of EPO, the inflammation level, and the maturity level, μ. We will simplify this for our first model to assume that death rate is not dependent on maturity level.

EPO prevents apoptosis, or programmed cell death, of progenitor cells [22]. We use a decreasing sigmoid function to describe this behavior.

Certain interferons, present under inflammatory conditions, can also cause death of progenitor cells, specifically CFU-E [33]. We assume that the death rate of progenitor cells depends on inflammation level, which is modeled by some increasing sigmoid function.

Finally, we assume that overall death rate is the sum of these two effects:

$$\delta_P(E,I) = \left(\delta_{P,E}^{max} - \delta_{P,E}^{min}\right) \frac{\left(c_{\delta,P,E}\right)^{k_{\delta,P,E}}}{\left(c_{\delta,P,E}\right)^{k_{\delta,P,E}} + E^{k_{\delta,P,E}}} + \delta_{P,E}^{min}$$
$$+ \left(\delta_{P,I}^{min} - \delta_{P,I}^{max}\right) \frac{\left(c_{\delta,P,I}\right)^{k_{\delta,P,I}}}{\left(c_{\delta,P,I}\right)^{k_{\delta,P,I}} + I^{k_{\delta,P,I}}} + \delta_{P,I}^{max}.$$

Now we consider the rate of change in population from maturity level μ to maturity level $\mu + \Delta\mu$.

rate of change in population on the interval $(\mu, \mu+\Delta\mu)$ =
(rate of cells entering the interval) − (rate of cells leaving the interval)
+ (birth rate term) − (death rate term)

$$\frac{\partial}{\partial t}\int_{\mu}^{\mu+\Delta\mu} P(t,\xi)d\xi = \rho_P P(t,\mu) - \rho_P P(t,\mu+\Delta\mu)$$
$$+ \int_{\mu}^{\mu+\Delta\mu} \beta_P(E)\, P(t,\xi)d\xi - \int_{\mu}^{\mu+\Delta\mu} \delta_P(E,I)P(t,\xi)d\xi$$

$$\frac{\partial}{\partial t}\int_{\mu}^{\mu+\Delta\mu} P(t,\xi)d\xi = -\rho_P\left[P(t,\mu+\Delta\mu) - P(t,\mu)\right]$$
$$+ \left[\beta_P(E) - \delta_P(E,I)\right]\int_{\mu}^{\mu+\Delta\mu} P(t,\xi)d\xi$$

Dividing by $\Delta\mu$ and then letting $\Delta\mu \to 0$, we obtain

$$\frac{\partial}{\partial t}P(t,\mu) = -\rho_P\frac{\partial}{\partial \mu}P(t,\mu) + \left[\beta_P(E) - \delta_P(E,I)\right]P(t,\mu),$$

and we have the boundary condition

$$P(t, 0) = R_P E(t).$$

2.6 Class $M(t, \nu)$

Class $M(t, \nu)$ consists of immature hematopoietic cells: proerythroblasts, basophilic erythroblasts, polychromatic erythroblasts, orthochromatic erythroblasts, and non-circulating reticulocytes (i.e. those that still reside in the bone marrow). Cells are recruited from class P and, upon maturation, feed into class O. Their development is influenced by EPO concentration.

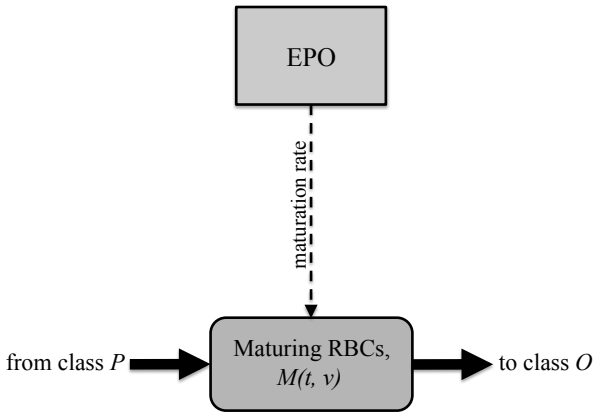

Figure 2.7: Maturing erythrocytes, $M(t, \nu)$.

We make the following assumptions:

(i) There is a smallest maturity level, $\nu_0 = 0$, and a largest maturity level, ν_f. That is, $0 \leq \nu \leq \nu_f$.

(ii) The maturation rate depends on the level of erythropoietin and the maturity level. However, for our initial model, we assume that maturation rate *does not* depend

on the maturity level.

EPO stimulates maturation [22], so we use an increasing sigmoid function for maturation rate, $\rho_M(E)$.

$$\rho_M(E) = \left(\rho_M^{min} - \rho_M^{max}\right) \frac{(c_{\rho,M})^{k_{\rho,M}}}{(c_{\rho,M})^{k_{\rho,M}} + E^{k_{\rho,M}}} + \rho_M^{max}.$$

(iii) The birth rate depends on the maturity level, but for our first model, we assume birth rate is a constant, $\tilde{\beta}_M$.

(iv) The number of cells at maturity level $\nu = 0$ is equal to the number of cells leaving the previous stage:

$$M(t, 0) = P(t, \mu_F).$$

(v) The death rate depends on the maturity level, ν and on the iron level. To simplify, we assume the death rate is a constant, δ_M.

As in the progenitor class, we can consider the rate of change in population from maturity level ν to maturity level $\nu + \Delta\nu$, then divide by $\Delta\nu$ and let $\Delta\nu \to 0$ to obtain

$$\frac{d}{dt}M(t,\nu) = -\rho_M(E)\frac{\partial}{\partial\nu}M(t,\nu) + \left[\tilde{\beta}_M - \delta_M\right] M(t,\nu).$$

Since we have made the assumption that the birth and death rates are both constant, it is clear that they will not both be identifiable. We replace the difference $\tilde{\beta}_M - \delta_M$ by the constant β_M, which then represents the net birth rate.

Hence, we have

$$\frac{\partial}{\partial t}M(t,\nu) = -\rho_M(E)\frac{\partial}{\partial\nu}M(t,\nu) + \beta_M M(t,\nu),$$

with the boundary condition

$$M(t, 0) = P(t, \mu_F).$$

It is worth noting again that as this is our first model of the system, we have made the assumption that iron level does not impact cell development until cells mature out of class M into class O. Specifically, we do not account for iron entering red blood cells

throughout class M and we ignore any impact this would have on death rate in class M. Future versions of the model will need to account for these interactions with the iron compartment.

2.7 Class $O(t, \psi)$

Unlike the classes P and M, class O does not represent *the number* of circulating reticulocytes and mature erythrocytes, because knowledge of the number of cells alone does not give us enough information to determine whether the cells contain the necessary amount of hemoglobin to carry oxygen at full capacity.

Erythrocytes begin hemoglobinization at the polychromatic erythroblast stage (in class M). They continue to acquire more hemoglobin throughout the orthochromatic erythroblast stage and into the reticulocyte stage, until the reticulocyte leaves the bone marrow, at which time it ceases hemoglobinization [48]. Hence, the oxygen carrying ability of a mature erythrocyte is determined by how much hemoglobin is available during the time interval when that cell is in class M.

In order to initially simplify computations, we assume that a cell's oxygen-carrying ability is based solely on the availability of iron at the time that the cell matures out of class M and begins circulating in the blood. As previously noted, the biology does not support this formulation of the problem, and this assumption will be reconsidered in future models.

Let us consider an example in order to elucidate this idea. Suppose we know that $k_{Fe} = 0.2$ mg/billion cells and that at some given time t, $Fe_{avail} = 8$ mg. Suppose also that at time t there are 100 billion cells maturing out of class M; that is, $M(t, \nu_f) = 100$. Then

$$Fe_{avail} < Fe_{needed} = k_{Fe} M(t, \nu_f) = 20 \text{ mg}.$$

Then, per equation (2.3), $Fe_{used} = Fe_{avail} = 8$ mg, which is only 40% of the 20 mg that would be needed for each cell maturing into class O to have full oxygen-carrying capacity. Then the 100 billion cells maturing into class O would have, on average, only 40% oxygen-carrying ability. It would be difficult to track both the number of circulating erythroid cells and the oxygen carrying capacity of each. Instead, we think of the 100 billion cells with 40% oxygen-carrying ability as 40 billion cells with 100% oxygen-carrying capacity. Hence, every "cell" in class O is assumed to have full-oxygen carrying capacity.

Now we present the assumptions we make about class O.

(i) We assume that there is a smallest maturity level, $\psi_0 = 0$, and a largest maturity level, ψ_f. That is, $0 \leq \psi \leq \psi_f$. In the future, we may wish to allow ψ_f to vary.

(ii) The maturation rate of cells in this class is a function of the maturity level. We will further assume, for simplification in this initial model, that the maturity rate is constant:

$$\frac{d\psi}{dt} = \rho_O$$

(iii) The birth rate is zero. Cells at this stage mature but do not proliferate [22].

(iv) The number of members of class O at maturity level $\psi = 0$ is equal to the number of cells leaving the previous stage multiplied by the ratio of Fe_{used} and Fe_{needed}:

$$\begin{aligned} O(t,0) &= \frac{Fe_{used}}{Fe_{needed}} \cdot M(t,\nu_f), \\ &= \frac{Fe_{used}}{k_{Fe}M(t,\nu_f)} \cdot M(t,\nu_f), \\ &= \frac{1}{k_{Fe}} Fe_{used}. \end{aligned} \tag{2.5}$$

As stated above, this assumption guarantees that each member of class O has full oxygen-carrying ability.

(v) The death rate of cells in the class $O(t,\psi)$, depends on the maturity level. We expect this to be an increasing function, because macrophages envelop mainly aging adult erythrocytes [48]. Therefore, we will use the increasing sigmoid function

$$\delta_O(\psi) = \left(\delta_O^{min} - \delta_O^{max}\right) \frac{(c_{\delta,O})^{k_{\delta,O}}}{(c_{\delta,O})^{k_{\delta,O}} + \psi^{k_{\delta,O}}} + \delta_O^{max}.$$

As in classes P and M, we can generate the partial differential equation

$$\frac{\partial}{\partial t}O(t,\psi) = -\rho_O \frac{\partial}{\partial \psi}O(t,\psi) - \delta_O(\psi)O(t,\psi)$$

with boundary condition (2.5).

2.8 Hemoglobin Concentration

We have already assumed that hemoglobin exists only in erythrocytes in class O. We compute the total number of members in class O at a given time t by

$$\int_0^{\psi_f} O(t,\psi)d\psi. \tag{2.6}$$

We previously made the assumption that each member of class O has exactly the same amount of iron. Specifically, if we multiply the quantity (2.6) by k_{Fe}, we have the amount of iron (in mg) circulating in erythrocytes at time t. We then multiply by a conversion factor to find the amount of hemoglobin circulating. Then we need only divide by blood volume, $BV(t)$, to determine the hemoglobin concentration.

Blood volume is difficult to determine and varies greatly in patients undergoing dialysis. Patients in ESRD are unable to clear fluids from their bodies. Fluids, for the most part, build up in the patient's body between dialysis treatments. Therefore, we assume that blood volume increases linearly between dialysis treatments and decreases linearly during a dialysis treatment. Initially we simulate patients undergoing dialysis (1) three times per week (i.e. Monday-Wednesday-Friday, or MWF), or (2) every third day (ETD), as in Figure 2.8.

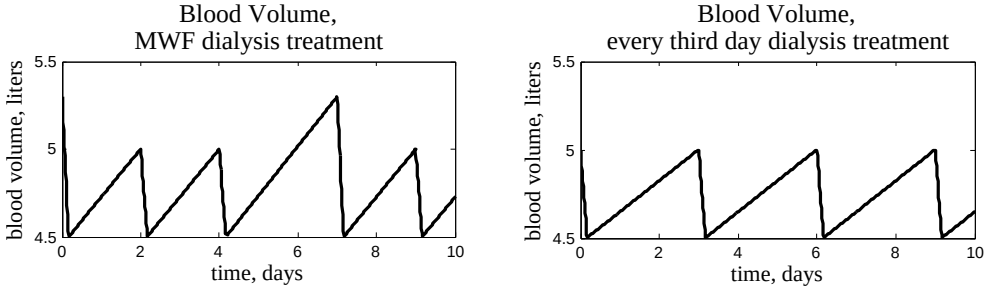

Figure 2.8: Blood volume over various treatment protocols.

Hence, hemoglobin concentration is a nonlinear function,

$$Hb(t) = \frac{k_{Fe}\int_0^{\psi_f} O(t,\psi)d\psi}{BV(t)}.$$

2.9 Modification to the Model

We now discuss how we produce a smooth approximation to the piecewise-defined function

$$f(E,I) = \begin{cases} f_{E<EPO_{th}}, & E < EPO_{th}, \\ 1, & E \geq EPO_{th}, \end{cases}$$

where

$$f_{E<EPO_{th}} = \frac{(c_{Fe,av})^{k_{Fe,av}}}{(c_{Fe,av})^{k_{Fe,av}} + I^{k_{Fe,av}}}.$$

For our initial simulations, we assume that inflammation remains constant. Hence, for a given inflammation level, f is a step function that oscillates between 1 and the constant $0 \leq f_{E<EPO_{th}} \leq 1$.

Rather than choose the constants $c_{Fe,av}$ and $k_{Fe,av}$, we choose two parameters $0 < f_1, f_{0.5} < 1$ such that when $E < EPO_{th}$,

$$f(E,1) = f_1 \text{ and } f(E,0.5) = f_{0.5}.$$

Thus,

$$\frac{(c_{Fe,av})^{k_{Fe,av}}}{(c_{Fe,av})^{k_{Fe,av}} + 1^{k_{Fe,av}}} = f_1 \tag{2.7}$$

and

$$\frac{(c_{Fe,av})^{k_{Fe,av}}}{(c_{Fe,av})^{k_{Fe,av}} + (0.5)^{k_{Fe,av}}} = f_{0.5}. \tag{2.8}$$

Then we solve (2.7) and (2.8) for the constants $c_{Fe,av}$ and $k_{Fe,av}$:

$$k_{Fe,av} = \frac{\ln f_{0.5} + \ln(1-f_1) - \ln f_1 - \ln(f_{0.5})}{\ln 2}$$

and

$$c_{Fe,av} = \left(\frac{1}{1-f_1}\right)^{\frac{\ln 2}{\ln f_{0.5} + \ln(1-f_1) - \ln f_1 - \ln(f_{0.5})}}.$$

We solve the EPO differential equation for a given treatment protocol. Then we use the solution to determine times $t_i = t_i(E)$ where EPO moves from above EPO_{th} to below EPO_{th} and vice versa, as in Figure 2.9.

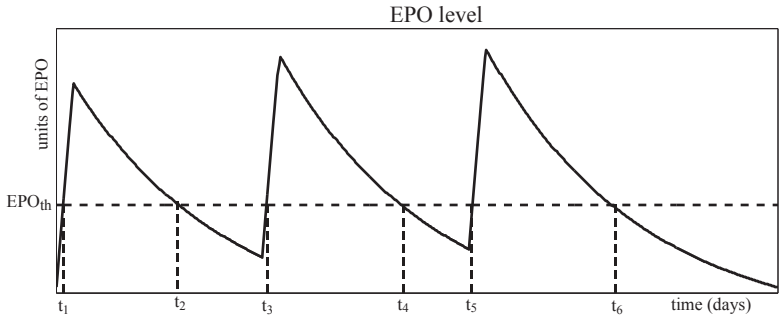

Figure 2.9: Determining the times t_i where $E(t) = EPO_{th}$.

We approximate f with

$$f^s(E, I, t) = h_{shift} + \sum_i h(i, I) H^s_{t_i}(t),$$

a linear combination of smoothed "heaviside" functions of the form

$$\begin{aligned} H^s_{t_i}(t) &= \frac{1}{2} + \frac{1}{2} \tanh\left(k_{heavy}(t - t_i)\right) \\ &= \frac{1}{1 + e^{-2k_{heavy}(t-t_i)}}. \end{aligned}$$

Choice of the parameter k_{heavy} determines the steepness of the approximation to each jump discontinuity. The coefficients $h(i, E)$ depend on (i) whether EPO level is passing from above EPO_{th} to below or vice versa, and (ii) the value of the quantity $f_{E<EPO_{th}}$, which depends on the level of inflammation.

Figure 2.10 shows an example of a function f (EPO three times per week, inflammation =0.5) with two smooth approximations, $k_{heavy} = 15$ and $k_{heavy} = 5$.

This formulation yields a function f^s that is smooth, approximates f, and has a smooth derivative. We replace f with f^s throughout the model and therefore we use the parameters f_1, $f_{0.5}$ and k_{heavy} in place of $c_{Fe,av}$ and $k_{Fe,av}$.

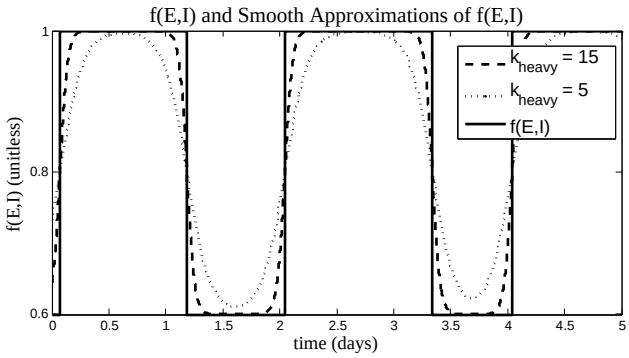

Figure 2.10: A smooth approximation of the function $f(E, I)$.

2.10 Model Summary

In summary, we have the system

$$\frac{\partial}{\partial t}P(t,\mu) = -\rho_P \frac{\partial}{\partial \mu}P(t,\mu) + \left[\beta_P(E) - \delta_P(E,I)\right] P(t,\mu), \tag{2.9}$$

$$\frac{\partial}{\partial t}M(t,\nu) = -\rho_M(E)\,\frac{\partial}{\partial \nu}M(t,\nu) + \beta_M M(t,\nu), \tag{2.10}$$

$$\frac{\partial}{\partial t}O(t,\psi) = -\rho_O \frac{\partial}{\partial \psi}O(t,\psi) - \delta_O(\psi)O(t,\psi), \tag{2.11}$$

$$\dot{Fe}(t) = k_{Fe}\int_0^{\psi_f} \delta_O(\psi)O(t,\psi)d\psi + \dot{Fe}_{ex}(t) - \rho_{Fe\to O} - \rho_{Fe,loss} \tag{2.12}$$

$$\dot{E}(t) = \rho_{EPO,basal} + \dot{E}_{ex}(t) - \frac{1}{t_{1/2}}\ln 2 \cdot E(t), \tag{2.13}$$

with boundary conditions

$$P(t,0) = R_P E(t), \tag{2.14}$$

$$M(t,0) = P(t,\mu_F), \tag{2.15}$$

$$O(t,0) = \frac{1}{k_{Fe}}Fe_{used}, \tag{2.16}$$

and initial conditions

$$P(0,\mu) = P_0(\mu), \tag{2.17}$$

$$M(0,\nu) = M_0(\nu), \tag{2.18}$$

$$O(0,\psi) = O_0(\psi), \tag{2.19}$$

$$Fe(0) = Fe_0, \tag{2.20}$$

$$E(0) = E_0. \tag{2.21}$$

Hemoglobin concentration is a time-dependent linear function of the amount of iron circulating,

$$Hb(t) = \frac{k_{Fe}\int_0^{\psi_f} O(t,\psi)d\psi}{BV(t)}. \tag{2.22}$$

Hence, we have a nonlinear coupled system of ordinary and partial differential equations with nontrivial boundary coupling with the following auxiliary equations.

$$\beta_P(E) = \left(\beta_P^{min} - \beta_P^{max}\right) \frac{\left(c_{\beta,P}\right)^{k_{\beta,P}}}{\left(c_{\beta,P}\right)^{k_{\beta,P}} + E^{k_{\beta,P}}} + \beta_P^{max} \tag{2.23}$$

$$\begin{aligned}\delta_P(E,I) = &\left(\delta_{P,E}^{max} - \delta_{P,E}^{min}\right) \frac{\left(c_{\delta,P,E}\right)^{k_{\delta,P,E}}}{\left(c_{\delta,P,E}\right)^{k_{\delta,P,E}} + E^{k_{\delta,P,E}}} + \delta_{P,E}^{min} \\ &+ \left(\delta_{P,I}^{min} - \delta_{P,I}^{max}\right) \frac{\left(c_{\delta,P,I}\right)^{k_{\delta,P,I}}}{\left(c_{\delta,P,I}\right)^{k_{\delta,P,I}} + I^{k_{\delta,P,I}}} + \delta_{P,I}^{max}\end{aligned} \tag{2.24}$$

$$\rho_M(E) = \left(\rho_M^{min} - \rho_M^{max}\right) \frac{\left(c_{\rho,M}\right)^{k_{\rho,M}}}{\left(c_{\rho,M}\right)^{k_{\rho,M}} + E^{k_{\rho,M}}} + \rho_M^{max} \tag{2.25}$$

$$\delta_O(\psi) = \left(\delta_O^{min} - \delta_O^{max}\right) \frac{\left(c_{\delta,O}\right)^{k_{\delta,O}}}{\left(c_{\delta,O}\right)^{k_{\delta,O}} + \psi^{k_{\delta,O}}} + \delta_O^{max} \tag{2.26}$$

$$f^s(E,I,t) = h_{shift} + \sum_i h(i,I) H_{t_i}^s(t) \tag{2.27}$$

$$H_{t_i}^s(t) = \frac{1}{1 + e^{-2k_{heavy}(t-t_i)}} \tag{2.28}$$

$$\rho_{Fe,loss}(Fe) = \begin{cases} \rho_{Fe,const}, & Fe \geq Fe_{th} \\ \rho_{Fe,frac} \cdot Fe, & Fe < Fe_{th} \end{cases} \tag{2.29}$$

$$\rho_{Fe \to O} = k_{\rho,Fe} Fe_{used} \tag{2.30}$$

$$Fe_{needed} = k_{Fe} M(t, \nu_f). \tag{2.31}$$

$$Fe_{avail} = k_{Fe,eff} f(E,I) Fe, \tag{2.32}$$

$$Fe_{used} = \min\left\{Fe_{needed},\ Fe_{avail}\right\} \tag{2.33}$$

Chapter 3

Numerical Implementation

3.1 Parameter Value Considerations

- Treatment Protocol:
  We perform simulations for two different "typical" treatment protocols: (1) a patient who goes in for dialysis every third day (ETD) and (2) a patient on a Monday, Wednesday, and Friday (MWF) treatment schedule. In both cases, dialysis is assumed to occur over a four-hour period during which time 5000 units of EPO are assumed to be administered at a constant rate. For those on the ETD schedule, iron is administered every ninth day; those on the the MWF schedule receive iron every Monday. We assume a standard preparation of 62.5 mg iron per administration.

- EPO:
  The half-life, $t_{1/2}$, of EPO is estimated to be 25 hours [48]. We assume the rate of EPO produced by the body, $\rho_{EPO,basal}$, is 100 units of EPO per day, chosen to be small relative to the amount provided intravenously.

- Iron: For this set of simulations, we assumed that the net amount of exogenous iron entering the system is equal to the net amount of iron losses in the system. For example, for a patient on MWF treatment schedule, exogenous iron treatment is 62.5 mg of iron every seventh day; therefore we assume that the rate of iron losses to be 62.5/7 mg iron per day.

- Blood volume:
  Typical adult blood volume is between 4.5 and 5 liters. We assume that blood

volume reaches its minimum, 4.5 liters, at the end of the four hours of dialysis. For a patient undergoing ETD treatment, we assume blood volume increases linearly to its maximum, 5 liters, just before they start a dialysis treatment. This is also true for a patient on MWF treatment, except that we assume the blood volume increases further, to 5.3 liters, over the weekend.

- Maturity Levels: Based on the literature [22], we assume $\mu_f = 3$ and $\nu_f = 2$. In healthy individuals, red blood cells have an average life span of approximately 120 days. In patients in ESRD, the life span of red blood cells is significantly shorter, so we assume that the *maximum* maturity level in class O is $\psi_f = 120$.

- k_{Fe} : In a healthy individual, each red blood cell (RBC) contains approximately 270 million hemoglobin molecules [21, 5, 37]. We use basic stoichiometry to determine k_{Fe} as follows:

$$\begin{aligned} k_{Fe} = & \frac{270 \times 10^6 \text{ Hg molecules}}{1 \text{ RBC}} \cdot \frac{10^9 \text{ RBCs}}{1 \text{ billion RBCs}} \cdot \frac{4 \text{ iron atoms}}{1 \text{ Hg molecule}} \\ & \cdot \frac{1 \text{ mol iron}}{6.022 \times 10^{23} \text{ iron atoms}} \cdot \frac{55.845 \text{ grams iron}}{1 \text{ mol iron}} \cdot \frac{10^3 \text{ mg iron}}{1 \text{ gram iron}} \\ = & \ 0.10015 \text{ mg iron / billion RBCs} \end{aligned}$$

- Other parameters: The remaining parameters were given nominal values that produced expected numbers of cells in classes P and M, and appropriate *Hb* concentrations. These parameters could be expected to vary among individuals. The remaining nominal parameter values we use appear in Appendix A.

3.2 Numerical Solution Methodologies

We solve our system in a sequential manner, beginning with (2.13). We then solve (2.9) numerically, using the solution of (2.13) in the boundary condition, (2.14). Similarly, use this solution in the boundary condition (2.15) to solve (2.10), and we use the solution of (2.10) when we solve (2.11) and (2.12) simultaneously. We solve using Matlab's ode23t solver.

We choose to solve the partial differential equations in the system using the finite element method. We initially use linear splines to perform the computations, but eventually

used quadratic splines (upwinding), as in [11], to determine if there was any advantage to using higher order elements. The derivations for those equations, therefore, are for the quadratic splines, but can easily be adapted to create linear splines by setting the upwinding parameter ω equal to zero.

Note that in class P (and also in class O), we have assumed that the maturation rate is constant (for simplification and lack of other biological information). Therefore,

$$\frac{\partial P}{\partial \mu} = \frac{\partial P}{\partial t} \cdot \frac{\partial t}{\partial \mu} = \frac{\partial P}{\partial t} \cdot \frac{1}{\rho_P}.$$

Hence, we could replace $\dfrac{\partial P}{\partial \mu}$ with $\dfrac{\partial P}{\partial t} \cdot \dfrac{1}{\rho_P}$ in (2.9), effectively reducing the problem. However, we proceed without making this reduction so that if, in future model revisions, our model assumptions change and we find that maturation rate is not constant, we will not have to make significant changes to our numerical methods.

3.2.1 EPO ODE

Since the EPO ODE does not receive input from any of the other classes/compartments, we solve the system

$$\dot{E}(t) = \rho_{EPO,basal} + \dot{E}_{ex}(t) - \frac{24}{25} \ln 2 \cdot E(t), \quad E(0) = E_0,$$

using ETD or MWF treatment protocol, as described in section 3.1.

3.2.2 Class P PDE

The progenitor class is influenced only by the EPO level and the inflammation level. We interpolate the EPO level for use in solving the PDE associated with the progenitor class, $P(t, \mu)$, on $0 = \mu_0 \leq \mu \leq \mu_f$.

Let

$$0 = \mu_1 < \mu_2 < \cdots < \mu_{N_P} = \mu_f$$

be a uniform partition of $N_P - 1$ subintervals, each of length $h_P = \frac{\mu_f}{N_P - 1}$. We define N_P

piecewise linear continuous functions

$$\phi_j^A, \quad j = 1, 2, \ldots, N_P,$$

which we will call *trial solution functions*, by

$$\phi_j^A(\mu) = \begin{cases} \dfrac{\mu - \mu_{j-1}}{h_P}, & \mu_{j-1} \le \mu \le \mu_j, \\ \dfrac{\mu_{j+1} - \mu}{h_P}, & \mu_j \le \mu \le \mu_{j+1}, \\ 0, & \mu < \mu_{j-1} \text{ or } \mu > \mu_{j+1}. \end{cases}$$

The derivative of such a function (when it exists) is given by

$$\phi_j^{A\prime}(\mu) = \begin{cases} \dfrac{1}{h_P}, & \mu_{j-1} < \mu < \mu_j, \\ -\dfrac{1}{h_P}, & \mu_j < \mu < \mu_{j+1}, \\ 0, & \mu < \mu_{j-1} \text{ or } \mu > \mu_{j+1}. \end{cases}$$

We will also use a set of *test functions* $\tilde{\phi}_j$. We begin by defining N_P continuous second-order spline functions

$$\chi_j^A, \quad j = 1, 2, \ldots, N_P,$$

by

$$\chi_j^A(\mu) = \begin{cases} \dfrac{(\mu - \mu_{j-1})(\mu_j - \mu)}{h_P^2}, & \mu_{j-1} \le \mu \le \mu_j, \\ -\dfrac{(\mu - \mu_j)(\mu_{j+1} - \mu)}{h_P^2}, & \mu_j \le \mu \le \mu_{j+1}, \\ 0, & \mu < \mu_{j-1} \text{ or } \mu > \mu_{j+1}. \end{cases}$$

Notice that by definition, $\chi_j^A(\mu_{j-1}) = \chi_j^A(\mu_j) = \chi_j^A(\mu_{j+1}) = 0$.

Let ω_P be a scalar parameter and define the test functions $\tilde{\phi}_j^A, j = 1, 2, \ldots, N_P$, by

$$\tilde{\phi}_j^A(\mu) = \phi_j^A(\mu) + \omega_P \chi_j^A(\mu).$$

Note that for all j,

$$\frac{d}{d\mu}\tilde{\phi}_j^A(\mu) = \phi_j^{A'}(\mu) + \omega_P \chi_j^{A'}(\mu)$$

and

$$\tilde{\phi}_j^A(\mu) = \phi_j^A(\mu) \text{ for } \mu = \mu_{j-i}, \mu_j, \mu_{j+1}.$$

Let $1 \leq j \leq N_P$ be arbitrary. We make a weak formulation of (2.9) by multiplying by the j^{th} test function and integrating over all maturity levels:

$$\begin{aligned}\int_0^{\mu_f} \frac{\partial}{\partial t} P(t,\mu)\tilde{\phi}_j^A(\mu)d\mu = & -\rho_P \int_0^{\mu_f} \frac{\partial}{\partial \mu} P(t,\mu)\tilde{\phi}_j^A(\mu)d\mu \\ & + \int_0^{\mu_f} \left[\beta_P(E) - \delta_P(E,I)\right] P(t,\mu)\tilde{\phi}_j^A(\mu)d\mu.\end{aligned}$$

Using integration by parts of the second term, we have

$$\begin{aligned}\int_0^{\mu_f} \frac{\partial}{\partial t} P(t,\mu)\tilde{\phi}_j^A(\mu)d\mu = & - \rho_P P(t,\mu)\tilde{\phi}_j^A(\mu)\Big|_{\mu=0}^{\mu=\mu_f} \\ & + \rho_P \int_0^{\mu_f} P(t,\mu)\frac{d}{d\mu}\tilde{\phi}_j^A(\mu)d\mu \\ & + \int_0^{\mu_f} \left[\beta_P(E) - \delta_P(E,I)\right] P(t,\mu)\tilde{\phi}_j^A(\mu)d\mu.\end{aligned}$$

$$\begin{aligned}\int_0^{\mu_f} \frac{\partial}{\partial t} P(t,\mu)\tilde{\phi}_j^A(\mu)d\mu = & -\rho_P P(t,\mu_f)\phi_j^A(\mu_f) + \rho_P P(t,0)\phi_j^A(0) \\ & + \rho_P \int_0^{\mu_f} P(t,\mu)\frac{d}{d\mu}\tilde{\phi}_j^A(\mu)d\mu \\ & + \int_0^{\mu_f} \left[\beta_P(E) - \delta_P(E,I)\right] P(t,\mu)\tilde{\phi}_j^A(\mu)d\mu.\end{aligned}$$

Now we can apply the boundary condition (2.14) to obtain

$$\begin{aligned}\int_0^{\mu_f} \frac{\partial}{\partial t} P(t,\mu)\tilde{\phi}_j^A(\mu)d\mu = & -\rho_P P(t,\mu_f)\phi_j^A(\mu_f) + \rho_P R_P E(t)\phi_j^A(0) \\ & + \rho_P \int_0^{\mu_f} P(t,\mu)\frac{d}{d\mu}\tilde{\phi}_j^A(\mu)d\mu \\ & + \int_0^{\mu_f} \left[\beta_P(E) - \delta_P(E,I)\right] P(t,\mu)\tilde{\phi}_j^A(\mu)d\mu. \end{aligned} \tag{3.1}$$

We define the Galerkin finite element approximation for P by

$$P(t,\mu) = \sum_{i=1}^{N_P} a_i(t)\phi_i^A(\mu), \tag{3.2}$$

which we substitute into equation (3.1), then rearrange the terms for convenience, as below.

$$\begin{aligned}\int_0^{\mu_f} \sum_{i=1}^{N_P} a_i'(t)\phi_i^A(\mu)\tilde{\phi}_j^A(\mu)d\mu = & -\rho_P \sum_{i=1}^{N_P} a_i(t)\phi_i^A(\mu_f)\phi_j^A(\mu_f) + \rho_P R_P E(t)\phi_j^A(0) \\ & + \rho_P \int_0^{\mu_f} \sum_{i=1}^{N_P} a_i(t)\phi_i^A(\mu)\frac{d}{d\mu}\tilde{\phi}_j^A(\mu)d\mu \\ & + \int_0^{\mu_f} \left[\beta_P(E) - \delta_P(E,I)\right] \sum_{i=1}^{N_P} a_i(t)\phi_i^A(\mu)\tilde{\phi}_j^A(\mu)d\mu. \end{aligned}$$

$$\begin{aligned}\sum_{i=1}^{N_P} a_i'(t) \int_0^{\mu_f} \phi_i^A(\mu)\tilde{\phi}_j^A(\mu)d\mu = & -\rho_P a_{N_P}(t)\phi_j^A(\mu_f) + \rho_P R_P E(t)\phi_j^A(0) \\ & + \sum_{i=1}^{N_P} a_i(t)\Bigg\{\rho_P \int_0^{\mu_f} \phi_i^A(\mu)\frac{d}{d\mu}\tilde{\phi}_j^A(\mu)d\mu \\ & + \left[\beta_P(E) - \delta_P(E,I)\right] \int_0^{\mu_f} \phi_i^A(\mu)\tilde{\phi}_j^A(\mu)d\mu\Bigg\}. \end{aligned}$$

$$\sum_{i=1}^{N_P} a_i'(t) \left[\int_0^{\mu_f} \phi_i^A(\mu)\phi_j^A(\mu)d\mu + \omega_P \int_0^{\mu_f} \phi_i^A(\mu)\chi_j^A(\mu)d\mu \right]$$
$$= -\rho_P a_{N_P}(t)\phi_j^A(\mu_f) + \rho_P R_P E(t)\phi_j^A(0)$$
$$+ \sum_{i=1}^{N_P} a_i(t) \Bigg\{ \rho_P \left[\int_0^{\mu_f} \phi_i^A(\mu)\phi_j^{A\prime}(\mu)d\mu + \omega_P \int_0^{\mu_f} \phi_i^A(\mu)\chi_j^{A\prime}(\mu)d\mu \right]$$
$$+ [\beta_P(E) - \delta_P(E,I)] \left[\int_0^{\mu_f} \phi_i^A(\mu)\phi_j^A(\mu)d\mu + \omega_P \int_0^{\mu_f} \phi_i^A(\mu)\chi_j^A(\mu)d\mu \right] \Bigg\}. \quad (3.3)$$

We can let j range from 1 to N_P to yield a system of N_P ordinary differential equations for the coefficients $a_i(t)$, which we will put in matrix form. Therefore, we introduce the following definitions:

$$x(t) = [a_1(t), a_2(t), \ldots, a_{N_P}(t)]^T,$$

$$\mathcal{A} = \begin{bmatrix} \int \phi_1^A \phi_1^A & \int \phi_2^A \phi_1^A & & & & \\ \int \phi_1^A \phi_2^A & \int \phi_2^A \phi_2^A & \int \phi_3^A \phi_2^A & & & \\ & \int \phi_2^A \phi_3^A & \int \phi_3^A \phi_3^A & \int \phi_4^A \phi_3^A & & \\ & & \ddots & \ddots & \ddots & \\ & & & \int \phi_{N_P-2}^A \phi_{N_P-1}^A & \int \phi_{N_P-1}^A \phi_{N_P-1}^A & \int \phi_{N_P}^A \phi_{N_P-1}^A \\ & & & & \int \phi_{N_P-1}^A \phi_{N_P}^A & \int \phi_{N_P}^A \phi_{N_P}^A \end{bmatrix}$$

$$= \frac{h_P}{6} \begin{bmatrix} 2 & 1 & & & & 0 \\ 1 & 4 & 1 & & & \\ & 1 & 4 & 1 & & \\ & & \ddots & \ddots & \ddots & \\ & & & 1 & 4 & 1 \\ 0 & & & & 1 & 2 \end{bmatrix},$$

$$\mathcal{A}' = \begin{bmatrix} \int \phi_1^A \phi_1^{A'} & \int \phi_2^A \phi_1^{A'} & & & & \\ \int \phi_1^A \phi_2^{A'} & \int \phi_2^A \phi_2^{A'} & \int \phi_3^A \phi_2^{A'} & & & \\ & \int \phi_2^A \phi_3^{A'} & \int \phi_3^A \phi_3^{A'} & \int \phi_4^A \phi_3^{A'} & & \\ & & \ddots & \ddots & \ddots & \\ & & & \int \phi_{N_P-2}^A \phi_{N_P-1}^{A\ \prime} & \int \phi_{N_P-1}^A \phi_{N_P-1}^{A\ \prime} & \int \phi_{N_P}^A \phi_{N_P-1}^{A\ \prime} \\ & & & & \int \phi_{N_P-1}^A \phi_{N_P}^{A\ \prime} & \int \phi_{N_P}^A \phi_{N_P}^{A\ \prime} \end{bmatrix}$$

$$= \frac{1}{2} \begin{bmatrix} -1 & -1 & & & & 0 \\ 1 & 0 & -1 & & & \\ & 1 & 0 & -1 & & \\ & & \ddots & \ddots & \ddots & \\ & & & 1 & 0 & -1 \\ 0 & & & & 1 & 1 \end{bmatrix},$$

$$\mathcal{X}_A = \begin{bmatrix} \int \phi_1^A \chi_1^A & \int \phi_2^A \chi_1^A & & & \\ \int \phi_1^A \chi_2^A & \int \phi_2^A \chi_2^A & \int \phi_3^A \chi_2^A & & \\ & \int \phi_2^A \chi_3^A & \int \phi_3^A \chi_3^A & \int \phi_4^A \chi_3^A & \\ & & \ddots & \ddots & \ddots \\ & & & \int \phi_{N_P-2}^A \chi_{N_P-1}^A & \int \phi_{N_P-1}^A \chi_{N_P-1}^A & \int \phi_{N_P}^A \chi_{N_P-1}^A \\ & & & & \int \phi_{N_P-1}^A \chi_{N_P}^A & \int \phi_{N_P}^A \chi_{N_P}^A \end{bmatrix}$$

$$= \frac{h_P}{12} \begin{bmatrix} -1 & -1 & & & & 0 \\ 1 & 0 & -1 & & & \\ & 1 & 0 & -1 & & \\ & & \ddots & \ddots & \ddots & \\ & & & 1 & 0 & -1 \\ 0 & & & & 1 & 1 \end{bmatrix},$$

$$\mathcal{X}'_A = \begin{bmatrix} \int \phi_1^A \chi_1^{A\prime} & \int \phi_2^A \chi_1^{A\prime} & & & \\ \int \phi_1^A \chi_2^{A\prime} & \int \phi_2^A \chi_2^{A\prime} & \int \phi_3^A \chi_2^{A\prime} & & \\ & \int \phi_2^A \chi_3^{A\prime} & \int \phi_3^A \chi_3^{A\prime} & \int \phi_4^A \chi_3^{A\prime} & \\ & & \ddots & \ddots & \ddots \\ & & & \int \phi_{N_P-2}^A \chi_{N_P-1}^{A\ \prime} & \int \phi_{N_P-1}^A \chi_{N_P-1}^{A\ \prime} & \int \phi_{N_P}^A \chi_{N_P-1}^{A\ \prime} \\ & & & & \int \phi_{N_P-1}^A \chi_{N_P}^{A\ \prime} & \int \phi_{N_P}^A \chi_{N_P}^{A\ \prime} \end{bmatrix}$$

$$= \frac{1}{6} \begin{bmatrix} -1 & 1 & & & & 0 \\ 1 & -2 & 1 & & & \\ & 1 & -2 & 1 & & \\ & & \ddots & \ddots & \ddots & \\ & & & 1 & -2 & 1 \\ 0 & & & & 1 & -1 \end{bmatrix},$$

$$M_P = \mathcal{A} + \omega_P \mathcal{X}_A,$$

$$A_P(E,I) = \rho_P \left\{ \mathcal{A}' + \omega_P \mathcal{X}_A' + \begin{bmatrix} 0 & \cdots & & 0 \\ \vdots & & & \vdots \\ 0 & \cdots & 0 & 0 \\ 0 & \cdots & 0 & -1 \end{bmatrix} \right\} + \left[\beta_P(E) - \delta_P(E,I)\right] \left\{\mathcal{A} + \omega_P \mathcal{X}_A\right\},$$

and

$$B_P(E) = \left[\rho_P R_P E(t), 0, 0, \ldots, 0\right]^T,$$

where

$$\begin{aligned}
\int \phi_i^A \phi_j^A \text{ means } & \int_0^{\mu_f} \phi_i^A(\mu)\phi_j^A(\mu)d\mu, \\
\int \phi_i^A \phi_j^{A'} \text{ means } & \int_0^{\mu_f} \phi_i^A(\mu)\chi_j^{A'}(\mu)d\mu, \\
\int \phi_i^A \chi_j^A \text{ means } & \int_0^{\mu_f} \phi_i^A(\mu)\chi_j^A(\mu)d\mu, \text{ and} \\
\int \phi_i^A \chi_j^{A'} \text{ means } & \int_0^{\mu_f} \phi_i^A(\mu)\chi_j^{A'}(\mu)d\mu.
\end{aligned}$$

Then (3.3) can be written as

$$M_P \dot{x}(t) = A_P(E,I)x(t) + B_P(E). \tag{3.4}$$

3.2.3 Classes M, O and Iron

The maturing class, $M(t,\nu)$, on $0 = \nu_0 \leq \nu \leq \nu_f$, is influenced by the EPO level, and depends on the progenitor class as its boundary condition. We linearly interpolate $E(t)$ and $a_{N_P}(t)$ from the solution to the previous two systems.

The process of converting (2.10) to a system of N_M ODEs is the same as for class P,

so the details for generating the matrix equation

$$M_M \dot{y}(t) = A_M(E)y(t) + B_M(E) \tag{3.5}$$

are omitted here but can be found in Appendix B.

Similarly, the class O PDE (2.11) can be converted into a system of N_O ODEs given in matrix from as

$$M_O \dot{z}(t) = A_O z(t) + B_O(t). \tag{3.6}$$

These will be solved simultaneously with (2.12), the differential equation for iron. The derivations for these equations can be found in Appendix C.

3.3 Validating the Code using Forcing Functions

In sections 3.2.2 and 3.2.3, we discussed how we convert the partial differential equations for states to systems of ordinary differential equations. Now we discuss how we solve these systems numerically and how we validate our code.

We use Matlab's ode23t command to solve the large systems of differential equations. In order to validate our code, we implement a forcing function strategy, as follows. For class P, for example, we solve a modified version of (2.9):

$$\frac{\partial}{\partial t}\tilde{P}(t,\mu) = -\rho_P \frac{\partial}{\partial \mu}\tilde{P}(t,\mu) + \left[\beta_P(E) - \delta_P(E,I)\right]\tilde{P}(t,\mu) + F(t,\mu). \tag{3.7}$$

We choose a function such as $\tilde{P}^*(t,\mu) = 10e^{-t/2} + 15e^{-\mu/3}$, which is smooth and decreases to zero with increasing time and maturity level, then determine the forcing function F that guarantees that $\tilde{P}^*$ is the exact solution of (3.7). We solve (3.7) numerically and compare our solution with the known exact solution.

It is well known that the solution to (2.9) will propagate along its characteristic curves, which we can think of as a "wave front." When we use standard linear splines ϕ_j as both the trial solution functions and the test functions, we introduce error at this wave front, which is propagated in time. In Figure 3.1.1, we see that the error can become large and that standard linear splines are insufficient to resolve the solution, as described in [28]. (We will discuss the error that is similar in both Figures 3.1.1 and 3.1.2 later.)

In order to alleviate this problem, we use a Petrov-Galerkin finite element method,

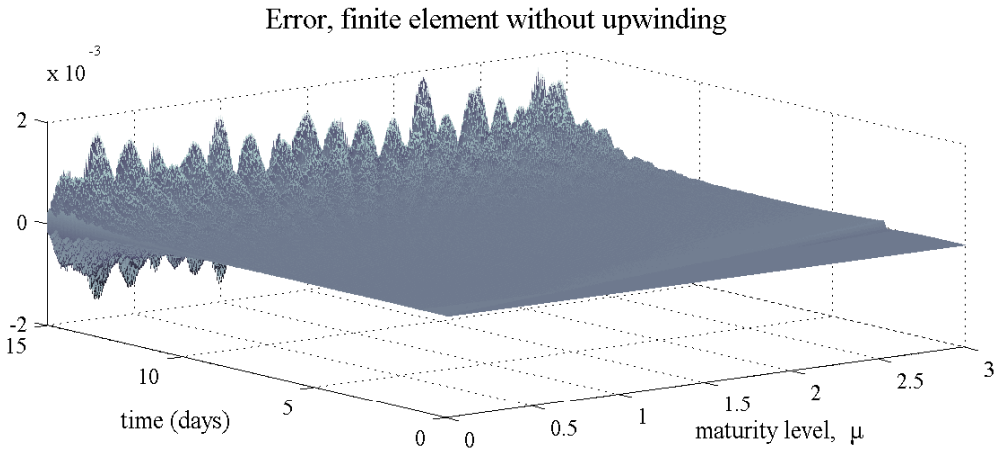

3.1.1: Error without using upwinding.

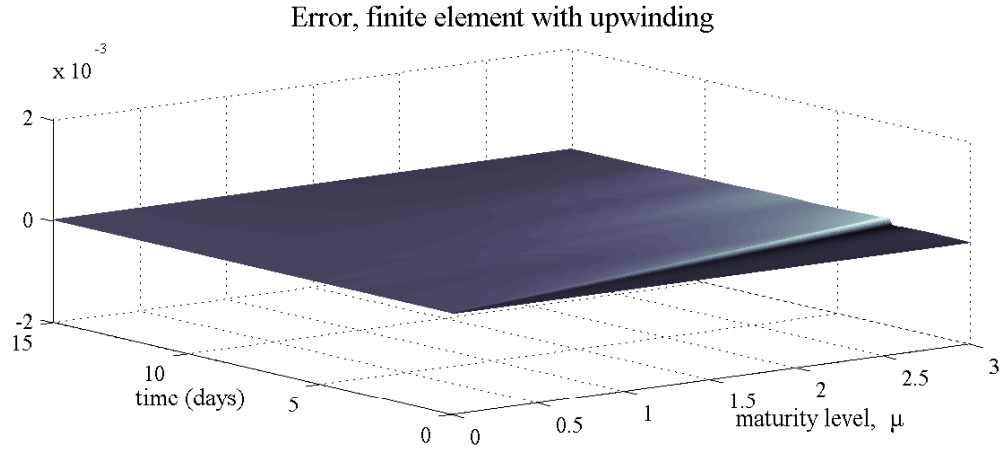

3.1.2: Error using upwinding.

Figure 3.1: Code validation. We using a forcing function strategy to compare the numerical solution to a known exact solution. Exact solution is of the order 10^2.

also known as upwinding. We continue using linear spline elements ϕ_j for the trial solution functions, but for the test functions we use second-order functions of the form $\phi_j + \omega\chi_j$, where

$$\chi_j(\mu) = \begin{cases} \dfrac{(\mu - \mu_{j-1})(\mu_j - \mu)}{h^2}, & \mu_{j-1} \le \mu \le \mu_j, \\ -\dfrac{(\mu - \mu_j)(\mu_{j+1} - \mu)}{h^2}, & \mu_j \le \mu \le \mu_{j+1}, \\ 0, & \mu < \mu_{j-1} \text{ or } \mu > \mu_{j+1}. \end{cases}$$

Figure 3.2 provides an example of standard test elements with varying levels of the upwinding parameter ω. Note that $\omega = 0$ corresponds to no upwinding, or standard linear spline elements.

When we solve (3.7) numerically using nonzero values of ω, and compare our solution with the exact solution, we see significant improvement, as in Figure 3.1.2.

We note that the small error seen in both Figure 3.1.1 and Figure 3.1.2 (that propagates along a linear characteristic from $t = 0$ to approximately $t = 3$) is due to a high order discontinuity between the boundary condition and initial condition at $(t, \mu) = (0, 0)$. This error diminishes with use of a finer mesh on the structure variable.

In order to determine an appropriate value for the parameter ω, we fix the number of elements and solve (3.7). Figure 3.3 shows the error using several values for the upwinding parameter.

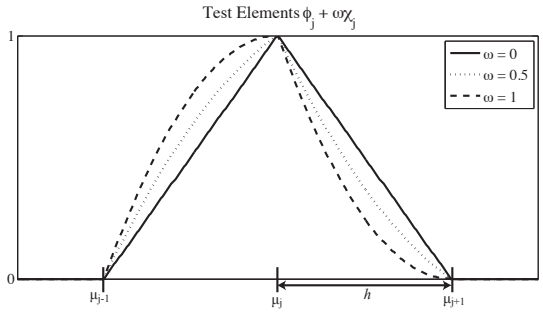

Figure 3.2: Test basis elements, with varying values of the upwinding parameter ω.

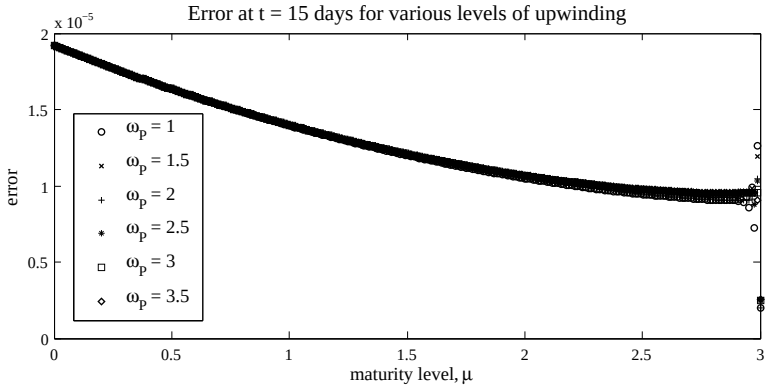

Figure 3.3: Effect of varying ω_P on error between numerical and exact solution at $t = 15$ for $N = 256$ spatial elements. Exact solution is of the order 10^2.

We note that the error is of the same order for several values of the parameter and we choose to continue our simulations with $\omega_P = 2.5$ as the upwinding parameter for class P.

As one final validation of our code, we sequentially increase the number of splines elements by a factor of two to confirm that the numerical solution converges to the exact solution and to observe the rate of convergence, which is essentially quadratic. The results appear in Table 3.1.

We repeated this process of validating the code for classes M and O. The results appear in Appendices D and E.

Table 3.1: Convergence of Solution–Maximum Error at $t = 15$ with $\omega_P = 2.5$ for an increasing number of splines. Exact solution is of the order 10^2.

N_P	Maximum error	(Max Error for N_P)/(Max Error for $2N_P$)
4	0.1298	5.2451
8	0.0247	4.5190
16	0.0055	4.2395
32	0.0013	4.1153
64	3.1384e-04	4.0566
128	7.7365e-05	4.0280
256	1.9207e-05	4.0140
512	4.7850e-06	1.7820
1024	2.6851e-06	

Chapter 4

Numerical Results and Discussion

4.1 Numerical Results and Discussion

We simulated two types of treatment (ETD and MWF) at each of seven inflammation levels (inflammation = 0, 0.25, 0.37, 0.5, 0.63, 0.75, and 1). The complete numerical results appear in Appendix F. We show first simulations of a patient at inflammation level 0.5, under the ETD treatment schedule and then the MWF treatment schedule. We also show some results comparing various inflammation levels.

4.1.1 Numerical results for a patient at inflammation level 0.5

An example of our numerical results is shown for a patient undergoing treatment on the ETD schedule with inflammation level 0.5. As expected, in Figure 4.1 we see the patient's EPO level increases every third day when exogenous EPO is provided, and decays between treatments.

In Figure 4.2, we observe that the boundary condition at $\mu = 0$ for class P mimics the shape of the EPO plot because the recruitment rate is directly proportional to the EPO level.

Cells in class P mature and divide at a rate of approximately one division per day. Cells in class P mature into class M, which is pictured in Figure 4.3.

Comparing Figures 4.2 and 4.3, we see that, as expected, $P(t, \mu_f) = M(t, 0)$ for all t. Cells in class M divide at a rate of approximately one division per day before they mature into class O.

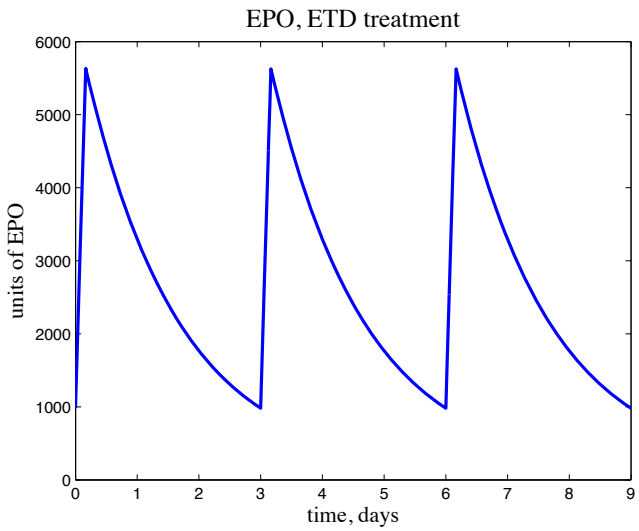

Figure 4.1: EPO level over time for a patient with inflammation = 0.5 undergoing ETD treatment.

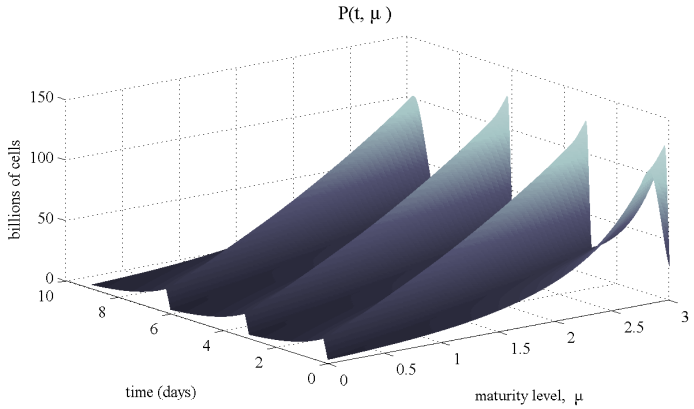

Figure 4.2: Number of cells in class P for a patient with inflammation = 0.5 undergoing ETD treatment.

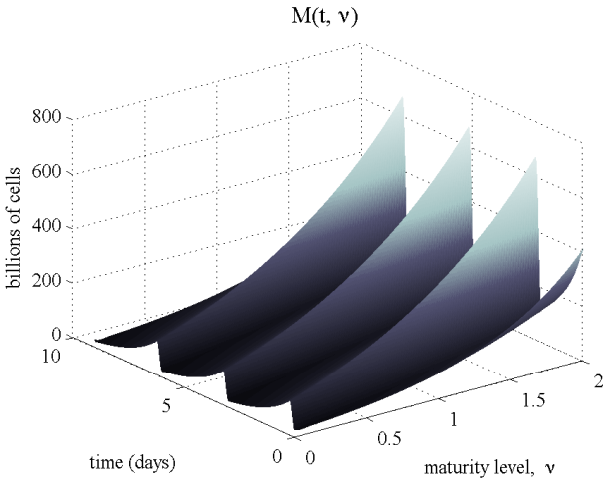

Figure 4.3: Number of cells in class M for a patient with inflammation = 0.5 undergoing ETD treatment.

As we consider Figure 4.4, it is worth noting that there has been a change in the time scale. This plot actually closely resembles the plots for classes P and M, but appears much different because results are shown over a time period of 120 days as opposed to just two or three days; this is not an example of the "noise" we discussed previously.

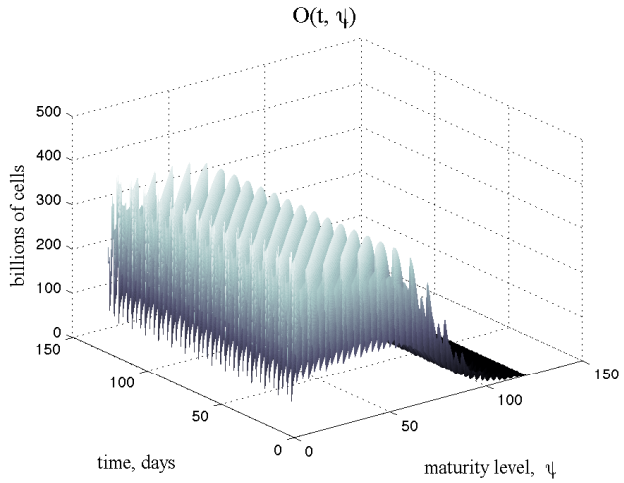

Figure 4.4: Number of cells in class O for a patient with inflammation = 0.5 undergoing ETD treatment.

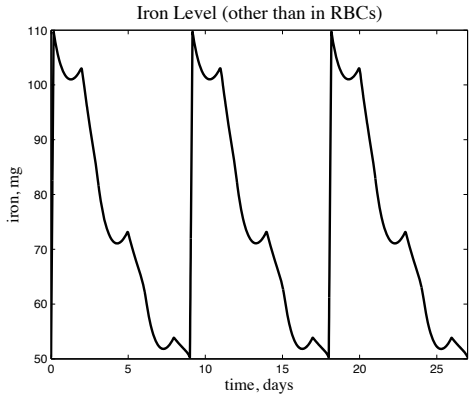

Figure 4.5: Iron level for a patient with inflammation = 0.5 undergoing ETD treatment.

The boundary condition, $O(t, 0)$, is not identical to $M(t, \nu_f)$ in Figure 4.3 because the number of cells maturing in to class O is also dependent on how much iron is available. Note also that cells in class O no longer divide; they simply mature and die.

The amount of iron (other than that being carried in RBCs), in Figure 4.5, is seen to increase greatly when exogenous iron is introduced (on days 0 and 9). Small increases are due to iron being recycled from RBCs that have died.

Finally, Figure 4.6 shows the resulting hemoglobin concentration. The desired range, 11 to 13 g/dL, is also shown.

Figure 4.7 shows similar results for a patient at inflammation level 0.5 undergoing MWF treatment.

The main output of interest in this work is the hemoglobin concentration. It is clear that the hemoglobin concentration is being driven by the blood volume. That is, as blood volume increases, concentration decreases. During the time a patient is undergoing treatment, their blood volume decreases drastically, and we hemoglobin concentration increase drastically in response.

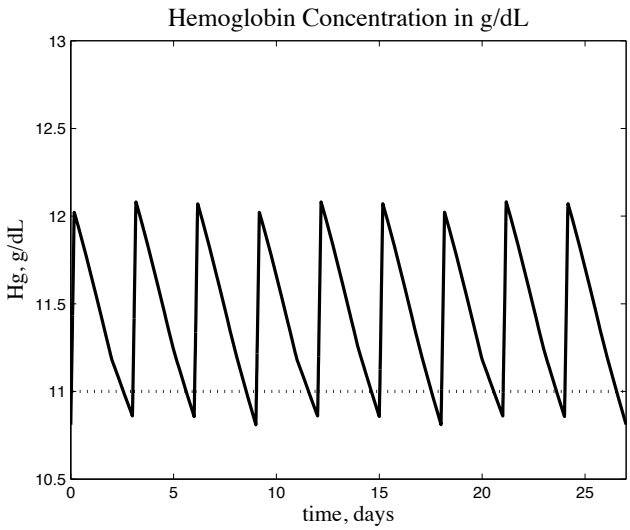

Figure 4.6: Hemoglobin concentration for a patient with inflammation = 0.5 undergoing ETD treatment.

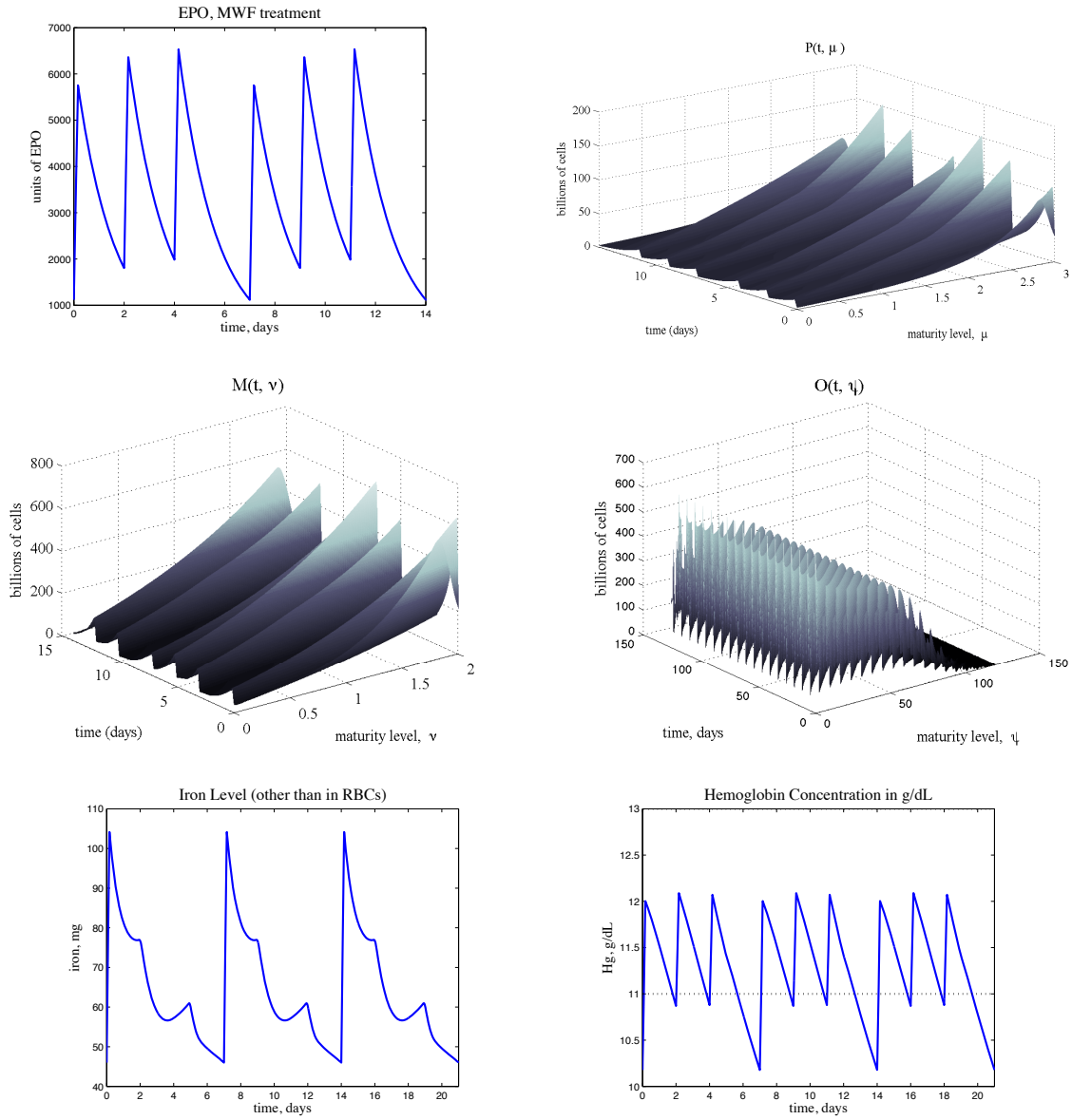

Figure 4.7: Numerical results for a patient with inflammation level 0.5 undergoing MWF treatment.

4.1.2 Numerical results, comparing inflammation levels

We also present some results of varying the inflammation level for both ETD (Figure 4.8) and MWF treatment (Figure 4.9).

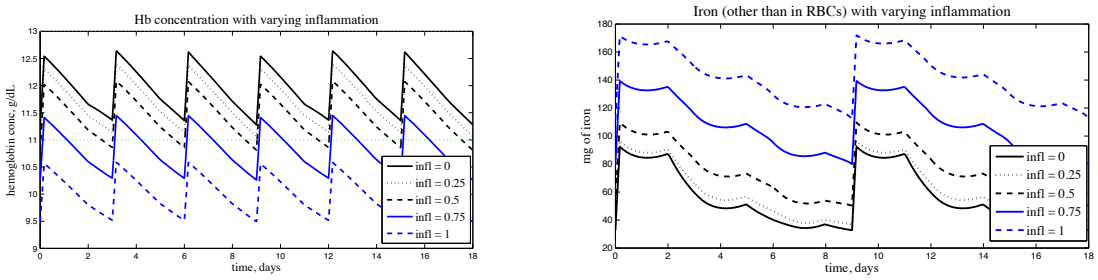

Figure 4.8: Hemoglobin concentration and iron with varying inflammation, ETD treatment.

It should be noted here that the solutions are dependent on the initial conditions, and therefore careful choice of initial conditions must be made in order to produce results that biologically reasonable. For example, if one starts with an an initial condition $O(t, 0)$ that is large, then the iron being carried in those cells eventually ends up in the iron compartment, which in turn affects the recruitment rate into class O. As a result, it is possible, for example, to produce a set of simulations such that the hemoglobin

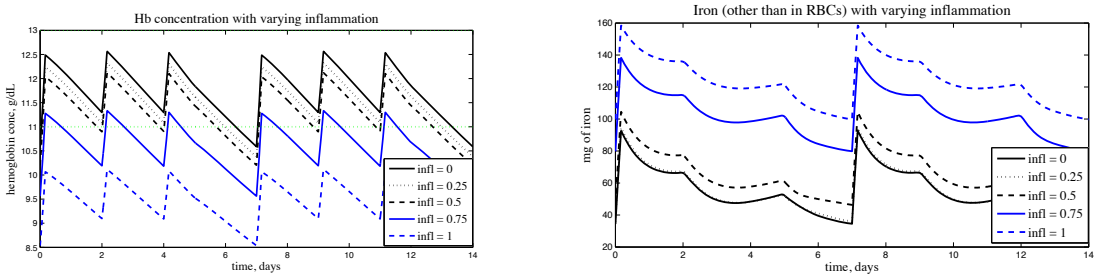

Figure 4.9: Hemoglobin concentration and iron with varying inflammation, MWF treatment.

concentration for a patient with inflammation level 0.5 is actually higher than for a patient with a lower inflammation level.

It is clear based on the plots of hemoglobin concentration that, as we described previously, hemoglobin concentration is largely driven by blood volume. This has potential treatment implications; keeping hemoglobin concentration within the desired band can be achieved by increasing the frequency of dialysis. In fact, it is possible that the quantities of EPO and iron administered will have little effect relative to the blood volume. This may not have a direct effect on dialysis practice, however, because it is certainly one of the goals of treatment to give patients increased autonomy. Requiring them to come for treatment every day, for example, might keep hemoglobin concentration within the desired band, but would not necessarily increase the patient's quality of life.

4.2 Comparing iron needed and iron available

For each treatment protocol, we also compare iron needed, Fe_{needed} and iron available, Fe_{avail}, over time at various levels of inflammation so that we might understand the role iron plays in determining the number of cells maturing in to class O (see Figures 4.10 through 4.19, which follow).

It is worth noting again that we assigned nominal parameter values and the solutions (in particular iron available) are absolutely dependent on the initial conditions. As such, the solutions should be viewed qualitatively, not quantitatively.

Iron-restricted erythropoiesis occurs when iron needed is greater than iron available. In this case, providing more iron might be beneficial for the patient. Understanding when iron-restricted erythropoiesis is occurring is, therefore, useful information for a practictioner. Based on the following simulations, iron-restricted erythropoiesis is evident following treatment that consists of an EPO administration but no iron administration. The implication might be that smaller, more frequent doses of iron are more desirable than the simulated treatment protocol.

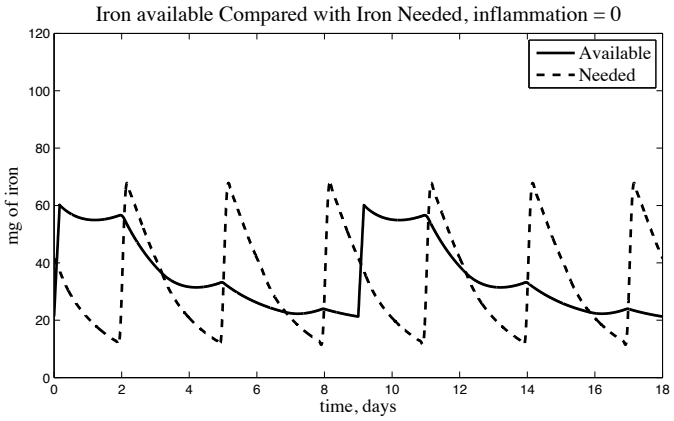

Figure 4.10: Fe_{needed} and Fe_{avail} : inflammation = 0, ETD treatment.

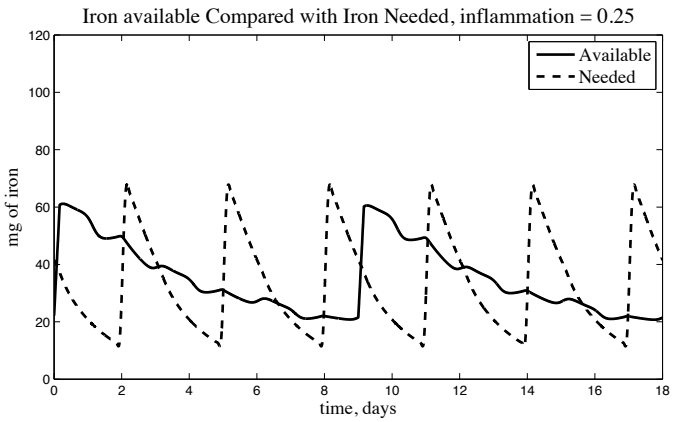

Figure 4.11: Fe_{needed} and Fe_{avail} : inflammation = 0.25, ETD treatment.

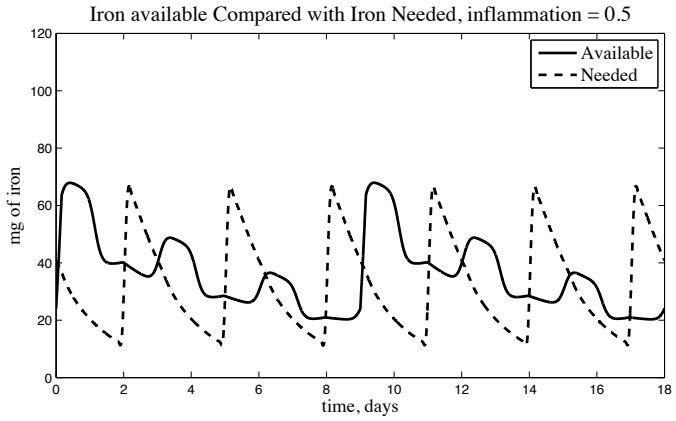

Figure 4.12: Fe_{needed} and Fe_{avail} : inflammation = 0.5, ETD treatment.

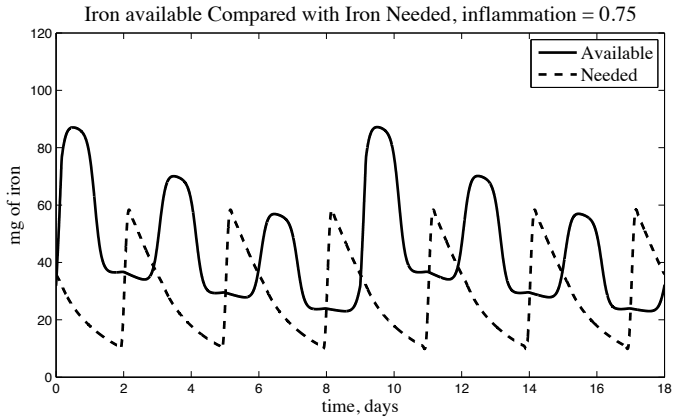

Figure 4.13: Fe_{needed} and Fe_{avail} : inflammation = 0.75, ETD treatment.

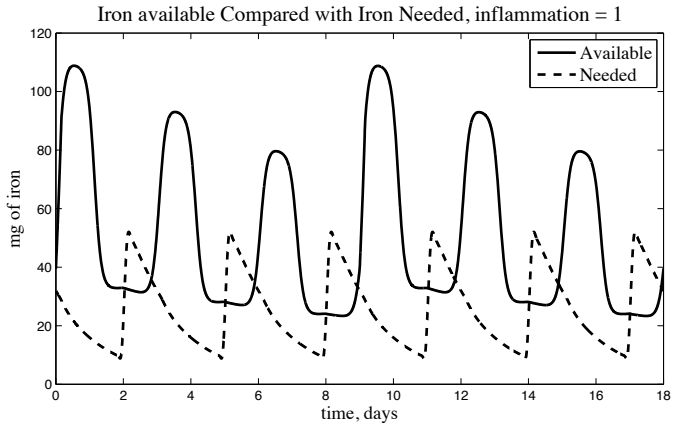

Figure 4.14: Fe_{needed} and Fe_{avail} : inflammation = 1, ETD treatment.

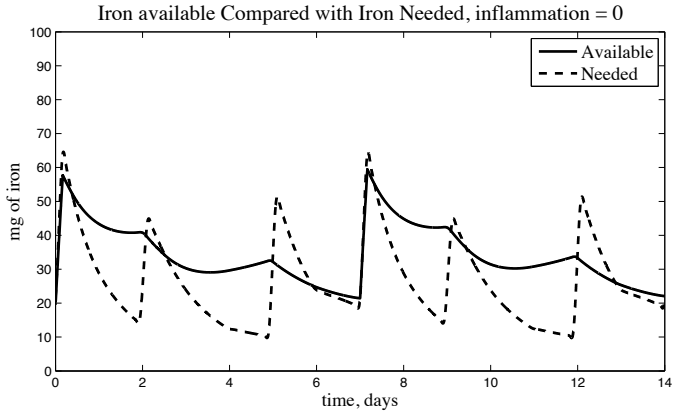

Figure 4.15: Fe_{needed} and Fe_{avail} : inflammation = 0, MWF treatment.

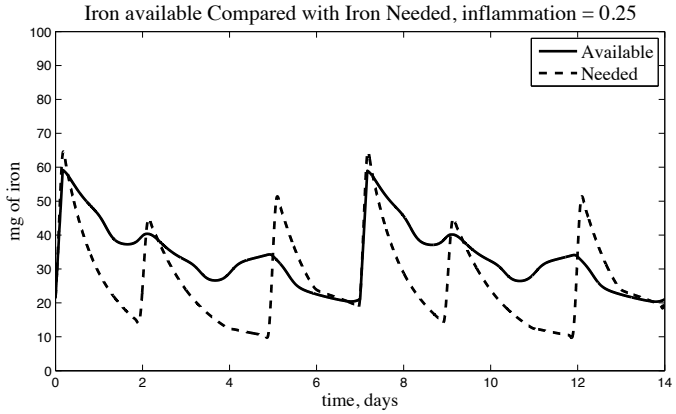

Figure 4.16: Fe_{needed} and Fe_{avail} : inflammation = 0.25, MWF treatment.

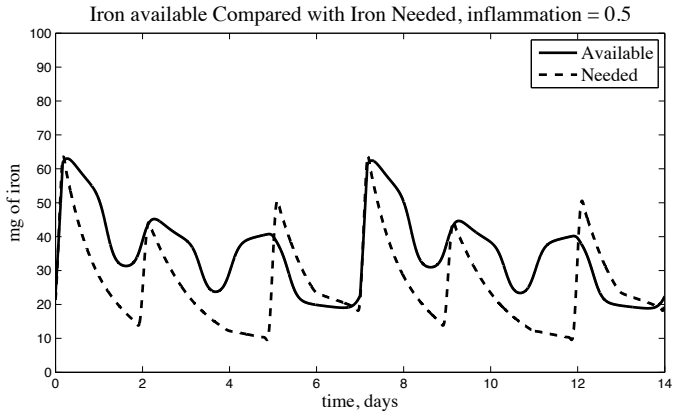

Figure 4.17: Fe_{needed} and Fe_{avail} : inflammation = 0.5, MWF treatment.

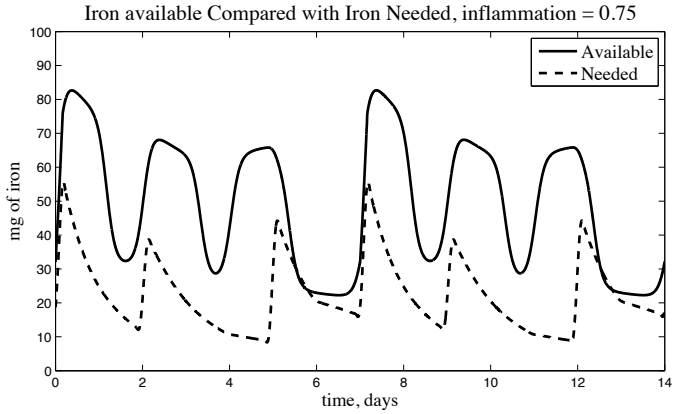

Figure 4.18: Fe_{needed} and Fe_{avail} : inflammation = 0.75, MWF treatment.

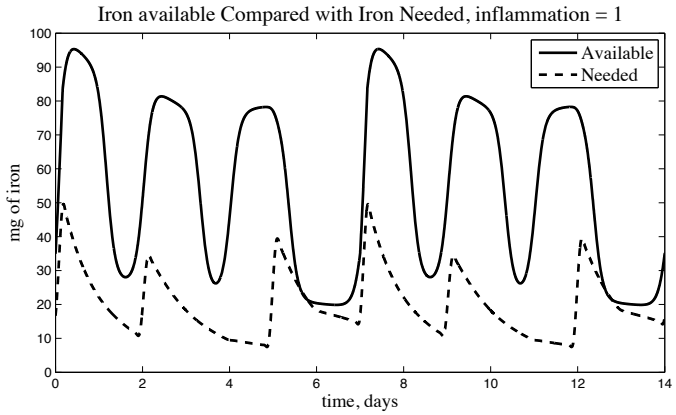

Figure 4.19: Fe_{needed} and Fe_{avail} : inflammation = 1, MWF treatment.

4.3 Summary

The model presented is capable of describing patients over a broad range of conditions, including various inflammation levels and treatment protocols. Parameter values were prescribed per the literature, when available, and numerical testing validates the use of our code in solving the model. Numerical results are presented, making note that the results are highly dependent on the initial conditions, which are estimated.

This model makes significant simplifications with regard to how iron is assimilated into red blood cells. As such, we continue our study by revisiting the model to determine a more biologically reasonable way to incorporate iron, which we do in Chapter 5, through the use of another structure variable which will account for the amount of iron in a cell.

This initial model is significant in that it addresses, for the first time, the roles inflammation and iron play in red blood cell dynamics, which are known to have a significant impact on red blood cell dynamics in patients with CKD. Results provide qualitative evidence to support a change in the administration of iron throughout a treatment protocol.

Chapter 5

Revisiting the Model

5.1 Introduction

We are motivated to revisit the model assumptions by a desire to incorporate iron into our model in a more biologically reasonable fashion. At moderate inflammation levels, iron-restricted erythropoiesis does occur, and our previous model may not be sufficient to capture the dynamics this behavior completely because we assumed that a cell acquired all of its iron at the moment it matured from class P to class M, rather than acquiring iron over time.

As such, we review the literature and revisit *all* of our model assumptions. We revise several aspects of the model, and begin by highlighting the ways in which the revised model differs from the previously used model. A complete description of the revised model follows in Section 5.2.

- *We divide the populations of cells into five compartments as opposed to three in the previous model.* Figure 5.1, a modification of a figure in [25], shows different aspects of the system we will model.

  This figure suggests five cell classes:

  - P_1 : early BFU-E
  - P_2 : late BFU-E, CFU-E, proerythroblasts, and early basophilic erythroblasts
  - P_3 : late basophilic erythroblasts and early polychromatic erythroblasts
  - P_4 : late polychromatic erythroblasts, orthochromatic erythroblasts, and non-circulating reticulocytes

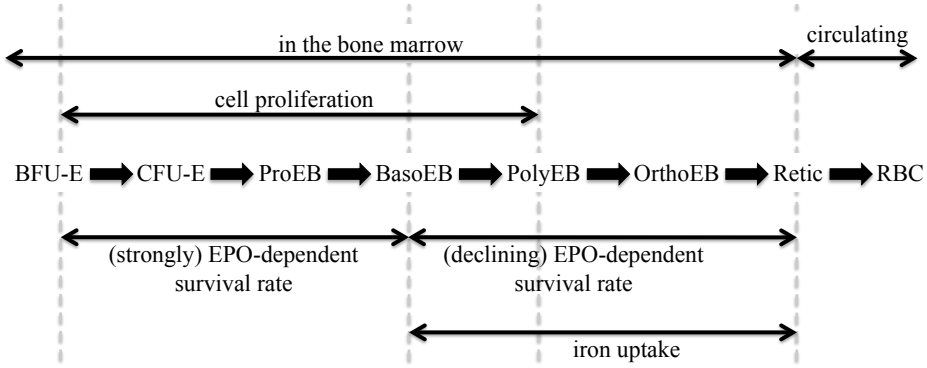

Figure 5.1: Stages of red blood cell production. We use the following short-hand notations: BFU-E = burst-forming unit–erythroid, CFU-E = colony-forming unit–erythroid, ProEB = proerythroblast, BasoEB = basophilic erythroblast, PolyEB = polychromatic erythroblast, OrthoEB = orthochromatic erythroblast, Retic = reticulocyte, RBC = red blood cell.

  - P_5 : mature erythrocytes and circulating reticulocytes

  We discuss each compartment individually in sections 5.2.1 through 5.2.5, but it should be noted that the original system chosen to name the erythroid cell progression was based on distinguishing characteristics when samples were taken, stained, and viewed through a microscope. It is not surprising that we choose our five classes of cells differently; we focus on the interactions with EPO and iron and the location of the cells (in the bone marrow or circulating).

- *EPO affects survival (and not necessarily proliferation) of RBC progenitors.* In the previous model, we assumed that a rise in EPO led to a increase in proliferation of precursor cells. In fact, research has shown that EPO is much more important for survival of the precursors [57, 44]. Even in healthy individuals, complete survival of progenitors would require an EPO level much higher than normal level; the normal production rate of RBCs represents survival of only a minority of progenitor cells [25].

- *We have incorporated the phenomenon known as neocytolysis.* In a healthy individual, an increase in blood oxygen level is detected by the kidneys, which in turn decrease production of EPO. Down-regulation of the RBC production is achieved by the increased death rate of RBC progenitors due to this decrease in EPO. However, it takes 18 to 21 days for cells to mature and be released into circulation, so this down-regulation has a long delay before it actually affects blood oxygen level. Additionally, down-regulation would only cause the circulating red cell mass to drop by about 1% per day [39].

  Neocytolysis been observed in astronauts entering space [3, 53] and in high altitude dwellers who descend to sea level [34, 41] who have higher aggregate RBC mass than needed. Their RBC mass was decreased by 10-15% in a few days, which could not be explained by simple down-regulation of RBC production.

  Neocytolysis, believed to be caused by a drop in EPO level, is a physiologic process that aids in this control of the red cell mass by causing the selective destruction of young circulating RBCs [39, 12]. Since these cells were circulating and contributing to blood oxygen level, their death has a much faster effect on blood oxygen level than the down-regulation of the production cycle. Neocytolysis has been determined to contribute to the anemia of renal disease [40, 4], as patients undergoing therapy have constantly fluctuating EPO levels.

- *We assume the role of inflammation in cellular iron uptake is independent of EPO level.* Inflammation alone can cause anemia (termed the anemia of chronic disease) [50, 24], but the specific mechanisms relating EPO and inflammation are not yet well-defined. Our model continues to remain vague with respect to inflammation, in that we are not tracking specific inflammation markers or trying to follow all of the pathways associated with inflammation. We know that inflammation disrupts iron metabolism [36, 55, 42], so we simply assume that as inflammation increases, availability of iron decreases (described in more detail later).

- *Cellular iron uptake occurs over time instead of at the moment a cell matures from one class into another.* In the previous model, we made the assumption that a RBC acquired all of its iron at the moment it transitioned from the bone marrow to the blood stream. This was never a biologically sound assumption, and was made only to simplify computations. We now assume that red blood cells uptake

iron gradually.

- *A cell's iron state affects its death rate.* We were unable to model this behavior in our previous model because we made the assumption that all members in class O contained the exact same amount of iron. Now that we are able to track the iron state, we can account for the fact that hypochromic RBCs (i.e., those that do not have a full complement of iron) have increased death rate [27].

5.2 The Model

We use a model with two structure variables, one for maturity level and one for cellular iron level. The inclusion of a structure variable for cellular iron level is what enables us to model the incorporation of iron in a more biologically reasonable fashion. The model is represented in Figure 5.2.

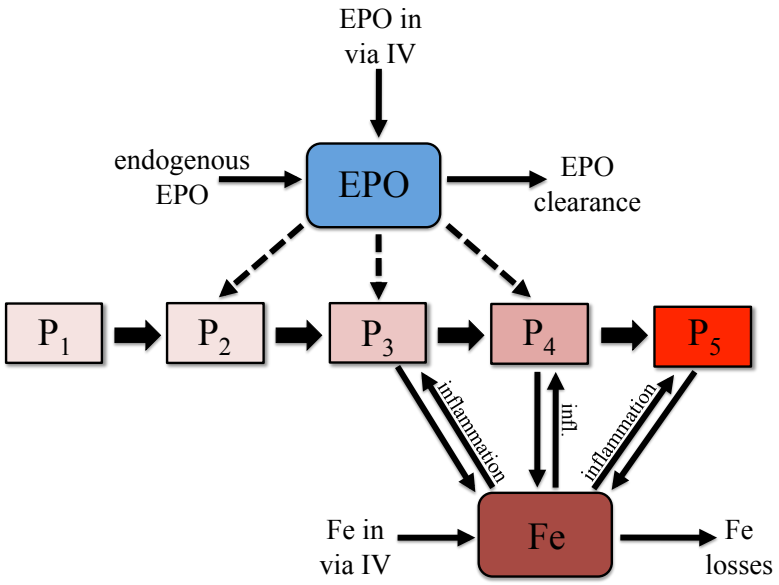

Figure 5.2: Model schematic. Note that the states variables are $P_1(t, \mu_1)$, $P_2(t, \mu_2)$, $P_3(t, \mu_3, \gamma)$, $P_4(t, \mu_4, \gamma)$, $P_5(t, \mu_5, \gamma)$, $EPO(t)$ and $Fe(t)$.

Throughout, we use β to represent birth/proliferation rate, δ to represent death rate, ρ to represent other rates (maturation rates, rates of treatment, etc.).

The structure variables μ_i and γ are unitless and represent the maturity level and iron state, respectively, of cells. Thus, $P_3(t^*, \mu_3^*, \gamma^*)$ is the number of cells (in billions) in population P_3 at time t^* that have maturity level μ^* and iron state γ^*. Each class is assumed to have a maximum maturity level, $(\mu_i)_f$.

We will assume that the iron state structure variable γ varies from 0 to γ_f, where $\gamma_{full} = \frac{\gamma_f}{3} = 1$ represents the amount of iron the "typical" RBC contains in a healthy individual (this quantity is to be estimated later). We will assume that when a cell divides, each daughter cell inherits half of the parent cell's iron. Therefore, when a cell with iron state γ^* divides, it leaves iron state γ^* and two cells enter iron state $\frac{\gamma^*}{2}$. Similarly, for each cell in iron class $2\gamma^*$ that divides, two cells enter iron class γ^*.

We derive equations for those classes that incorporate iron by considering, at some time t, an incremental area of size $\Delta\mu$ by $\Delta\gamma$, with $0 \leq \gamma \leq \frac{\gamma_f}{2}$, as in Figure 5.3.

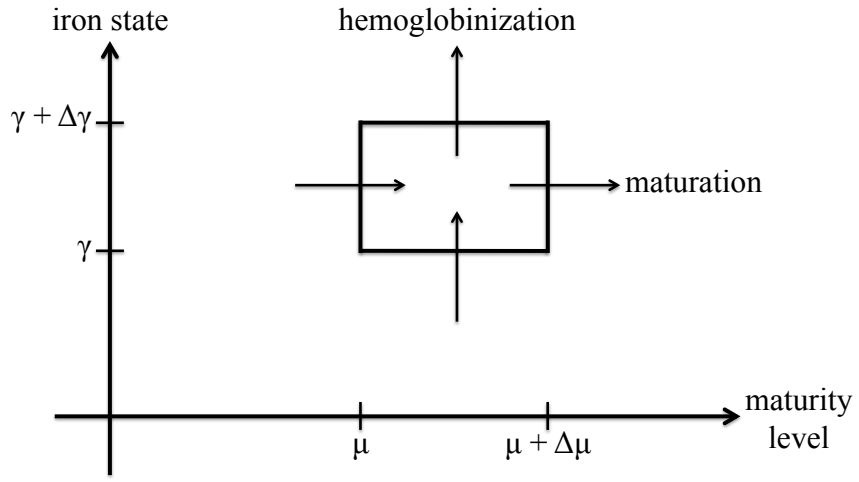

Figure 5.3

We think of this region as a compartment and consider the time rate of change of the cell population in the compartment.

$$\begin{aligned}\frac{\partial}{\partial t}\int_{\gamma}^{\gamma+\Delta\gamma}\int_{\mu}^{\mu+\Delta\mu} P(t,\xi,\zeta)d\xi d\zeta &= 2(\text{birth rate at iron state } 2\gamma) - (\text{birth rate at iron state } \gamma)\\ &\quad - (\text{death rate}) + (\text{rate of maturation in})\\ &\quad - (\text{rate of maturation out})\\ &\quad + (\text{rate of hemoglobinization in})\\ &\quad - (\text{rate of hemoglobinization out})\end{aligned}$$

$$\begin{aligned}&= 2\int_{\gamma}^{\gamma+\Delta\gamma}\int_{\mu}^{\mu+\Delta\mu} \beta P(t,\xi,2\zeta)d\xi d\zeta\\ &\quad - \int_{\gamma}^{\gamma+\Delta\gamma}\int_{\mu}^{\mu+\Delta\mu} \beta P(t,\xi,\zeta)d\xi d\zeta\\ &\quad - \int_{\gamma}^{\gamma+\Delta\gamma}\int_{\mu}^{\mu+\Delta\mu} \delta P(t,\xi,\zeta)d\xi d\zeta\\ &\quad + \int_{\gamma}^{\gamma+\Delta\gamma} \rho P(t,\mu,\zeta)d\zeta - \int_{\gamma}^{\gamma+\Delta\gamma} \rho P(t,\mu+\Delta\mu,\zeta)d\zeta\\ &\quad + \int_{\mu}^{\mu+\Delta\mu} hP(t,\xi,\gamma)d\xi - \int_{\mu}^{\mu+\Delta\mu} hP(t,\xi,\gamma+\Delta\gamma)d\xi,\end{aligned}$$

where $0 \le \mu \le \mu_f$, β is the proliferation rate, δ is the death rate, ρ is the maturation rate, and h is the hemoglobinization rate, equivalent to the rate of iron uptake.

We rearrange,

$$\begin{aligned}\frac{\partial}{\partial t}\int_{\gamma}^{\gamma+\Delta\gamma}\int_{\mu}^{\mu+\Delta\mu} P(t,\xi,\zeta)d\xi d\zeta &= 2\int_{\gamma}^{\gamma+\Delta\gamma}\int_{\mu}^{\mu+\Delta\mu} \beta P(t,\xi,2\zeta)d\xi d\zeta\\ &\quad - \int_{\gamma}^{\gamma+\Delta\gamma}\int_{\mu}^{\mu+\Delta\mu} [\beta+\delta]P(t,\xi,\zeta)d\xi d\zeta\\ &\quad - \int_{\gamma}^{\gamma+\Delta\gamma} \rho\left[P(t,\mu+\Delta\mu,\zeta) - P(t,\mu,\zeta)\right]d\zeta\\ &\quad - \int_{\mu}^{\mu+\Delta\mu} h\left[P(t,\xi,\gamma+\Delta\gamma) - P(t,\xi,\gamma)\right]d\xi,\end{aligned}$$

then divide by $\Delta\mu\Delta\gamma$:

$$\begin{aligned}\frac{\partial}{\partial t}\left[\frac{1}{\Delta\gamma}\int_{\gamma}^{\gamma+\Delta\gamma}\frac{1}{\Delta\mu}\int_{\mu}^{\mu+\Delta\mu}P(t,\xi,\zeta)d\xi d\zeta\right] &= \frac{2}{\Delta\gamma}\int_{\gamma}^{\gamma+\Delta\gamma}\frac{1}{\Delta\mu}\int_{\mu}^{\mu+\Delta\mu}\beta P(t,\xi,2\zeta)d\xi d\zeta \\ &\quad -\frac{1}{\Delta\gamma}\int_{\gamma}^{\gamma+\Delta\gamma}\frac{1}{\Delta\mu}\int_{\mu}^{\mu+\Delta\mu}[\beta+\delta]P(t,\xi,\zeta)d\xi d\zeta \\ &\quad -\frac{1}{\Delta\gamma}\int_{\gamma}^{\gamma+\Delta\gamma}\rho\frac{P(t,\mu+\Delta\mu,\zeta)-P(t,\mu,\zeta)}{\Delta\mu}d\zeta \\ &\quad -\frac{1}{\Delta\mu}\int_{\mu}^{\mu+\Delta\mu}h\frac{P(t,\xi,\gamma+\Delta\gamma)-P(t,\xi,\gamma)}{\Delta\gamma}d\xi.\end{aligned}$$

When we allow $\Delta\mu\to 0$ and $\Delta\gamma\to 0$, we obtain

$$\begin{aligned}\frac{\partial}{\partial t}P(t,\mu,\gamma) &= 2\beta P(t,\mu,2\gamma)-[\beta+\delta]P(t,\mu,\gamma)-\frac{\partial}{\partial\mu}\rho P(t,\mu,\gamma) \\ &\quad -\frac{\partial}{\partial\gamma}hP(t,\mu,\gamma), \qquad 0\le\gamma\le\frac{\gamma_f}{2}, \quad (5.1)\end{aligned}$$

the general form of the equations governing cells in classes P_3 through P_5. Note that the rates β, δ, ρ and h could be functions that depend on μ, γ or other states in the system.

By our assumptions, the maximum iron state is γ_f, so cell division cannot yield a cell with iron state $\gamma > \frac{\gamma_f}{2}$. Thus, for cells with iron states greater than $\frac{\gamma_f}{2}$, we omit the birth rate term associated with iron state 2γ, as below:

$$\frac{\partial}{\partial t}P(t,\mu,\gamma) = -[\beta+\delta]P(t,\mu,\gamma)-\frac{\partial}{\partial\mu}\rho P(t,\mu,\gamma)-\frac{\partial}{\partial\gamma}hP(t,\mu,\gamma), \qquad \frac{\gamma_f}{2}\le\gamma\le\gamma_f. \tag{5.2}$$

Cells in classes $P_1(t,\mu_1)$ and $P_2(t,\mu_2)$ do not incorporate iron, so they are functions of only time and maturity level. The general form of the partial differential equations governing these classes, derived in [6], is

$$\frac{\partial}{\partial t}P(t,\mu) = [\beta-\delta]P(t,\mu)-\frac{\partial}{\partial\mu}\rho P(t,\mu), \tag{5.3}$$

where β is the proliferation rate, δ is the death rate, and ρ is the maturation rate.

5.2.1 Class $P_1(t, \mu_1)$

Class P_1 consists of early BFU-E. These are the most immature cells that are committed to the erythroid lineage. We make the following assumptions about cells in this class.

1. The maturation rate is constant, ρ_1.

2. BFU-E differentiate into CFU-E in approximately seven days [46, 43]. BFU-E begin expressing EPO receptors (EPORs), which means that, in time, they do become influenced by EPO. Hence, we allow for cells to reside in class P_1 for three days (during which they are not influenced by EPO), while late BFU-E are in class P_2 (where they are under the influence of EPO). Therefore we choose the maximum maturity level to be $(\mu_1)_f = 3$.

3. The majority of cell proliferation happens in later classes [25, 26], so we set birth rate equal to death rate for cells in this class.

Hence, for class P_1, equation (5.3) becomes

$$\frac{\partial}{\partial t}P_1(t, \mu_1) = -\rho_1 \frac{\partial}{\partial \mu_1}P_1(t, \mu_1)$$

with initial condition

$$P_1(0, \mu_1) = P_1^{init}(\mu_1)$$

and boundary condition

$$P_1(t, 0) = P_1^{bdy}(t).$$

5.2.2 Class $P_2(t, \mu_2)$

Class P_2 consists of late BFU-E, CFU-E, proerythroblasts, and early basophilic erythroblasts. We make the following assumptions about cells in class P_2.

1. The maturation rate is constant, ρ_2.

2. Cells reside in this class for twelve days [18, 43], and therefore $(\mu_2)_f = 12$.

3. During the time cells reside in class P_2, they undergo approximately 6 cell divisions [25, 18, 19, 20]. We assume that the birth rate is a constant, β_2.

4. Cells in this class express EPORs [26, 45], and this interaction of EPO with EPOR is the most important control point for erythropoiesis [18]. Cells at this stage depend absolutely on EPO for their survival and will undergo apoptosis in its absence [46, 26]. Therefore we choose the death rate to be a decreasing function of the EPO level:

$$\delta_2(EPO) = \left(\delta_2^{max} - \delta_2^{min}\right) \cdot \frac{\left(c_{\delta_2}\right)^{k_{\delta_2}}}{\left(c_{\delta_2}\right)^{k_{\delta_2}} + \left(EPO\right)^{k_{\delta_2}}} + \delta_2^{min}.$$

Thus, using equation (5.3), the state equation for class P_2 is given by

$$\frac{\partial}{\partial t}P_2(t,\mu_2) = [\beta_2 - \delta_2(EPO)]P_2(t,\mu_2) - \rho_2\frac{\partial}{\partial \mu_2}P_2(t,\mu_2),$$

with initial condition

$$P_2(0,\mu_2) = P_2^{init}(\mu_2)$$

and boundary condition

$$P_2(t,0) = P_1\big(t,(\mu_1)_f\big).$$

5.2.3 Class $P_3(t,\mu_3,\gamma)$

Class P_3 consists of late basophilic erythroblasts and early polychromatic erythroblasts. We assume the following.

1. The maturation rate is constant, ρ_3.
2. Cells reside in this class for 1 day [18, 43], and therefore $(\mu_3)_f = 1$.
3. Cells in this stage continue to proliferate [18], with a constant rate β_3.
4. Cells in class P_3 continue to express EPORs, but the level of expression declines significantly as cells mature through this class [13]. Hence, cells in this class become less dependent on EPO for survival. We model this as

$$\delta_3(\mu_3, EPO) = \delta_3^{max}(\mu_3) \cdot \frac{\left(c_{\delta_3}\right)^{k_{\delta_3}}}{\left(c_{\delta_3}\right)^{k_{\delta_3}} + \left(EPO\right)^{k_{\delta_3}}}$$

where $\delta_3^{max}(\mu_3)$ is a decreasing function, which we assume to be linear for this model, as below:

$$\delta_3^{max}(\mu_3) = -m_3\mu_3 + b_3, \qquad m_3 > 0, \quad b_3 > m_3 \cdot (\mu_3)_f.$$

The function $\delta_3(\mu_3, EPO)$, for a fixed maturity level μ_3, is a decreasing sigmoid function of EPO. That is, at a fixed maturity level, as EPO increases, the death rate decreases. If we consider instead a fixed EPO level, then increasing maturation level causes a decrease in the maximum death rate. That is, low EPO affects younger cells in this class more than it affects more mature cells. Both the fixed maturity level and fixed EPO level phenomena are depicted in Figure 5.4.

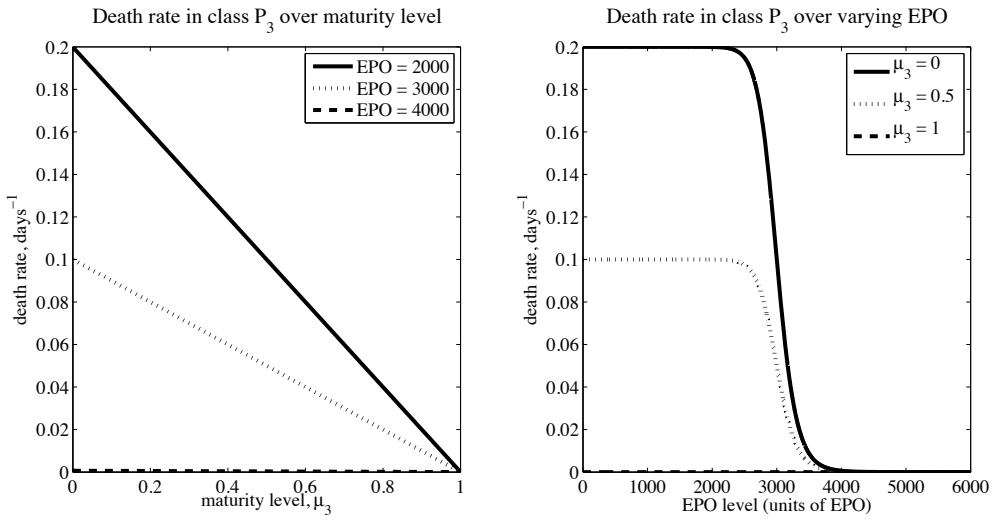

Figure 5.4: Death rate in class P_3 is a function of both maturity level, μ_3, and EPO level. For a fixed EPO level, death rate decreases as maturity level increases. For a fixed maturity level, death rate is larger when EPO is small. These plots were generated with parameter values $m_3 = 0.2$, $b_3 = 0.2$, $c_{\delta_3} = 3000$ and $k_{\delta_3} = 20$.

5. Cells in class P_3 express transferrin receptors (Tfr) and begin the process of taking in iron and synthesizing hemoglobin [25, 18]. The rate of hemoglobinization (or

equivalently iron uptake) is a function of iron level (in the iron compartment), inflammation level, and iron state (of a cell). A full description of the hemoglobinization rate, $h_3(Fe, I, \gamma)$, appears in Section 5.3.

Hence, for class P_3, equations (5.1) and (5.2) become

$$\frac{\partial}{\partial t}P_3(t,\mu_3,\gamma) = 2\beta_3 P_3(t,\mu_3,2\gamma) - [\beta_3 + \delta_3(\mu_3, EPO)]P_3(t,\mu_3,\gamma) - \rho_3\frac{\partial}{\partial \mu_3}P_3(t,\mu_3,\gamma) - \frac{\partial}{\partial \gamma}\Big[h_3(Fe,I,\gamma)P_3(t,\mu_3,\gamma)\Big], \qquad 0 \le \gamma \le \frac{\gamma_f}{2}$$

and

$$\frac{\partial}{\partial t}P_3(t,\mu_3,\gamma) = -[\beta_3 + \delta_3(\mu_3, EPO)]P_3(t,\mu_3,\gamma) - \rho_3\frac{\partial}{\partial \mu_3}P_3(t,\mu_3,\gamma) - \frac{\partial}{\partial \gamma}\Big[h_3(Fe,I,\gamma)P_3(t,\mu_3,\gamma)\Big], \qquad \frac{\gamma_f}{2} \le \gamma \le \gamma_f$$

with initial condition

$$P_3(0,\mu_3,\gamma) = P_3^{init}(\mu_3,\gamma)$$

and boundary conditions

$$P_3(t,0,\gamma) = \begin{cases} P_2\big(t,(\mu_2)_f\big), & \gamma = 0 \\ 0, & \gamma \neq 0 \end{cases}$$

and

$$P_3(t,\mu_3,0) = \begin{cases} P_2\big(t,(\mu_2)_f\big), & \mu_3 = 0 \\ P_3^{bdy,\gamma}(t,\mu_3), & \mu_3 \neq 0. \end{cases}$$

5.2.4 Class $P_4(t, \mu_4, \gamma)$

Class P_4 contains late polychromatic erythroblasts, orthochromatic erythroblasts, and non-circulating reticulocytes, the last stages of erythroid cells residing in the bone marrow. We make the following assumptions about cells in class P_4.

1. The maturation rate is constant, ρ_4.

2. Cells reside in this class for 2 days [18, 43], and therefore $(\mu_4)_f = 2$.

3. Cells in this class have stopped proliferating [25, 18]. Thus, $\beta_4 = 0$.

4. It is well-documented that red blood cells have a shorter life span in individuals with iron deficiency [54, 15, 14, 10]. Hence, we assume that cells at this stage that are severely iron deficient have increased mortality.

   We begin by defining $c_{\delta_4}(\mu_4)$ as an increasing function of μ_4. For simplicity, we choose a linear function:

   $$c_{\delta_4}(\mu_4) = m_4\mu_4 + b_4, \qquad m_4 > 0, \quad b_4 \geq 0,$$

   with the added restriction that $0 < c_{\delta_4}(\mu_4) < (\mu_4)_f$ for all μ_4.

   We assume now that if the cellular iron state is above a certain critical level, $0 < \gamma_{crit,4} < \frac{\gamma_f}{3}$, (say, for example, 80% of "typical" iron level for a heathy individual) then the death rate is small, say δ_4^{min}. If, however, the iron state is below the critical level, then the death rate depends on the iron state and the maturity level, as below:

   $$\delta_4(\mu_4, \gamma) = \begin{cases} \delta_4^{min}, & \gamma \geq \gamma_{crit,4} \\ \left(\delta_4^{max} - \delta_4^{min}\right) \cdot \dfrac{\left(c_{\delta_4}(\mu_4)\right)^{k_{\delta_4}}}{\left(c_{\delta_4}(\mu_4)\right)^{k_{\delta_4}} + \left(\gamma\right)^{k_{\delta_4}}} + \delta_4^{min}, & \gamma < \gamma_{crit,4}. \end{cases}$$

   Notice that when γ is relatively small, $\delta_4(\mu_4, \gamma)$ is close to δ_4^{max}, and when γ is relatively large, $\delta_4(\mu_4, \gamma)$ is close to δ_4^{min}. However, the "relativity" is affected by $c_{\delta_4}(\mu_4)$ when $\gamma < \gamma_{crit,4}$. As cells mature through class P_4 (i.e. as μ_4 increases), then $c_{\delta_4}(\mu_4)$ increases, which means that the death rate for a given iron level γ also increases (we choose $k_{\delta_4} > 1$). Hence, a cell having only a little iron when it arrives in class P_4 is less likely to die than a cell with that same level of iron that is about to mature out of class P_4. Figure 5.5 shows $\delta_4(\mu_4, \gamma)$ over varying μ_4 and γ.

5. These cells continue to collect iron and synthesize hemoglobin [25, 18] at a rate $h_4(Fe, I, \gamma)$, explained further in Section 5.3.

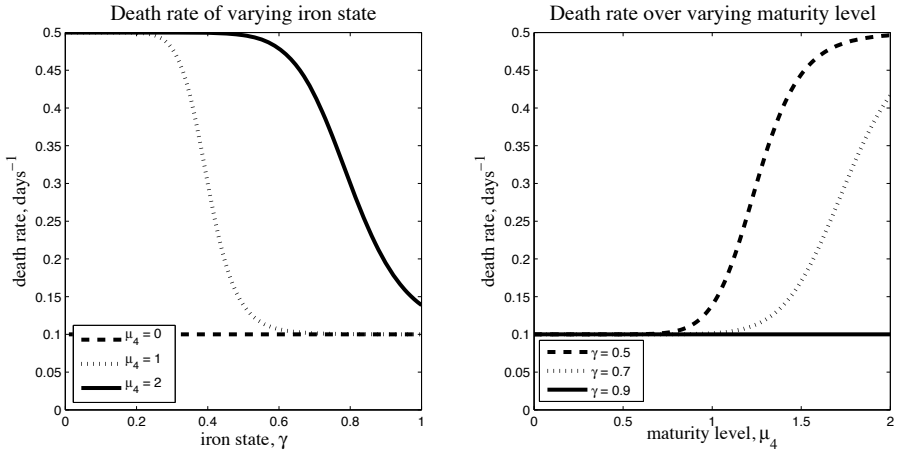

Figure 5.5: Death rate in class P_4 is a function of both maturity level, μ_4, and cellular iron state, γ. For a fixed maturity level μ_4, death rate decreases as iron state γ increases. That is, for a given maturity level, cells with little iron are more likely to die. For a iron state $\gamma < \gamma_{crit,4}$, death rate is increases as maturity level increases. These plots were generated with parameter values $\gamma_{crit,4} = 0.8$, $\delta_4^{min} = 0.1$, $\delta_4^{max} = 0.5$, $m_4 = 0.4$, and $b_4 = 0$.

Thus, using equation (5.1), the state equation is given by

$$\begin{aligned}\frac{\partial}{\partial t}P_4(t,\mu_4,\gamma) = & -\delta_4(\mu_4,\gamma)P_4(t,\mu_4,\gamma) - \rho_4\frac{\partial}{\partial \mu_4}P_4(t,\mu_4,\gamma) \\ & - \frac{\partial}{\partial \gamma}\Big[h_4(Fe,I,\gamma)P_4(t,\mu_4,\gamma)\Big],\end{aligned}$$

with initial condition

$$P_4(0,\mu_4,\gamma) = P_4^{init}(\mu_4,\gamma)$$

and boundary conditions

$$P_4(t,0,\gamma) = P_3\big(t,(\mu_3)_f,\gamma\big)$$

and

$$P_4(t,\mu_4,0) = \begin{cases} P_3\big(t,(\mu_3)_f,0\big), & \mu_4 = 0 \\ P_4^{bdy,\gamma}(t,\mu_4), & \mu_4 \neq 0. \end{cases}$$

5.2.5 Class $P_5(t, \mu_5, \gamma)$

Cells in class P_5 are mature erythrocytes and circulating reticulocytes. For cells in this class, we make the following assumptions.

1. The maturation rate is constant, ρ_5.

2. The average life span of a red blood cell in a patient with chronic kidney disease is about 70 days, significantly shorter than for healthy persons [51, 47, 29]. We set the maximum maturity level to be $(\mu_5)_f = 150$ days^{-1}, but the death rate is set such that practically no cells reach the maximum maturity level.

3. As they have no nuclei, cells in this stage do not proliferate [18], and therefore $\beta_5 = 0$.

4. Death rate in this class is assumed to have three components: death due to low cellular iron, death due to aging, and death due to neocytolysis.

   (a) *Death due to low cellular iron.* As in the previous class, cells that lack a full complement of iron have increased mortality. As in class P_4, we have

   $$c_{\delta_{5,\gamma}}(\mu_5) = m_5\mu_5 + b_5, \qquad m_5 > 0$$

   and

   $$\delta_{5,\gamma}(\mu_5, \gamma) = \begin{cases} \delta_{5,\gamma}^{min}, & \gamma \geq \gamma_{crit,5} \\ \left(\delta_{5,\gamma}^{max} - \delta_{5,\gamma}^{min}\right) \cdot \dfrac{\left(c_{\delta_{5,\gamma}}(\mu_5)\right)^{k_{\delta_{5,\gamma}}}}{\left(c_{\delta_{5,\gamma}}(\mu_5)\right)^{k_{\delta_{5,\gamma}}} + \left(\gamma\right)^{k_{\delta_{5,\gamma}}}} + \delta_{5,\gamma}^{min}, & \gamma < \gamma_{crit,5}. \end{cases}$$

   (b) *Death due to aging.* Senescent (aged) erythrocytes are enveloped and destroyed in the spleen [18], so death rate in this class is also a function of maturity level. This process occurs independent of cellular iron state.

   $$\delta_{5,\mu}(\mu_5) = \left(\delta_{\mu_5}^{max} - \delta_{\mu_5}^{min}\right) \cdot \frac{\left(c_{\delta_{\mu_5}}\right)^{k_{\delta_{\mu_5}}}}{\left(c_{\delta_{\mu_5}}\right)^{k_{\delta_{\mu_5}}} + \left(\mu_5\right)^{k_{\delta_{\mu_5}}}} + \delta_{\mu_5}^{min}$$

(c) *Death due to neocytolysis.* Neocytolysis targets RBCs between 14-21 days old (i.e., for maturity level $14 \leq \mu_5 \leq 21$) [3, 39]. These cells have increased death rate when EPO level drops, but the mechanisms are still not clear, and we don't know if the mechanisms are related to a large drop in EPO level (i.e., a large negative rate of change of EPO level) and/or simply a low EPO level. We account for both in this model, with tuning parameters α_1 and α_2 to account for the relative effects.

We begin with the assumption that neocytolysis is a response to low EPO level. We choose a decreasing sigmoid function for the maximum death rate:

$$\delta_{5,neo,1}^{max}(EPO) = \delta_{5,neo}^{max,1} \cdot \frac{\left(c_{\delta_5}^{neo}\right)^{k_{\delta_5}^{neo}}}{\left(c_{\delta_5}^{neo}\right)^{k_{\delta_5}^{neo}} + \left(EPO\right)^{k_{\delta_5}^{neo}}}.$$

Then the death rate is given by

$$\delta_{5,neo,1}(\mu_5, EPO) = \delta_{5,neo,1}^{max}(EPO)\left[\frac{1}{1+e^{-2k_{h,1}(\mu_5-15)}} - \frac{1}{1+e^{-2k_{h,1}(\mu_5-20)}}\right],$$

the sum of smoothed heaviside functions. Note that when $k_{h,1}$ is chosen large enough, the death rate is zero when $\mu_5 < 14$ and $\mu_5 > 21$. Also, for maturity levels $14 \leq \mu_5 \leq 21$, when EPO level is small, the maximum death rate is large. Figure 5.6 demonstrates the output of the death rate function $\delta_{5,neo,1}(\mu_5, EPO)$, for both the case of a fixed maturity level and varying EPO and the case of fixed EPO and varying maturity level.

For the assumption that neocytolysis is a response to large negative rate of change of EPO, we choose a decreasing function for the maximum death rate:

$$\delta_{5,neo,2}^{max}\left(\frac{d}{dt}EPO\right) = \begin{cases} \dfrac{-\delta_{5,neo}^{max,2}}{1+e^{-2k_{h,3}(\frac{d}{dt}EPO-\rho_{EPO,crit})}}, & \frac{d}{dt}EPO < 0 \\ 0, & \frac{d}{dt}EPO \geq 0. \end{cases}$$

(Note here that we do not use a sigmoid function (as we did for $\delta_{5,neo,1}^{max}(EPO)$) because the area of interest includes negative values of $\frac{d}{dt}EPO$.) The death

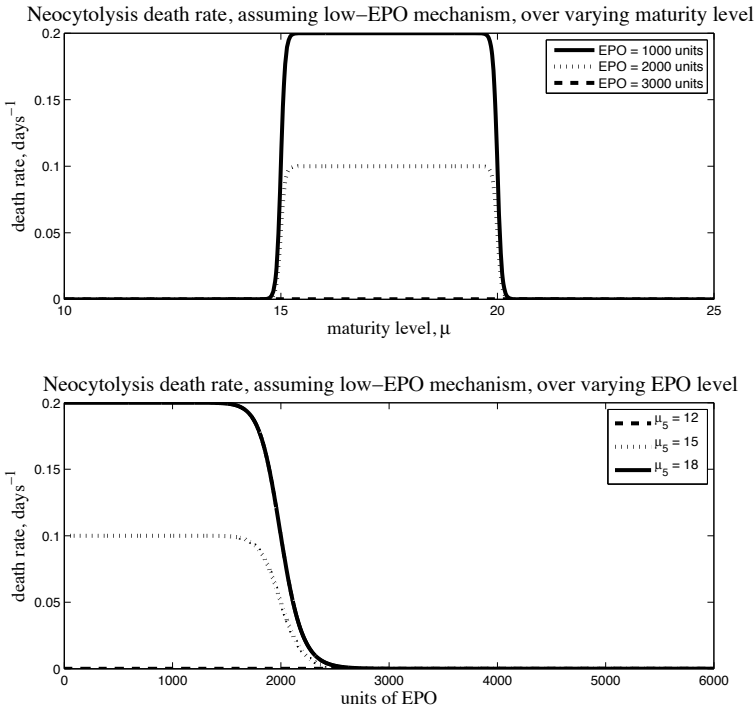

Figure 5.6: Low-EPO neocytolysis death rate in class P_5 is a function of maturity level μ_5 and EPO level. In the first plot, we fix EPO and show the death rate over varying maturity level. Notice that neocytolysis affects cells such that $14 \leq \mu_5 \leq 21$. Also, as EPO increases, the effects of neocytolysis diminish. This fact is demonstrated again in the second plot. To produce these plots, we chose parameter values $\delta_{5,neo}^{max,1} = 0.2$, $c_{\delta_5}^{neo} = 2000$, $k_{\delta_5}^{neo} = 20$ and $k_{h,1} = 10$.

rate, given by

$$\delta_{5,neo,2}\left(\mu_5, \frac{d}{dt}EPO\right) = \delta_{5,neo,2}^{max}\left(\frac{d}{dt}EPO\right)\left[\frac{1}{1+e^{-2k_{h,2}(\mu_5-15)}} - \frac{1}{1+e^{-2k_{h,2}(\mu_5-20)}}\right],$$

is plotted in Figure 5.7.

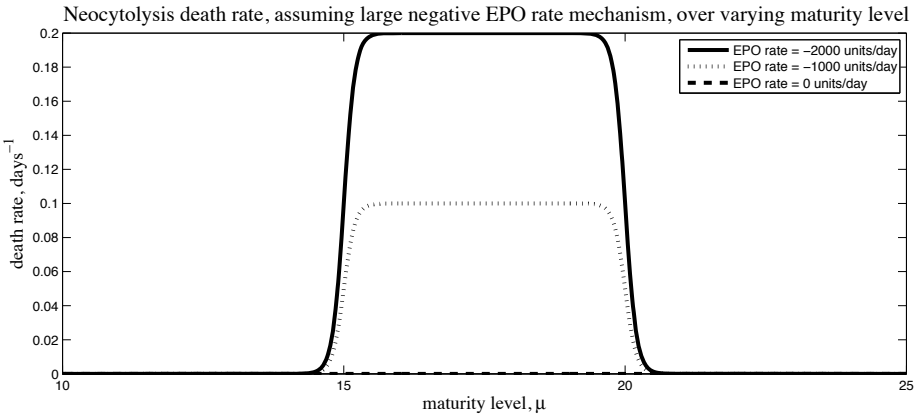

Figure 5.7: Large negative EPO rate neocytolysis death rate in class P_5 is a function of maturity level μ_5 and EPO rate. Note that neocytolysis targets cells with maturity level $14 \leq \mu_5 \leq 21$. As EPO rate attains large negative values, the death rate due to neocytolysis increases. To produce these plots, we chose parameter values $\delta_{5,neo}^{max,2} = 0.2$, $k_{h,3} = 0.5$, $\rho_{EPO,crit}$ and $k_{h,2} = 5$.

Then the death rate due to neocytolysis is given by

$$\delta_{5,neo}\left(\mu_5, EPO, \frac{d}{dt}EPO\right) = \alpha_1\delta_{5,neo,1}\left(\mu_5, EPO\right) + \alpha_2\delta_{5,neo,2}\left(\mu_5, \frac{d}{dt}EPO\right).$$

We assume that these phenomena occur independently and that the resultant death rate for class P_5 is the sum of these three components,

$$\delta_5\left(\mu_5, \gamma, EPO, \frac{d}{dt}EPO\right) = \delta_{5,\gamma}(\mu_5, \gamma) + \delta_{5,\mu}(\mu_5) + \delta_{5,neo}\left(\mu_5, EPO, \frac{d}{dt}EPO\right).$$

5. Only reticulocytes at this stage are still able to collect iron, and at a smaller rate than previous cell classes [18, 16, 9]. As before, the hemoglobinization rate, $h_5(Fe, I, \gamma)$, for cells in class P_5 is discussed in Section 5.3.

Using equation (5.1), cells in class P_5 are governed by the equation

$$\frac{\partial}{\partial t}P_5(t,\mu_5,\gamma) = -\delta_5\left(\mu_5,\gamma,EPO,\frac{d}{dt}EPO\right)P_5(t,\mu_5,\gamma) - \rho_5\frac{\partial}{\partial \mu_5}P_5(t,\mu_5,\gamma) - \frac{\partial}{\partial \gamma}\Big[h_5(Fe,I,\gamma)P_5(t,\mu_5,\gamma)\Big],$$

with initial condition

$$P_5(0,\mu_5,\gamma) = P_5^{init}(\mu_5,\gamma)$$

and boundary conditions

$$P_5(t,0,\gamma) = P_4\big(t,(\mu_4)_f,\gamma\big)$$

and

$$P_5(t,\mu_5,0) = \begin{cases} P_4\big(t,(\mu_4)_f,0\big), & \mu_5 = 0 \\ P_5^{bdy,\gamma}(t,\mu_5), & \mu_5 \neq 0. \end{cases}$$

5.2.6 EPO compartment

We use the same equation for EPO used previously in [6],

$$\frac{d}{dt}EPO(t) = \rho_{EPO,endog} + \rho_{EPO,exog}(t) - \frac{1}{t_{1/2}}\ln 2 EPO(t),$$

with initial condition

$$EPO(0) = E_0,$$

where $\rho_{EPO,endog}$ is the (assumed constant) rate of endogenous EPO production, $\rho_{EPO,exog}(t)$ is the rate of exogenous EPO provided during treatment, and $t_{1/2}$ is the half-life of EPO.

5.2.7 Iron compartment

For the iron compartment, we consider rates of iron entering and leaving the compartment as follows:

$$\begin{aligned}\frac{d}{dt}Fe(t) = &\text{(rate of exogenous iron from treatment)} - \text{(rate of iron losses)} \\ &- \text{(rate of iron entering classes } P_3,\ P_4 \text{ and } P_5) \\ &+ \text{(rate of iron ``recycled'' from classes } P_3,\ P_4 \text{ and } P_5)\end{aligned}$$

$$\begin{aligned}= \rho_{Fe,exog}(t) - \rho_{Fe,loss} - k_{Fe}\sum_{i=3}^{5}\int_0^{\gamma_f}\int_0^{(\mu_i)_f} h_i(Fe,I,\gamma)P_i(t,\mu_i,\gamma)d\mu_i d\gamma \\ + k_{Fe}\Bigg[\int_0^{\gamma_f}\int_0^{(\mu_3)_f}\delta_3 P_3(t,\mu_3,\gamma)d\mu_3 d\gamma \\ + \int_0^{\gamma_f}\int_0^{(\mu_4)_f}\delta_4(\mu_4,\gamma)P_4(t,\mu_4,\gamma)d\mu_4 d\gamma \\ + \int_0^{\gamma_f}\int_0^{(\mu_5)_f}\delta_5\left(\mu_5,\gamma,EPO,\frac{d}{dt}EPO\right)P_5(t,\mu_5,\gamma)d\mu_5 d\gamma\Bigg].\end{aligned}$$

Note that we have assumed that iron losses are constant. We also have initial condition

$$Fe(0) = Fe_0$$

5.2.8 Blood Volume and Hemoglobin Concentration

We model blood volume exactly as we did in [6].

As in our previous model, only cells that are circulating can contribute to hemoglobin concentration. For this model, only cells in class P_5 are circulating, so we have

$$Hb(t) = \frac{k_{Fe}\displaystyle\int_0^{\gamma_f}\int_0^{(\mu_5)_f}\gamma P_5(t,\mu_5,\gamma)d\mu_5 d\gamma}{BV(t)}.$$

5.3 Hemoglobization

Cells in classes P_3, P_4 and P_5 participate in iron uptake for the purposes of synthesizing hemoglobin. We use γ as a unitless structure variable that indicates the level of iron in a given cell. Recall that $0 \leq \gamma \leq \gamma_f$, where $\frac{\gamma_f}{3} = 1$ represents the amount of iron the "typical" RBC contains in a healthy individual. Recall also that when a cell divides, we assume that each of the daughter cells receives half of the parent cell's iron endowment.

In order to determine the rate of iron moving from the iron compartment and entering RBCs, we compare the rate of iron required for cells to be hemoglobinized at the maximum rate with the rate of iron available in the iron compartment (which is restricted by inflammation). Then we can determine if there is enough iron available to hemoglobinize at the maximum rate if hemoglobinization is occurring in an iron-restricted fashion.

We assume that the fastest a cell could obtain a full complement of hemoglobin is 3 days. A cell beginning hemoglobinization in class P_3 is undergoing cell division at a rate of 1 division per day. While we model hemoglobinization and proliferation as continuous processes, the following considerations in discrete time nodes indicate that the maximum rate of iron uptake for class P_3 should be set to $\frac{8}{7}\gamma_{full}$ days^{-1}.

$$\begin{aligned}
\text{day 0:} &\quad \gamma = 0 \\
\text{day 1 before cell division:} &\quad \gamma = \tfrac{8}{7}\gamma_{full} \\
\text{day 1 after cell division:} &\quad \gamma = \tfrac{4}{7}\gamma_{full} \\
\text{day 2 before cell division:} &\quad \gamma = \tfrac{4}{7}\gamma_{full} + \tfrac{8}{7}\gamma_{full} = \tfrac{12}{7}\gamma_{full} \\
\text{day 2 after cell division:} &\quad \gamma = \tfrac{6}{7}\gamma_{full} \\
\text{day 3 before cell division:} &\quad \gamma = \tfrac{6}{7}\gamma_{full} + \tfrac{8}{7}\gamma_{full} = 2\gamma_{full} \\
\text{day 3 after cell division:} &\quad \gamma = \gamma_{full}
\end{aligned}$$

Cells in class P_3 can uptake iron at this rate until their iron state is about $2\gamma_{full}$ (we allow for twice the normal iron state because cells in this class have the potential to divide). Cells in class P_4 can uptake iron at this rate until their iron state reaches γ_{full}, at which point they stop taking in iron. Reticulocytes in class P_5 (i.e., cells in class P_5 with maturity level $0 \leq \mu_5 \leq 2$) are circulating in the blood. While they are still capable of iron uptake until they reach iron state γ_{full}, the rate of uptake is smaller [18],

so we multiply the rate for class P_4 by the constant $0 < k_5 < 1$. Therefore we define the maximum iron uptake rate functions $h_3^{max}(\gamma)$, $h_4^{max}(\gamma)$, and $h_5^{max}(\gamma)$, pictured in Figure 5.8, as below.

$$h_3^{max}(\gamma) = \left(\frac{8}{7}\gamma_{full}\right) \cdot \frac{\left(2\gamma_{full}\right)^k_{h,3,max}}{\left(2\gamma_{full}\right)^k_{h,3,max} + \left(\gamma\right)^k_{h,3,max}}$$

$$h_4^{max}(\gamma) = \left(\frac{8}{7}\gamma_{full}\right) \cdot \frac{\left(\gamma_{full}\right)^k_{h,4,max}}{\left(\gamma_{full}\right)^k_{h,4,max} + \left(\gamma\right)^k_{h,4,max}}$$

$$h_5^{max}(\mu_5, \gamma) = \begin{cases} k_5 h_4^{max}(\gamma), & 0 \leq \mu_5 \leq 2 \\ 0, & \mu_5 > 2. \end{cases}$$

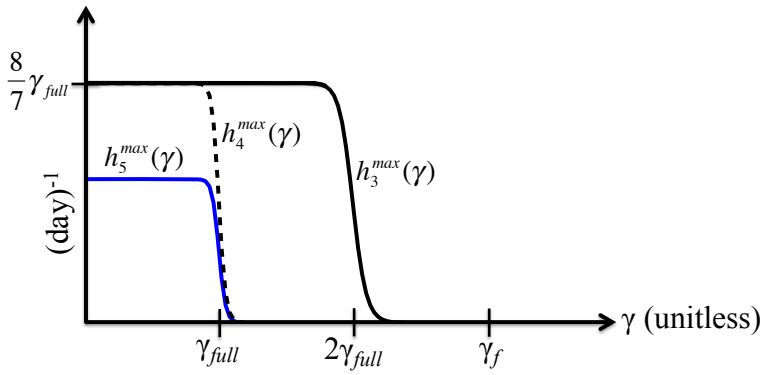

Figure 5.8: Maximum iron uptake rate.

Then the rate of iron needed for each cell to become hemoglobinized at its maximum rate is

$$\begin{aligned}\rho_{Fe,needed} &= (\text{max rate iron needed in class } P_3) + (\text{max rate iron needed in class } P_4) \\ &\quad + (\text{max rate iron needed in class } P_5)\end{aligned}$$

$$\begin{aligned}= k_{Fe}\Bigg[&\int_0^{\gamma_f}\int_0^{(\mu_3)_f} h_3^{max}(\gamma)P_3(t,\mu_3,\gamma)d\mu_3 d\gamma \\ &+ \int_0^{\gamma_f}\int_0^{(\mu_4)_f} h_4^{max}(\gamma)P_4(t,\mu_4,\gamma)d\mu_4 d\gamma \\ &+ \int_0^{\gamma_f}\int_0^{2} h_5^{max}(\mu_5,\gamma)P_5(t,\mu_5,\gamma)d\mu_5 d\gamma\Bigg].\end{aligned}$$

We compare this with the rate of iron available at time t, which depends on the inflammation level. We assume that as inflammation increases, the iron availability decreases, and define the function $0 \le f(I) \le 1$ as follows:

$$f(I) = \left(1 - f^{min}\right) \cdot \frac{(c_I)^{k_I}}{(c_I)^{k_I} + (I)^{k_I}} + f^{min}$$

Then the rate of iron availability is given by

$$\rho_{Fe,avail} = k_{Fe,eff} f(I) Fe(t),$$

where $0 < k_{Fe,eff} \le 1$ days^{-1} is a rate constant that indicates the maximum rate of iron available in the absence of inflammation.

We define the iron availability rate fraction, $0 < k_{Fe,avail} \le 1$, to be

$$k_{Fe,avail} = \begin{cases} 1, & \rho_{Fe,needed} \le \rho_{Fe,avail}, \\ \dfrac{\rho_{Fe,avail}}{\rho_{Fe,needed}}, & \rho_{Fe,needed} > \rho_{Fe,avail}. \end{cases}$$

Then the actual rates of iron uptake are given by

$$h_i(Fe, I, \gamma) = k_{Fe,avail} h_i^{max}(\gamma), \qquad i = 3, 4, 5.$$

5.4 Model Summary

We have the following system:

$$\frac{\partial}{\partial t}P_1(t,\mu_1) = -\rho_1\frac{\partial}{\partial \mu_1}P_1(t,\mu_1), \tag{5.4}$$

$$\frac{\partial}{\partial t}P_2(t,\mu_2) = [\beta_2 - \delta_2(EPO)]P_2(t,\mu_2) - \rho_2\frac{\partial}{\partial \mu_2}P_2(t,\mu_2), \tag{5.5}$$

$$\begin{aligned}\frac{\partial}{\partial t}P_3(t,\mu_3,\gamma) = {} & 2\beta_3 P_3(t,\mu_3,2\gamma) - [\beta_3 + \delta_3(\mu_3,EPO)]P_3(t,\mu_3,\gamma) - \rho_3\frac{\partial}{\partial \mu_3}P_3(t,\mu_3,\gamma) \\ & - \frac{\partial}{\partial \gamma}\left[h_3(Fe,I,\gamma)P_3(t,\mu_3,\gamma)\right], \qquad 0 \le \gamma \le \frac{\gamma_f}{2},\end{aligned} \tag{5.6}$$

$$\begin{aligned}\frac{\partial}{\partial t}P_3(t,\mu_3,\gamma) = {} & -[\beta_3 + \delta_3(\mu_3,EPO)]P_3(t,\mu_3,\gamma) - \rho_3\frac{\partial}{\partial \mu_3}P_3(t,\mu_3,\gamma) \\ & - \frac{\partial}{\partial \gamma}\left[h_3(Fe,I,\gamma)P_3(t,\mu_3,\gamma)\right], \qquad \frac{\gamma_f}{2} \le \gamma \le \gamma_f,\end{aligned} \tag{5.7}$$

$$\begin{aligned}\frac{\partial}{\partial t}P_4(t,\mu_4,\gamma) = {} & -\delta_4(\mu_4,\gamma)P_4(t,\mu_4,\gamma) - \rho_4\frac{\partial}{\partial \mu_4}P_4(t,\mu_4,\gamma) \\ & - \frac{\partial}{\partial \gamma}\left[h_4(Fe,I,\gamma)P_4(t,\mu_4,\gamma)\right],\end{aligned} \tag{5.8}$$

$$\frac{\partial}{\partial t}P_5(t,\mu_5,\gamma) = -\delta_5\left(\mu_5,\gamma,EPO,\frac{d}{dt}EPO\right)P_5(t,\mu_5,\gamma) - \rho_5\frac{\partial}{\partial \mu_5}P_5(t,\mu_5,\gamma) \tag{5.9}$$

$$- \frac{\partial}{\partial \gamma}\left[h_5(Fe,I,\gamma)P_5(t,\mu_5,\gamma)\right], \tag{5.10}$$

$$\frac{d}{dt}EPO(t) = \rho_{EPO,endog} + \rho_{EPO,exog}(t) - \frac{1}{t_{1/2}}\ln 2 EPO(t), \tag{5.11}$$

$$\begin{aligned}\frac{d}{dt}Fe(t) = {} & \rho_{Fe,exog}(t) - \rho_{Fe,loss} - k_{Fe}\sum_{i=3}^{5}\int_0^{\gamma_f}\int_0^{(\mu_i)_f} h_i(Fe,I,\gamma)P_i(t,\mu_i,\gamma)d\mu_i d\gamma \\ & + k_{Fe}\Bigg[\int_0^{\gamma_f}\int_0^{(\mu_3)_f}\delta_3 P_3(t,\mu_3,\gamma)d\mu_3 d\gamma \\ & \quad + \int_0^{\gamma_f}\int_0^{(\mu_4)_f}\delta_4(\mu_4,\gamma)P_4(t,\mu_4,\gamma)d\mu_4 d\gamma \\ & \quad + \int_0^{\gamma_f}\int_0^{(\mu_5)_f}\delta_5\left(\mu_5,\gamma,EPO,\frac{d}{dt}EPO\right)P_5(t,\mu_5,\gamma)d\mu_5 d\gamma\Bigg],\end{aligned} \tag{5.12}$$

with initial conditions

$$P_1(0,\mu_1) = P_1^{init}(\mu_1), \tag{5.13}$$
$$P_2(0,\mu_2) = P_2^{init}(\mu_2), \tag{5.14}$$
$$P_3(0,\mu_3,\gamma) = P_3^{init}(\mu_3,\gamma), \tag{5.15}$$
$$P_4(0,\mu_4,\gamma) = P_4^{init}(\mu_4,\gamma), \tag{5.16}$$
$$P_5(0,\mu_5,\gamma) = P_5^{init}(\mu_5,\gamma), \tag{5.17}$$
$$EPO(0) = E_0, \tag{5.18}$$
$$Fe(0) = Fe_0, \tag{5.19}$$

and boundary conditions

$$P_1(t,0) = P_1^{bdy}(t), \tag{5.20}$$
$$P_2(t,0) = P_1\big(t,(\mu_1)_f\big), \tag{5.21}$$
$$P_3(t,0,\gamma) = \begin{cases} P_2\big(t,(\mu_2)_f\big), & \gamma = 0, \\ 0, & \gamma \neq 0, \end{cases} \tag{5.22}$$
$$P_3(t,\mu_3,0) = \begin{cases} P_2\big(t,(\mu_2)_f\big), & \mu_3 = 0, \\ P_3^{bdy,\gamma}(t,\mu_3), & \mu_3 \neq 0, \end{cases} \tag{5.23}$$
$$P_4(t,0,\gamma) = P_3\big(t,(\mu_3)_f,\gamma\big) \tag{5.24}$$
$$P_4(t,\mu_4,0) = \begin{cases} P_3\big(t,(\mu_3)_f,0\big), & \mu_4 = 0, \\ P_4^{bdy,\gamma}(t,\mu_4), & \mu_4 \neq 0, \end{cases} \tag{5.25}$$
$$P_5(t,0,\gamma) = P_4\big(t,(\mu_4)_f,\gamma\big), \tag{5.26}$$
$$P_5(t,\mu_5,0) = \begin{cases} P_4\big(t,(\mu_4)_f,0\big), & \mu_5 = 0, \\ P_5^{bdy,\gamma}(t,\mu_5), & \mu_5 \neq 0. \end{cases} \tag{5.27}$$

We also have the following auxiliary equations:

$$\delta_2(EPO) = \Big(\delta_2^{max} - \delta_2^{min}\Big) \cdot \frac{\Big(c_{\delta_2}\Big)^{k_{\delta_2}}}{\Big(c_{\delta_2}\Big)^{k_{\delta_2}} + \Big(EPO\Big)^{k_{\delta_2}}} + \delta_2^{min} \tag{5.28}$$

$$\delta_3^{max}(\mu_3) = -m_3\mu_3 + b_3, \qquad m_3 > 0, \quad b_3 > m_3 \cdot (\mu_3)_f \tag{5.29}$$

$$\delta_3(\mu_3, EPO) = \delta_3^{max}(\mu_3) \cdot \frac{\Big(c_{\delta_3}\Big)^{k_{\delta_3}}}{\Big(c_{\delta_3}\Big)^{k_{\delta_3}} + \Big(EPO\Big)^{k_{\delta_3}}} \tag{5.30}$$

$$c_{\delta_4}(\mu_4) = m_4\mu_4 + b_4, \qquad m_4 > 0, \quad b_4 \geq 0, \tag{5.31}$$

$$\delta_4(\mu_4, \gamma) = \begin{cases} \delta_4^{min}, & \gamma \geq \gamma_{crit,4} \\ \Big(\delta_4^{max} - \delta_4^{min}\Big) \cdot \dfrac{\Big(c_{\delta_4}(\mu_4)\Big)^{k_{\delta_4}}}{\Big(c_{\delta_4}(\mu_4)\Big)^{k_{\delta_4}} + \big(\gamma\big)^{k_{\delta_4}}} + \delta_4^{min}, & \gamma < \gamma_{crit,4}. \end{cases} \tag{5.32}$$

$$c_{\delta_{5,\gamma}}(\mu_5) = m_5\mu_5 + b_5, \qquad m_5 > 0 \tag{5.33}$$

$$\delta_{5,\gamma}(\mu_5, \gamma) = \begin{cases} \delta_{5,\gamma}^{min}, & \gamma \geq \gamma_{crit,5} \\ \Big(\delta_{5,\gamma}^{max} - \delta_{5,\gamma}^{min}\Big) \cdot \dfrac{\Big(c_{\delta_{5,\gamma}}(\mu_5)\Big)^{k_{\delta_{5,\gamma}}}}{\Big(c_{\delta_{5,\gamma}}(\mu_5)\Big)^{k_{\delta_{5,\gamma}}} + \big(\gamma\big)^{k_{\delta_{5,\gamma}}}} + \delta_{5,\gamma}^{min}, & \gamma < \gamma_{crit,5} \end{cases} \tag{5.34}$$

$$\delta_{5,\mu}(\mu_5) = \Big(\delta_{\mu_5}^{max} - \delta_{\mu_5}^{min}\Big) \cdot \frac{\Big(c_{\delta_{\mu_5}}\Big)^{k_{\delta_{\mu_5}}}}{\Big(c_{\delta_{\mu_5}}\Big)^{k_{\delta_{\mu_5}}} + \big(\mu_5\big)^{k_{\delta_{\mu_5}}}} + \delta_{\mu_5}^{min} \tag{5.35}$$

$$\delta_{5,neo,1}^{max}(EPO) = \delta_{5,neo}^{max,1} \cdot \frac{\big(c_{\delta_5}^{neo}\big)^{k_{\delta_5}^{neo}}}{\big(c_{\delta_5}^{neo}\big)^{k_{\delta_5}^{neo}} + \big(EPO\big)^{k_{\delta_5}^{neo}}} \tag{5.36}$$

$$\delta_{5,neo,1}(\mu_5, EPO) = \delta_{5,neo,1}^{max}(EPO) \left[\frac{1}{1 + e^{-2k_{h,1}(\mu_5 - 15)}} - \frac{1}{1 + e^{-2k_{h,1}(\mu_5 - 20)}}\right] \tag{5.37}$$

$$\delta_{5,neo,2}^{max}\left(\frac{d}{dt}EPO\right)=\begin{cases}\frac{-\delta_{5,neo}^{max,2}}{1+e^{-2k_{h,3}(\frac{d}{dt}EPO-\rho_{EPO,crit})}}, & \frac{d}{dt}EPO<0\\ 0, & \frac{d}{dt}EPO\geq 0.\end{cases} \tag{5.38}$$

$$\delta_{5,neo,2}\left(\mu_5,\frac{d}{dt}EPO\right)=\delta_{5,neo,2}^{max}\left(\frac{d}{dt}EPO\right)\left[\frac{1}{1+e^{-2k_{h,2}(\mu_5-15)}}-\frac{1}{1+e^{-2k_{h,2}(\mu_5-20)}}\right] \tag{5.39}$$

$$\delta_{5,neo}\left(\mu_5,EPO,\frac{d}{dt}EPO\right)=\alpha_1\delta_{5,neo,1}\left(\mu_5,EPO\right)+\alpha_2\delta_{5,neo,2}\left(\mu_5,\frac{d}{dt}EPO\right) \tag{5.40}$$

$$\delta_5\left(\mu_5,\gamma,EPO,\frac{d}{dt}EPO\right)=\delta_{5,\gamma}(\mu_5,\gamma)+\delta_{5,\mu}(\mu_5)+\delta_{5,neo}\left(\mu_5,EPO,\frac{d}{dt}EPO\right) \tag{5.41}$$

$$Hb(t)=\frac{k_{Fe}\int_0^{\gamma_f}\int_0^{(\mu_5)_f}\gamma P_5(t,\mu_5,\gamma)d\mu_5 d\gamma}{BV(t)} \tag{5.42}$$

$$h_3^{max}(\gamma)=\left(\frac{8}{7}\gamma_{full}\right)\cdot\frac{\left(2\gamma_{full}\right)_{h,3,max}^{k}}{\left(2\gamma_{full}\right)_{h,3,max}^{k}+\left(\gamma\right)_{h,3,max}^{k}} \tag{5.43}$$

$$h_4^{max}(\gamma)=\left(\frac{8}{7}\gamma_{full}\right)\cdot\frac{\left(\gamma_{full}\right)_{h,4,max}^{k}}{\left(\gamma_{full}\right)_{h,4,max}^{k}+\left(\gamma\right)_{h,4,max}^{k}} \tag{5.44}$$

$$h_5^{max}(\mu_5,\gamma)=\begin{cases}k_5h_4^{max}(\gamma), & 0\leq\mu_5\leq 2\\ 0, & \mu_5>2.\end{cases} \tag{5.45}$$

$$\rho_{Fe,needed} = k_{Fe}\Bigg[\int_0^{\gamma_f}\int_0^{(\mu_3)_f} h_3^{max}(\gamma)P_3(t,\mu_3,\gamma)d\mu_3 d\gamma + \int_0^{\gamma_f}\int_0^{(\mu_4)_f} h_4^{max}(\gamma)P_4(t,\mu_4,\gamma)d\mu_4 d\gamma + \int_0^{\gamma_f}\int_0^{2} h_5^{max}(\mu_5,\gamma)P_5(t,\mu_5,\gamma)d\mu_5 d\gamma\Bigg] \tag{5.46}$$

$$f(I) = \left(1 - f^{min}\right)\cdot\frac{(c_I)^{k_I}}{(c_I)^{k_I} + (I)^{k_I}} + f^{min} \tag{5.47}$$

$$\rho_{Fe,avail} = k_{Fe,eff} f(I) Fe(t) \tag{5.48}$$

$$k_{Fe,avail} = \begin{cases} 1, & \rho_{Fe,needed} \leq \rho_{Fe,avail}, \\ \dfrac{\rho_{Fe,avail}}{\rho_{Fe,needed}}, & \rho_{Fe,needed} > \rho_{Fe,avail}. \end{cases} \tag{5.49}$$

$$h_i(Fe,I,\gamma) = k_{Fe,avail} h_i^{max}(\gamma), \qquad i = 3,4,5. \tag{5.50}$$

Chapter 6

Conclusions and Future Work

6.1 Conclusions

We developed an initial mathematical model for red blood cell dynamics in patients with CKD undergoing hemodialysis, including the assumptions made. We discussed the numerical implementation of the model, including the need to add upwinding to our finite element scheme. We also demonstrated the validity of our code using a forcing function strategy that shows the numerical solution converging to a pre-determined exact solution.

We then presented numerical solutions. We observed the dynamics of our model various treatment protocols and inflammation levels, and made comparisons among various inflammation levels. We discussed the solutions qualitatively and what implications they might have for practitioners determining patient treatment protocol.

Finally, we introduced an improved but more complicated mathematical model. We revisited all model assumptions and made significant changes to the original model. Most importantly, with the inclusion of a second structure variable, we are able to account for uptake of iron by cells over time (instead of at one instant in time, as the previous model did) and track cellular iron level over time. Additionally, we incorporate the phenomenon of neocytolysis, which has been shown to affect patients with CKD. This model is more in line with the known understanding of the biology of the problem, but this poses a more difficult numerical implementation. Future work will determine if the increased effort required to compute solutions of the revised model yields results which provide increased understanding of the dynamics.

6.2 Numerical Implementation of the Revised Model

We intend continue using a finite element approach to implement the revised model numerically. In our initial model, we approximated a partial differential equation with N ordinary differential equations, where N is the number of elements. That is, N determines how coarse the numerical solution is. Increasing N produces a finer approximation, but also increases computation time.

However, classes P_3 through P_5 have *two* structure variables, μ for age-structuring and γ for cellular iron content. Hence we will assume a solution of the form

$$P(t, \mu, \gamma) = \sum_{i=1}^{N} \sum_{j=1}^{M} a_{ij}(t)\phi_i(\mu)\tilde{\phi}_j(\gamma).$$

As a result, we must replace this partial differential equation by N *times* M ordinary differential equations.

Additionally, our previous formulation led to a tridiagonal coefficient matrix for efficient computation. The addition of the second structure variable will, unfortunately, disrupt this structure somewhat in that the resultant coefficient matrix will be block tridiagonal.

Hence, implementing the revised model will dramatically increase run-time, which is already a concern (see Section 6.5).

6.3 Iron Homeostasis

One of the main advances of this work as that incorporates the role of iron in erythropoiesis. As erythrocytes are little more than containers for hemoglobin (and, thus, iron), previous models that did not account for iron made the implicit assumption that iron availability was never an issue. That is, they assumed that iron-restricted erythropoiesis never occurred.

We know that iron-restricted erythropoiesis does occur in patients with CKD, and even our initial model demonstrates this (see Section 4.2). The revised model provides allows for improved incorporation of iron from the iron compartment into erythrocytes.

However, neither of our models attempts to portray the many aspects of iron homeostasis. That is, we provide an extremely simplistic version of the iron compartment.

Iron homeostasis is influenced by many hormones and is still not well understood. In fact, hepcidin, the major regulating hormone in homeostasis, was not widely recognized as such until relatively recently. The body of literature describing the action and interactions of hepcidin is therefore small but growing.

The utility of our models to practitioners as more than a qualitative tool for understanding dynamics depends intimately on the ability to accurately gauge iron availability. Therefore, a model for iron homeostasis with a more dynamic iron compartment, is likely a necessary component.

6.4 Inflammation

In both our initial and our revised models, we simply assign a number between zero and one to describe inflammation level.

Inflammation is a broad term for an entire host of responses with a vast array of causes. There are literally hundreds of hormones involved in an inflammatory response, and their interactions are nontrivial. We decided early on in the modeling process to focus our attention on other aspects of the model, and therefore to make broad simplifications with regard to inflammation.

Improvements can certainly be made in this area by determining which hormones have the most impact on red blood cell dynamics. The literature in this area is not explicit. It is clear that inflammation affects hepcidin production (and therefore iron availability), but the mechanisms and specific hormone pathways are not yet clear. Also, many hormones associated with inflammation are known to affect EPO production. An increased understanding of inflammation can contribute positively to multiple aspects of our model.

6.5 Optimization

The goal of future optimization efforts would be to keep hemoglobin within an acceptable band (11 to 13 g/dL) while keeping iron level (specifically, iron not being carried by RBCs) below a toxic level by providing treatment with EPO and iron.

This is a broad goal, but one could begin efforts in this direction by assuming a treatment schedule. (For the purposes of this discussion, we use the initial model.) For

example, if we assume that a patient will come to treatment on a MWF schedule, then we can define E_M, E_W and E_F to be the amount of EPO administered on Monday, Wednesday and Friday, respectively. We define Fe_M, Fe_W and Fe_F similarly. One example of a possible cost function j is

$$J(t_f) = \alpha_1 \int_0^{t_f} |Hb(t) - 12| dt + \alpha_2 (E_M + E_W + E_F) + \alpha_3 \int_0^{t_f} Fe(t) dt.$$

This cost functional is small when (i) hemoglobin level is close to 12 g/dL from $t = 0$ to $t = t_f$, (ii) the amount of EPO administered is small, and (iii) the amount of iron (other than that being carried in RBCs) is small. The constants α_i can be used to weight the components of the cost function depending on which goals are most important.

Early efforts in this area quickly demonstrated the difficulties in computing an optimal treatment protocol, with the first difficulty being the 30 minute forward simulation run time. Also, there is a wide range over which to search. For example, EPO treatment can be as much as 30000 units of EPO per treatment (recall that we used 5000 units per treatment during in our previous simulations). Perhaps the biggest impediment to optimization efforts is the fact that, based on our simulations, blood volume seems to drive the hemoglobin concentration much more than EPO and iron administration.

6.6 Parameter Estimation

Our model currently provides mainly qualitative understanding of red blood cell dynamics. With data, we could hope to contribute quantitative understanding as well.

Both models have many more parameters than state equations, so we would not expect to be able to identify all of the parameters. A sensitivity analysis could be conducted to determine which parameters are most identifiable. The remaining parameters could be estimated using the entire data set. Finally, we would consider a patient's prior data to estimate the patient-specific set of identifiable parameters.

This would not be an easy task in practice. Running the entire forward simulation for the initial model has a run time of approximately 30 minutes, so the inverse problem could be expected to take much longer.

Assuming that we did successfully estimate the identifiable parameters, we could potentially compute a patient-specific optimal course of treatment (see Section 6.5).

REFERENCES

[1] A. Ackleh, K. Deng, K. Ito, and J. Thibodeaux. A structured erythropoiesis model with nonlinear cell maturation velocity and hormone decay rate. *Mathematical Biosciences*, 204(1):21 – 48, 2006.

[2] Suhail Ahmad. *Manual of Clinical Dialysis, Second Edition*. Springer Science + Business Media, LLC, New York, 2009.

[3] Calrence P. Alfrey, Mark M. Udden, Carolyn Leach-Huntoon, Theda Driscoll, and Mark H. Pickett. Control of red blood cell mass in spaceflight. *Journal of Applied Physiology*, 81:98–104, 1996.

[4] Clarence P. Alfrey and Stephen Fishbane. Implications of neocytolysis for optimal management of anemia in chronic kidney disease. *Nephron Clinical Practice*, 106:c149–c156, 2007.

[5] Nancy C. Andrews and Paul J. Schmidt. Iron homeostasis. *Annual Review of Physiology*, 69:69–85, 2007.

[6] H. T. Banks, Karen M. Bliss, Peter Kotanko, and Hien Tran. A computational model of red blood cell dynamics in patients with chronic kidney disease. *Center for Research in Scientific Computation at North Carolina State University*, TR11-03, 2011.

[7] H. T. Banks, C. Cole, P. Schlosser, and H. T. Tran. Modeling and optimal regulation of erythropoiesis subject to benzene intoxication. *Mathematical Biosciences and Engineering*, 1(1):15–48, June 2004.

[8] J. Belair, M. Mackey, and J. Mahaffy. Age-structured and two-delay models for erythropoiesis. *Mathematical Biosciences*, 128(1-2):317 – 346, 1995.

[9] Francesco M. Van Bockxmeer and Evan H. Morgan. Transferrin receptors during rabbit reticulocyte maturation. *Biochemica et Biophysica Acta*, 584:76–83, 1979.

[10] Robert T. Card and Lewis R. Weintraub. Metabolic abnormalities of erythrocytes in severe iron deficiency. *Blood*, 37:725–732, 1971.

[11] Graham F. Carey and J. Tinsley Oden. *Finite Elements, Computational Aspects, Volume III*. Prentice Hall, Inc., 1984.

[12] Chung-Che Chang, Yayan Chen, Kapil Modi, Omar Awar, Clarence P. Alfrey, and Lawrence Rice. Changes of red blood cell surface markers in a blood doping model of neocytolysis. *Journal of Investigative Medicine*, 57(5):650–654, 2009.

[13] Stefan N. Constantinescu. Mechanism of erythropoietin receptor activation. In S. G. Elliot, M. A. Foote, and G. Molineaux, editors, *Erythropoietins, Erythropoietic Factors and Erythropoiesis*, pages 175–196. Birkhauser Verlag/Switzerland, 2009.

[14] Maria Diez-Ewald and Miguel Layrisse. Mechanisms of hemolysis in iron deficiency anemia. further studies. *Blood*, 32:884–894, 1968.

[15] Z. Farid, J. H. Nichols, S. Bassily, and A. R. Schulert. Blood loss in pure *Ancylostoma Duodenale* infection in egyptian farmers. *American Journal of Tropical Medicine and Hygiene*, 14:375–378, 1965.

[16] Janet L. Frazier, Jennifer H. Caskey, Mark Yoffe, and Paul A. Seligman. Studies of the transferrin receptor on both human reticulocytes and nucleated human cells in culture. *Journal of Clinical Investigation*, 69:853–865, 1982.

[17] Tomas Ganz. Iron homeostasis: Fitting the puzzle pieces together. *Cell Metabolism*, 7(4):288 – 290, 2008.

[18] John P. Greer, John Foerster, George M. Rodgers, Frixos Paraskevas, Bertil Glader, Daniel A. Arber, and Jr. Robert T. Means. *Wintrobe's Clinical Hematology*. Lippincott Williams and Wilkins, 12 edition, 2009.

[19] Connie J. Gregory and Allen C. Eaves. Human marrow cells capable of erythropoietic differentiation in vitro: definition of three erythroid colony responses. *Blood*, 49:855–864, 1977.

[20] Connie J. Gregory and Allen C. Eaves. Three stages of erythropoietic progenitor cell differentiation distinguished by a number of physical and biologic properties. *Blood*, 51:527–537, 1978.

[21] John M. Higgins and L. Mahadevan. Physiological and pathological population dynamics of circulating human red blood cells. *Proceedings of the National Academy of Sciences of the United States of America*, 107(47):2058720592, 2010.

[22] L. Israels and E. Israels. Erythropoiesis: an overview. In *Erythropoietins and Erythropoiesis: Molecular, Cellular, Preclinical and Clinical Biology*. Birkhäuser Verlag, 2003.

[23] W. Jelkmann. Erythropoietin: structure, control of production, and function, 1992.

[24] Rafael L. Jurado. Iron, infections, and anemia of inflammation. *Clinical Infectious Diseases*, 25(4):888–895, 1997.

[25] Mark J. Koury and Prem Ponka. New Insights into Erythropoiesis: The Roles of Folate, Vitamin B12, and Iron. *Annual Review of Nutrition*, 24:105–131, 2004.

[26] Sanford B. Krantz. Erythropoietin. *Blood*, 77:419–434, 1991.

[27] Daniela S. Lempe, Phillipp A. Lang, Christophe Duranton, Ahmad Akel, Karl S. Lang, Stephan M. Huber, Thomas Wieder, and Florian Lang. Enhanced programmed cell death of iron-deficient erythrocytes. *The Journal of the Federation of American Societies for Experimental Biology Express Article*, 10.1096/fj.05-4872fje, Published online December 21, 2005.

[28] Shengtai Li and Linda Petzold. Moving mesh methods with upwinding schemes for time-dependent pdes. *Journal of Computational Physics*, 131:368–377, 1997.

[29] Joseph Ly, Rosa Marticorena, and Sandra Donnelly. Red blood cell survival in chronic renal failure. *American Journal of Kidney Diseases*, 44(4):715–719, 2004.

[30] I. Macdougall. Use of recombinant erythropoietins in the setting of renal disease. In S.G. Elliot G. Molineaux, M.A. Foote, editor, *Erythropoietins and Erythropoiesis: Molecular, Cellular, Preclinical and Clinical Biology*, pages 153–9. Birkhäuser Verlag, 2003.

[31] I. Macdougall and A. Cooper. Erythropoietin resistance: the role of inflammation and pro-inflammatory cytokines. *Nephrol. Dial. Transplant.*, 17:39–43, 2002.

[32] J. Mahaffy, J. Belair, and M. Mackey. Hematopoietic model with moving boundary condition and state dependent delay: applications in erythropoiesis. *Journal of Theoretical Biology*, 190(2):135, 1998.

[33] R. Means Jr. and S. Krantz. Inhibition of human erythroid colony-forming units by interferons alpha and beta: differing mechanisms despite shared receptor. *Experimental Hematology*, 24(2):204, 1996.

[34] Cesar F. Merino. Studies on blood formation and destruction in the polycythemia of high altitude. *Blood*, 5:1–31, 1950.

[35] National Kidney Foundation Kidney Disease Outcomes Quality Initiative. KDOQI Clinical Practice Guidline and Clinical Practice Recommendations for Anemia in Chronic Kidney Disease: 2007 Update of Hemoglobin Target. *American Journal of Kidney Diseases*, 50(3):471–530, September 2007.

[36] Gael Nicolas, Caroline Chauvet, Lydie Viatte, Jean Louis Danan, Xavier Bigard, Isabelle Devaux, Carole Beaumont, Axel Kahn, and Sophie Vaulont. The gene encoding the iron regulatory peptide hepcidin is regulated by anemia, hypoxia and inflammation. *Journal of Clinical Investigation*, 110(7):1037–1044, 2002.

[37] Myron Pollycove and Robert Mortimer. The quantitative determination of iron kinetics and hemoglobin synthesis in human subjects. *Journal of Clinical Investigation*, 40:753–782, 1961.

[38] R. Ramakrishnan, W. Cheung, M. Wacholtz, N. Minton, and W. Jusko. Pharmacokinetic and pharmacodynamic modeling of human erythropoietin after single and multiple doses in healthy volunteers. *The Journal of Clinical Pharmacology*, 44:991–1002, 2004.

[39] Lawrence Rice and Clarence Alfrey. The negative regulation of red cell mass by neocytolysis: Physiologic and pathophysiologic manifestations. *Cellular Physiology and Biochemistry*, 15:245–250, 2005.

[40] Lawrence Rice, Clarence P. Alfrey, Theda Driscoll, Carl E. Whitley, David L. Hachey, and Wadi Suki. Neocytolysis contributes to the anemia of renal disease. *American Journal of Kidney Disease*, 33(1):59–62, 1999.

[41] Lawrence Rice, Wilson Rulz, Theda Driscoll, Carl E. Whitley, Rosario Tapia, David L. Hachey, Gustavo F. Gonzales, and Clarence P. Alfrey. Neocytolysis on descent from altitude: A newly recognized mechanism for the control of red cell mass. *Annals of Internal Medicine*, 134(8):652–656, 2001.

[42] Jr. Robert T. Means and Sanford B. Krantz. Progress in understanding the pathogenesis of the anemia of chronic disease. *Blood*, 80(7):1639–1647, 1992.

[43] Bernadette F. Rodak, George A. Fritsma, and Kathryn Doig. *Hematology: Clinical Principles and Applications*. Saunders Elsevier, 3 edition, 2007.

[44] Pradeep Sathyanarayana, Arvind Dev, Jing Fang, Estelle Houde, Olga Bogacheva, Oleg Bogachev, Madhu Menon, Sarah Browne, Anamika Pradeep, Christine Emerson, and Don M. Wojchowski. Epo receptor circuits for primary erythroblast survival. *Blood*, 111(11), 2008.

[45] K. Sawada, S. B. Krantz, S-H. Dai, S. T. Koury, S. T. Horn, A. D. Glick, and C. I. Civin. Purification of human blood burst-forming units-erythroid and demonstration of the evolution of erythropoietin receptors. *Journal of Cellular Physiology*, 142:219–230, 1990.

[46] K. Sawada, S. B. Krantz, J. S. Kans, E. N. Dessypris, S. Sawyer, A. D. Glick, and C. I. Civin. Purification of Human Erythroid Colony-forming Units and Demonstration of Specific Binding of Erythropoietin. *Journal of Clinical Investigation*, 80(2):357–366, 1987.

[47] A. B. Shaw. Haemolysis in chronic renal failure. *British Medical Journal*, 2:213–216, 1967.

[48] A. Simmons. *Basic Hematology*. Charles C Thomas, Springfield, Illinois, 1973.

[49] P. Stenvinkel. The role of inflammation in the anaemia of end-stage renal disease. *Nephrology, Dialysis, Transplantation*, 16(Suppl 7):36–40, 2001.

[50] Peter Stenvinkel, Olof Heimburger, Furcy Paultre, Ulf Diczfalusy, Tao Wang, Lars Berglund, and Tomas Jogestrand. Strong association between malnutrition, inflammation, and artherosclerosis in chronic renal failure. *Kidney International*, 55:1899–1911, 1999.

[51] J. H. Stewart. Haemolytic anemia in acute and chronic renal failure. *QJM*, 36(1):85–105, 1967.

[52] U.S. Renal Data System. *USRDS 2008 Annual Data Report: Atlas of Chronic Kidney Disease and End-Stage Renal Disease in the United States*. National Institutes of Health, National Institute of Diabetes and Digestive and Kidney Diseases, Bethesda, MD, 2008.

[53] M. M. Udden, T. B. Driscoll, M. H. Pickett, C. S. Leach-Huntoon, and C. P. Alfrey. Decreased production of red blood cells in human subjects exposed to microgravity. *Journal of Laboratory and Clinical Medicine*, 125(4):442–449, 1995.

[54] M. C. Verloop, M. Van der Wolk, and A. J. Heier. Radioactive iron studies in patients with iron deficiency anemia with concurrent abnormal hemolysis. *Blood*, 15:791–806, 1960.

[55] Guenter Weiss and Lawrence T. Goodnough. Anemia of chronic disease. *New England Journal of Medicine*, 352:1011–1023, 2005.

[56] S. Woo, W. Krzyzanski, and W. Jusko. Pharmacokinetic and pharmacodynamic modeling of recombinant human erythropoietin after intravenous and subcutaneous administration in rats. *Journal of Pharmacology and Experimental Therapeutics*, 319(3):1297–1306, 2006.

[57] Hong Wu, Xin Liu, Rudolf Jaenisch, and Harvey F. Lodish. Generation of committed erythroid bfu-e and cfu-e progenitors does not require erythropoietin or the erythropoietin receptor. *Cell*, 83:59–67, 1995.

APPENDICES

Appendix A

Model Parameter Values

Table A.1: Model Parameters and Units, Part 1

Parameter	Units	Parameter value
ρ_P	day^{-1}	1
β_P^{max}	day^{-1}	0.2
β_P^{min}	day^{-1}	0.1
$c_{\beta,P}$	unitless	5250
$k_{\beta,P}$	unitless	5
$\delta_{P,E}^{max}$	day^{-1}	0.03
$\delta_{P,E}^{min}$	day^{-1}	0
$c_{\delta,P,E}$	unitless	1800
$k_{\delta,P,E}$	unitless	6
$\delta_{P,I}^{max}$	day^{-1}	0.05
$\delta_{P,I}^{min}$	day^{-1}	0
$c_{\delta,P,I}$	unitless	0.75
$k_{\delta,P,I}$	unitless	7
R_P	billions of cells/unit EPO	0.018
ρ_M^{max}	day^{-1}	1.2
ρ_M^{min}	day^{-1}	1
$c_{\rho,M}$	unitless	5500
$k_{\rho,M}$	unitless	10
β_M	day^{-1}	0.25
ρ_O	day^{-1}	1
δ_O^{max}	day^{-1}	0.13

Table A.2: Model Parameters and Units, Part 2

δ_O^{min}	day^{-1}	0
$c_{\delta,O}$	unitless	80
$k_{\delta,O}$	unitless	7
$k_{Fe,eff}$	unitless	0.65
f_1	unitless	0.3
$f_{0.5}$	unitless	0.6
k_{heavy}	unitless	5
EPO_{th}	units of EPO	3000
$k_{\rho,Fe}$	day^{-1}	0.993
$\rho_{Fe,frac}$	day^{-1}	0.3
Fe_{th}	mg	15

Appendix B

Derivation for class M

Let

$$0 = \nu_1 < \nu_2 < \cdots < \nu_{N_M} = \nu_f$$

be a uniform partition of $N_M - 1$ subintervals, each of length $h_M = \frac{\nu_f}{N_M - 1}$. We define N_M piecewise linear continuous functions

$$\phi_j^B, \quad j = 1, 2, \ldots, N_M$$

by

$$\phi_j^B(\nu) = \begin{cases} \dfrac{\nu - \nu_{j-1}}{h_M}, & \nu_{j-1} \leq \nu \leq \nu_j, \\ \dfrac{\nu_{j+1} - \nu}{h_M}, & \nu_j \leq \nu \leq \nu_{j+1}, \\ 0, & \nu < \nu_{j-1} \text{ or } \nu > \nu_{j+1} \end{cases}$$

The derivative of such a function (when it exists) is given by

$$\phi_j^{B'}(\nu) = \begin{cases} \dfrac{1}{h_M}, & \nu_{j-1} < \nu < \nu_j, \\ -\dfrac{1}{h_M}, & \nu_j < \nu < \nu_{j+1}, \\ 0, & \nu < \nu_{j-1} \text{ or } \nu > \nu_{j+1} \end{cases}$$

Similarly, we define N_M continuous second-order spline functions

$$\chi_j^B, \quad j = 1, 2, \ldots, N_M,$$

by

$$\chi_j^B(\nu) = \begin{cases} \dfrac{(\nu - \nu_{j-1})(\nu_j - \nu)}{h_M^2}, & \nu_{j-1} \le \nu \le \nu_j, \\ -\dfrac{(\nu - \nu_j)(\nu_{j+1} - \nu)}{h_M^2}, & \nu_j \le \nu \le \nu_{j+1}, \\ 0, & \nu < \nu_{j-1} \text{ or } \nu > \nu_{j+1}. \end{cases}$$

Notice that by definition, $\chi_j^B(\nu_{j-1}) = \chi_j^B(\nu_j) = \chi_j^B(\mu_{j+1}) = 0$.

Let ω_M be a scalar parameter and define the function $\tilde{\phi}_j^B, j = 1, 2, \ldots, N_M$, by

$$\tilde{\phi}_j^B(\nu) = \phi_j^B(\nu) + \omega_M \chi_j^B(\nu).$$

Note that for all j,

$$\frac{d}{d\nu}\tilde{\phi}_j^B(\nu) = \phi_j^{B\prime}(\nu) + \omega_M \chi_j^{B\prime}(\nu)$$

and

$$\tilde{\phi}_j^B(\nu) = \phi_j^B(\nu) \text{ for } \nu = \nu_{j-i}, \nu_j, \nu_{j+1}.$$

Let $1 \le j \le N_M$ be arbitrary. We multiply (2.10) by the jth function, $\tilde{\phi}_j^B(\nu)$, and integrate from $\nu = 0$ to $\nu = \nu_f$.

$$\int_0^{\nu_f} \frac{\partial}{\partial t} M(t,\nu)\tilde{\phi}_j^B(\nu)d\nu = -\rho_M(E)\int_0^{\nu_f} \frac{\partial}{\partial \nu} M(t,\nu)\tilde{\phi}_j^B(\nu)d\nu + \beta_M \int_0^{\nu_f} M(t,\nu)\tilde{\phi}_j^B(\nu)d\nu$$

After integration by parts of the second term we have

$$\begin{aligned} \int_0^{\nu_f} \frac{\partial}{\partial t} M(t,\nu)\tilde{\phi}_j^B(\nu)d\nu = & -\rho_M(E)M(t,\nu)\tilde{\phi}_j^B(\nu)\Big|_{\nu=0}^{\nu=\nu_f} + \rho_M(E)\int_0^{\nu_f} M(t,\nu)\frac{d}{d\nu}\tilde{\phi}_j^B(\nu)d\nu \\ & + \beta_M \int_0^{\nu_f} M(t,\nu)\tilde{\phi}_j^B(\nu)d\nu \\ = & -\rho_M(E)M(t,\nu_f)\phi_j(\nu_f) + \rho_M(E)M(t,0)\phi_j(0) \\ & + \rho_M(E)\int_0^{\nu_f} M(t,\nu)\frac{d}{d\nu}\tilde{\phi}_j^B(\nu)d\nu \\ & + \beta_M \int_0^{\nu_f} M(t,\nu)\tilde{\phi}_j^B(\nu)d\nu. \end{aligned}$$

Now we can apply the boundary condition (2.15) to obtain

$$\begin{aligned}\int_0^{\nu_f} \frac{\partial}{\partial t} M(t,\nu)\tilde{\phi}_j^B(\nu)d\nu = & -\rho_M(E)M(t,\nu_f)\phi_j(\nu_f) + \rho_M(E)P(t,\mu_f)\phi_j(0) \\ & + \rho_M(E)\int_0^{\nu_f} M(t,\nu)\frac{d}{d\nu}\tilde{\phi}_j^B(\nu)d\nu \\ & + \beta_M \int_0^{\nu_f} M(t,\nu)\tilde{\phi}_j^B(\nu)d\nu \\ = & -\rho_M(E)M(t,\nu_f)\phi_j(\nu_f) + \rho_M(E)a_{N_P}(t)\phi_j(0) \\ & + \rho_M(E)\int_0^{\nu_f} M(t,\nu)\frac{d}{d\nu}\tilde{\phi}_j^B(\nu)d\nu \\ & + \beta_M \int_0^{\nu_f} M(t,\nu)\tilde{\phi}_j^B(\nu)d\nu. \end{aligned} \tag{B.1}$$

We define the Galerkin finite element approximation for M by

$$M(t,\nu) = \sum_{i=1}^{N_M} b_i(t)\phi_i^B(\nu), \tag{B.2}$$

which we substitute into equation (B.1), and then rearrange the terms for convenience, as below.

$$\begin{aligned}\int_0^{\nu_f} \sum_{i=1}^{N_M} b_i'(t)\phi_i^B(\nu)\tilde{\phi}_j^B(\nu)d\nu = & -\rho_M(E)b_{N_M}(t)\phi_j^B(\nu_f) + \rho_M(E)a_{N_P}(t)\phi_j^B(0) \\ & + \rho_M(E)\int_0^{\nu_f} \sum_{i=1}^{N_M} b_i(t)\phi_i^B(\nu)\frac{d}{d\nu}\tilde{\phi}_j^B(\nu)d\nu \\ & + \beta_M \int_0^{\nu_f} \sum_{i=1}^{N_M} b_i(t)\phi_i^B(\nu)\tilde{\phi}_j^B(\nu)d\nu. \end{aligned}$$

$$\sum_{i=1}^{N_M} b_i'(t) \left[\int_0^{\nu_f} \phi_i^B(\nu) \tilde{\phi}_j^B(\nu) d\nu \right] = -\rho_M(E) b_{N_M}(t) \phi_j^B(\nu_f) + \rho_M(E) a_{N_P}(t) \phi_j^B(0) + \sum_{i=1}^{N_M} b_i(t) \left[\rho_M(E) \int_0^{\nu_f} \phi_i^B(\nu) \frac{d}{d\nu} \tilde{\phi}_j^B(\nu) d\nu + \beta_M \int_0^{\nu_f} \phi_i^B(\nu) \tilde{\phi}_j^B(\nu) d\nu \right].$$

$$\sum_{i=1}^{N_M} b_i'(t) \left[\int_0^{\nu_f} \phi_i^B(\nu) \phi_j^B(\nu) d\nu + \omega_M \int_0^{\nu_f} \phi_i^B(\nu) \chi_j^B(\nu) d\nu \right] = -\rho_M(E) b_{N_M}(t) \phi_j^B(\nu_f) + \rho_M(E) a_{N_P}(t) \phi_j^B(0) + \sum_{i=1}^{N_M} b_i(t) \left\{ \rho_M(E) \left[\int_0^{\nu_f} \phi_i^B(\nu) \phi_j^{B\prime}(\nu) d\nu + \omega_M \int_0^{\nu_f} \phi_i^B(\nu) \chi_j^{B\prime}(\nu) d\nu \right] + \beta_M \left[\int_0^{\nu_f} \phi_i^B(\nu) \phi_j^B(\nu) d\nu + \omega_M \int_0^{\nu_f} \phi_i^B(\nu) \chi_j^B(\nu) d\nu \right] \right\}. \quad \text{(B.3)}$$

We can let j range from 1 to N_M to yield a system of N_M ordinary differential equations for the coefficients $b_i(t)$, which we convert to matrix form. To this end, we introduce the following definitions:

$$y(t) = \left[b_1(t), b_2(t), \ldots, b_{N_M}(t) \right]^T,$$

$$\mathcal{B} = \begin{bmatrix} \int \phi_1^B \phi_1^B & \int \phi_2^B \phi_1^B & & & & \\ \int \phi_1^B \phi_2^B & \int \phi_2^B \phi_2^B & \int \phi_3^B \phi_2^B & & & \\ & \int \phi_2^B \phi_3^B & \int \phi_3^B \phi_3^B & \int \phi_4^B \phi_3^B & & \\ & & \ddots & \ddots & \ddots & \\ & & & \int \phi_{N_M-2}^B \phi_{N_M-1}^B & \int \phi_{N_M-1}^B \phi_{N_M-1}^B & \int \phi_{N_M}^B \phi_{N_M-1}^B \\ & & & & \int \phi_{N_M-1}^B \phi_{N_M}^B & \int \phi_{N_M}^B \phi_{N_M}^B \end{bmatrix}$$

$$= \frac{h_M}{6} \begin{bmatrix} 2 & 1 & & & & 0 \\ 1 & 4 & 1 & & & \\ & 1 & 4 & 1 & & \\ & & \ddots & \ddots & \ddots & \\ & & & 1 & 4 & 1 \\ 0 & & & & 1 & 2 \end{bmatrix},$$

$$\mathcal{B}' = \begin{bmatrix} \int \phi_1^B \phi_1^{B'} & \int \phi_2^B \phi_1^{B'} & & & & \\ \int \phi_1^B \phi_2^{B'} & \int \phi_2^B \phi_2^{B'} & \int \phi_3^B \phi_2^{B'} & & & \\ & \int \phi_2^B \phi_3^{B'} & \int \phi_3^B \phi_3^{B'} & \int \phi_4^B \phi_3^{B'} & & \\ & & \ddots & \ddots & \ddots & \\ & & & \int \phi_{N_M-2}^B \phi_{N_M-1}^{B\ \prime} & \int \phi_{N_M-1}^B \phi_{N_M-1}^{B\ \prime} & \int \phi_{N_M}^B \phi_{N_M-1}^{B\ \prime} \\ & & & & \int \phi_{N_M-1}^B \phi_{N_M}^{B\ \prime} & \int \phi_{N_M}^B \phi_{N_M}^{B\ \prime} \end{bmatrix}$$

$$= \frac{1}{2} \begin{bmatrix} -1 & -1 & & & & 0 \\ 1 & 0 & -1 & & & \\ & 1 & 0 & -1 & & \\ & & \ddots & \ddots & \ddots & \\ & & & 1 & 0 & -1 \\ 0 & & & & 1 & 1 \end{bmatrix},$$

$$\mathcal{X}_B = \begin{bmatrix} \int \phi_1^B \chi_1^B & \int \phi_2^B \chi_1^B & & & & \\ \int \phi_1^B \chi_2^B & \int \phi_2^B \chi_2^B & \int \phi_3^B \chi_2^B & & & \\ & \int \phi_2^B \chi_3^B & \int \phi_3^B \chi_3^B & \int \phi_4^B \chi_3^B & & \\ & & \ddots & \ddots & \ddots & \\ & & & \int \phi_{N_M-2}^B \chi_{N_M-1}^B & \int \phi_{N_M-1}^B \chi_{N_M-1}^B & \int \phi_{N_M}^B \chi_{N_M-1}^B \\ & & & & \int \phi_{N_M-1}^B \chi_{N_M}^B & \int \phi_{N_M}^B \chi_{N_M}^B \end{bmatrix}$$

$$= \frac{h_M}{12} \begin{bmatrix} -1 & -1 & & & & 0 \\ 1 & 0 & -1 & & & \\ & 1 & 0 & -1 & & \\ & & \ddots & \ddots & \ddots & \\ & & & 1 & 0 & -1 \\ 0 & & & & 1 & 1 \end{bmatrix},$$

$$\mathcal{X}'_B = \begin{bmatrix} \int \phi_1^B \chi_1^{B'} & \int \phi_2^B \chi_1^{B'} & & & & \\ \int \phi_1^B \chi_2^{B'} & \int \phi_2^B \chi_2^{B'} & \int \phi_3^B \chi_2^{B'} & & & \\ & \int \phi_2^B \chi_3^{B'} & \int \phi_3^B \chi_3^{B'} & \int \phi_4^B \chi_3^{B'} & & \\ & & \ddots & \ddots & \ddots & \\ & & & \int \phi_{N_M-2}^B \chi_{N_M-1}^{B\ \prime} & \int \phi_{N_M-1}^B \chi_{N_M-1}^{B\ \prime} & \int \phi_{N_M}^B \chi_{N_M-1}^{B\ \prime} \\ & & & & \int \phi_{N_M-1}^B \chi_{N_M}^{B\ \prime} & \int \phi_{N_M}^B \chi_{N_M}^{B\ \prime} \end{bmatrix}$$

$$= \frac{1}{6} \begin{bmatrix} -1 & 1 & & & & 0 \\ 1 & -2 & 1 & & & \\ & 1 & -2 & 1 & & \\ & & \ddots & \ddots & \ddots & \\ & & & 1 & -2 & 1 \\ 0 & & & & 1 & -1 \end{bmatrix},$$

$$M_M = \mathcal{B} + \omega_M \mathcal{X}_B,$$

$$A_M(E) = \rho_M(E) \left\{ \mathcal{B}' + \omega_M \mathcal{X}'_B + \begin{bmatrix} 0 & \cdots & & 0 \\ \vdots & & & \vdots \\ 0 & \cdots & 0 & 0 \\ 0 & \cdots & 0 & -1 \end{bmatrix} \right\} + \beta_M \left\{ \mathcal{B} + \omega_M \mathcal{X}_B \right\},$$

and

$$B_M(E) = \left[\rho_M(E) a_{N_P}(t), 0, 0, \ldots, 0 \right]^T,$$

where

$$\begin{aligned}
\int \phi_i^B \phi_j^B \text{ means } & \int_0^{\nu_f} \phi_i^B(\nu) \phi_j^B(\nu) d\nu, \\
\int \phi_i^B \phi_j^{B'} \text{ means } & \int_0^{\nu_f} \phi_i^B(\nu) \chi_j^{B'}(\nu) d\nu, \\
\int \phi_i^B \chi_j^B \text{ means } & \int_0^{\nu_f} \phi_i^B(\nu) \chi_j^B(\nu) d\nu, \text{ and} \\
\int \phi_i^B \chi_j^{B'} \text{ means } & \int_0^{\nu_f} \phi_i^B(\nu) \chi_j^{B'}(\nu) d\nu.
\end{aligned}$$

Then (B.3) can be written as

$$M_M \dot{y}(t) = A_M(E) y(t) + B_M(E).$$

Appendix C

Derivation for class O

We define a uniform partition of $N_O - 1$ subintervals,

$$0 = \psi_1 < \psi_2 < \cdots < \psi_{N_O} = \psi_f$$

each of length $h_O = \frac{\psi_f}{N_O - 1}$. Then we define N_O piecewise linear continuous functions

$$\phi_j^D, \quad j = 1, 2, \ldots, N_O$$

by

$$\phi_j^D(\psi) = \begin{cases} \dfrac{\psi - \psi_{j-1}}{h_O}, & \psi_{j-1} \leq \psi \leq \psi_j, \\ \dfrac{\psi_{j+1} - \psi}{h_O}, & \psi_j \leq \psi \leq \psi_{j+1}, \\ 0, & \psi < \psi_{j-1} \text{ or } \psi > \psi_{j+1}. \end{cases}$$

The derivative of such a function (when it exists) is given by

$$\phi_j^{D\prime}(\psi) = \begin{cases} \dfrac{1}{h_O}, & \psi_{j-1} < \psi < \psi_j, \\ -\dfrac{1}{h_O}, & \psi_j < \psi < \psi_{j+1}, \\ 0, & \psi < \psi_{j-1} \text{ or } \psi > \psi_{j+1}. \end{cases}$$

Similarly, we define N_O continuous second-order spline functions

$$\chi_j^D, \quad j = 1, 2, \ldots, N_O,$$

by

$$\chi_j^D(\psi) = \begin{cases} \dfrac{(\psi - \psi_{j-1})(\psi_j - \psi)}{h_O^2}, & \psi_{j-1} \le \psi \le \psi_j, \\ -\dfrac{(\psi - \psi_j)(\psi_{j+1} - \psi)}{h_O^2}, & \psi_j \le \psi \le \psi_{j+1}, \\ 0, & \psi < \psi_{j-1} \text{ or } \psi > \psi_{j+1}. \end{cases}$$

Notice that by definition, $\chi_j^D(\psi_{j-1}) = \chi_j^D(\psi_j) = \chi_j^D(\psi_{j+1}) = 0$.

Let ω_O be a scalar parameter and define the function $\tilde{\phi}_j^D, j = 1, 2, \ldots, N_O$, by

$$\tilde{\phi}_j^B(\psi) = \phi_j^B(\psi) + \omega_M \chi_j^B(\psi).$$

Note that for all j,

$$\frac{d}{d\psi}\tilde{\phi}_j^D(\psi) = \phi_j^{D\prime}(\psi) + \omega_O \chi_j^{D\prime}(\psi)$$

and

$$\tilde{\phi}_j^D(\psi) = \phi_j^D(\psi) \text{ for } \psi = \psi_{j-i}, \psi_j, \psi_{j+1}.$$

Let $1 \le j \le N_O$ be arbitrary. We multiply (2.11) by the jth function, $\tilde{\phi}_j^D(\psi)$, and integrate from $\psi = 0$ to $\psi = \psi_f$.

$$\int_0^{\psi_f} \frac{\partial}{\partial t} O(t,\psi)\tilde{\phi}_j^D(\psi)d\psi = -\rho_O \int_0^{\psi_f} \frac{\partial}{\partial \psi} O(t,\psi)\tilde{\phi}_j^D(\psi)d\psi - \int_0^{\psi_f} \delta_O(\psi) O(t,\psi)\tilde{\phi}_j^D(\psi)d\psi$$

We use integration by parts on the second term to obtain

$$\int_0^{\psi_f} \frac{\partial}{\partial t} O(t,\psi)\tilde{\phi}_j^D(\psi)d\psi = -\rho_O O(t,\psi)\tilde{\phi}_j^D(\psi)\Big|_{\psi=0}^{\psi=\psi_f} + \rho_O \int_0^{\psi_f} O(t,\psi)\frac{d}{d\psi}\tilde{\phi}_j^D(\psi)d\psi - \int_0^{\psi_f} \delta_O(\psi) O(t,\psi)\tilde{\phi}_j^D(\psi)d\psi$$

$$\int_0^{\psi_f} \frac{\partial}{\partial t} O(t,\psi)\tilde{\phi}_j^D(\psi)d\psi = -\rho_O O(t,\psi_f)\phi_j^D(\psi_f) + \rho_O O(t,0)\phi_j^D(0) + \rho_O \int_0^{\psi_f} O(t,\psi)\frac{d}{d\psi}\tilde{\phi}_j^D(\psi)d\psi - \int_0^{\psi_f} \delta_O(\psi)O(t,\psi)\tilde{\phi}_j^D(\psi)d\psi \qquad \text{(C.1)}$$

We would like to apply the boundary condition (2.16),

$$O(t,0) = \frac{1}{k_{Fe}} Fe_{used}.$$

As such, we introduce

$$\begin{aligned} Fe_{needed} &= k_{Fe} M(t,\nu_f), \qquad \text{by (2.31)}, \\ &= k_{Fe} b_{N_M}(t), \qquad \text{by (B.2)}, \end{aligned}$$

$$Fe_{avail} = k_{Fe,eff} f(E,I) Fe, \qquad \text{by (2.32), and}$$

$$Fe_{used} = \min\left\{Fe_{needed},\ Fe_{avail}\right\}, \qquad \text{by (2.33).}$$

We interpolate $b_{N_M}(t)$ and $E(t)$ from the previously computed solution vectors for use in these equations.

Now we can substitute the boundary condition (2.16) in (C.1) to obtain

$$\int_0^{\psi_f} \frac{\partial}{\partial t} O(t,\psi)\tilde{\phi}_j^D(\psi)d\psi = -\rho_O O(t,\psi_f)\phi_j^D(\psi_f) - \frac{\rho_O}{k_{Fe}} Fe_{used}\phi_j^D(0) + \rho_O \int_0^{\psi_f} O(t,\psi)\frac{d}{d\psi}\tilde{\phi}_j^D(\psi)d\psi - \int_0^{\psi_f} \delta_O(\psi)O(t,\psi)\tilde{\phi}_j^D(\psi)d\psi \qquad \text{(C.2)}$$

We define the Galerkin finite element approximation for O by

$$O(t,\psi) = \sum_{i=1}^{N_O} d_i(t)\phi_i^D(\psi), \tag{C.3}$$

and substitute this into equation (C.2), then rearrange the terms for convenience, as below.

$$\begin{aligned}\int_0^{\psi_f} \sum_{i=1}^{N_O} d_i'(t)\phi_i^D(\psi)\tilde{\phi}_j^D(\psi)d\psi = & -\rho_O d_{N_O}(t)\phi_j^D(\psi_f) + \frac{\rho_O}{k_{Fe}} Fe_{used}\phi_j^D(0) \\ & + \rho_O \int_0^{\psi_f} \sum_{i=1}^{N_O} d_i(t)\phi_i^D(\psi)\frac{d}{d\psi}\tilde{\phi}_j^D(\psi)d\psi \\ & - \int_0^{\psi_f} \delta_O(\psi) \sum_{i=1}^{N_O} d_i(t)\phi_i^D(\psi)\tilde{\phi}_j^D(\psi)d\psi\end{aligned}$$

$$\begin{aligned}\sum_{i=1}^{N_O} d_i'(t)\left[\int_0^{\psi_f} \phi_i^D(\psi)\tilde{\phi}_j^D(\psi)d\psi\right] = & -\rho_O d_{N_O}(t)\phi_j^D(\psi_f) + \frac{\rho_O}{k_{Fe}} Fe_{used}\phi_j^D(0) \\ & + \sum_{i=1}^{N_O} d_i(t)\left\{\rho_O \int_0^{\psi_f} \phi_i^D(\psi)\frac{d}{d\psi}\tilde{\phi}_j^D(\psi)d\psi \right. \\ & \left. - \int_0^{\psi_f} \delta_O(\psi)\phi_i^D(\psi)\tilde{\phi}_j^D(\psi)d\psi\right\}\end{aligned}$$

$$\sum_{i=1}^{N_O} d_i'(t)\left[\int_0^{\psi_f}\phi_i^D(\psi)\phi_j^D(\psi)d\psi+\omega_O\int_0^{\psi_f}\phi_i^D(\psi)\chi_j^D(\psi)d\psi\right]$$
$$=-\rho_O d_{N_O}(t)\phi_j^D(\psi_f)+\frac{\rho_O}{k_{Fe}}Fe_{used}\phi_j^D(0)$$
$$+\sum_{i=1}^{N_O} d_i(t)\Bigg\{\rho_O\left[\int_0^{\psi_f}\phi_i^D(\psi)\phi_j^{D\prime}(\psi)d\psi+\omega_O\int_0^{\psi_f}\phi_i^D(\psi)\chi_j^{D\prime}(\psi)d\psi\right]$$
$$-\int_0^{\psi_f}\delta_O(\psi)\phi_i^D(\psi)\phi_j^D(\psi)d\psi$$
$$-\omega_O\int_0^{\psi_f}\delta_O(\psi)\phi_i^D(\psi)\chi_j^D(\psi)d\psi\Bigg\} \tag{C.4}$$

We can let j range from 1 to N_O to yield a system of N_O ordinary differential equations for the coefficients $d_i(t)$, which we put in matrix form. As such, we introduce the following definitions:

$$z(t)=\left[d_1(t),d_2(t),\ldots,d_{N_O}(t)\right]^T,$$

$$\mathcal{D}=\begin{bmatrix}\int\phi_1^D\phi_1^D & \int\phi_2^D\phi_1^D & & & & & \\ \int\phi_1^D\phi_2^D & \int\phi_2^D\phi_2^D & \int\phi_3^D\phi_2^D & & & & \\ & \int\phi_2^D\phi_3^D & \int\phi_3^D\phi_3^D & \int\phi_4^D\phi_3^D & & & \\ & & \ddots & \ddots & \ddots & & \\ & & & \int\phi_{N_O-2}^D\phi_{N_O-1}^D & \int\phi_{N_O-1}^D\phi_{N_O-1}^D & \int\phi_{N_O}^D\phi_{N_O-1}^D \\ & & & & \int\phi_{N_O-1}^D\phi_{N_O}^D & \int\phi_{N_O}^D\phi_{N_O}^D\end{bmatrix}$$
$$=\frac{h_O}{6}\begin{bmatrix}2&1&&&&0\\1&4&1&&&\\&1&4&1&&\\&&\ddots&\ddots&\ddots&\\&&&1&4&1\\0&&&&1&2\end{bmatrix},$$

$$\mathcal{D}' = \begin{bmatrix} \int \phi_1^D \phi_1^{D\prime} & \int \phi_2^D \phi_1^{D\prime} & & & & \\ \int \phi_1^D \phi_2^{D\prime} & \int \phi_2^D \phi_2^{D\prime} & \int \phi_3^D \phi_2^{D\prime} & & & \\ & \int \phi_2^D \phi_3^{D\prime} & \int \phi_3^D \phi_3^{D\prime} & \int \phi_4^D \phi_3^{D\prime} & & \\ & & \ddots & \ddots & \ddots & \\ & & & \int \phi_{N_O-2}^D {\phi_{N_O-1}^D}' & \int \phi_{N_O-1}^D {\phi_{N_O-1}^D}' & \int \phi_{N_O}^D {\phi_{N_O-1}^D}' \\ & & & & \int \phi_{N_O-1}^D {\phi_{N_O}^D}' & \int \phi_{N_O}^D {\phi_{N_O}^D}' \end{bmatrix}$$

$$= \frac{1}{2} \begin{bmatrix} -1 & -1 & & & & 0 \\ 1 & 0 & -1 & & & \\ & 1 & 0 & -1 & & \\ & & \ddots & \ddots & \ddots & \\ & & & 1 & 0 & -1 \\ 0 & & & & 1 & 1 \end{bmatrix},$$

$$\mathcal{X}_D = \begin{bmatrix} \int \phi_1^D \chi_1^D & \int \phi_2^D \chi_1^D & & & & \\ \int \phi_1^D \chi_2^D & \int \phi_2^D \chi_2^D & \int \phi_3^D \chi_2^D & & & \\ & \int \phi_2^D \chi_3^D & \int \phi_3^D \chi_3^D & \int \phi_4^D \chi_3^D & & \\ & & \ddots & \ddots & \ddots & \\ & & & \int \phi_{N_O-2}^D \chi_{N_O-1}^D & \int \phi_{N_O-1}^D \chi_{N_O-1}^D & \int \phi_{N_O}^D \chi_{N_O-1}^D \\ & & & & \int \phi_{N_O-1}^D \chi_{N_O}^D & \int \phi_{N_O}^D \chi_{N_O}^D \end{bmatrix}$$

$$= \frac{h_O}{12} \begin{bmatrix} -1 & -1 & & & & 0 \\ 1 & 0 & -1 & & & \\ & 1 & 0 & -1 & & \\ & & \ddots & \ddots & \ddots & \\ & & & 1 & 0 & -1 \\ 0 & & & & 1 & 1 \end{bmatrix},$$

$$\mathcal{X}'_D = \begin{bmatrix} \int \phi_1^D \chi_1^{D\prime} & \int \phi_2^D \chi_1^{D\prime} & & & & & \\ \int \phi_1^D \chi_2^{D\prime} & \int \phi_2^D \chi_2^{D\prime} & \int \phi_3^D \chi_2^{D\prime} & & & & \\ & \int \phi_2^D \chi_3^{D\prime} & \int \phi_3^D \chi_3^{D\prime} & \int \phi_4^D \chi_3^{D\prime} & & & \\ & & \ddots & \ddots & \ddots & & \\ & & & \int \phi_{N_O-2}^D \chi_{N_O-1}^{D\ \prime} & \int \phi_{N_O-1}^D \chi_{N_O-1}^{D\ \prime} & \int \phi_{N_O}^D \chi_{N_O-1}^{D\ \prime} \\ & & & & \int \phi_{N_O-1}^D \chi_{N_O}^{D\ \prime} & \int \phi_{N_O}^D \chi_{N_O}^{D\ \prime} \end{bmatrix}$$

$$= \frac{1}{6} \begin{bmatrix} -1 & 1 & & & & 0 \\ 1 & -2 & 1 & & & \\ & 1 & -2 & 1 & & \\ & & \ddots & \ddots & \ddots & \\ & & & 1 & -2 & 1 \\ 0 & & & & 1 & -1 \end{bmatrix},$$

$$\mathcal{D}_\delta = \begin{bmatrix} \int \delta_O \phi_1^D \phi_1^D & \int \delta_O \phi_2^D \phi_1^D & & & & \\ \int \delta_O \phi_1^D \phi_2^D & \int \delta_O \phi_2^D \phi_2^D & \int \delta_O \phi_3^D \phi_2^D & & & \\ & \int \delta_O \phi_2^D \phi_3^D & \int \delta_O \phi_3^D \phi_3^D & \int \delta_O \phi_4^D \phi_3^D & & \\ & & \ddots & \ddots & \ddots & \\ & & & \int \delta_O \phi_{N_O-2}^D \phi_{N_O-1}^D & \int \delta_O \phi_{N_O-1}^D \phi_{N_O-1}^D & \int \delta_O \phi_{N_O}^D \phi_{N_O-1}^D \\ & & & & \int \delta_O \phi_{N_O-1}^D \phi_{N_O}^D & \int \delta_O \phi_{N_O}^D \phi_{N_O}^D \end{bmatrix},$$

$$\mathcal{X}_\delta = \begin{bmatrix} \int \delta_O \phi_1^D \chi_1^D & \int \delta_O \phi_2^D \chi_1^D & & & & \\ \int \delta_O \phi_1^D \chi_2^D & \int \delta_O \phi_2^D \chi_2^D & \int \delta_O \phi_3^D \chi_2^D & & & \\ & \int \delta_O \phi_2^D \chi_3^D & \int \delta_O \phi_3^D \chi_3^D & \int \delta_O \phi_4^D \chi_3^D & & \\ & & \ddots & \ddots & \ddots & \\ & & & & & \\ & & & & & \\ & & & \int \delta_O \phi_{N_O-2}^D \chi_{N_O-1}^D & \int \delta_O \phi_{N_O-1}^D \chi_{N_O-1}^D & \int \delta_O \phi_{N_O}^D \chi_{N_O-1}^D \\ & & & & \int \delta_O \phi_{N_O-1}^D \chi_{N_O}^D & \int \delta_O \phi_{N_O}^D \chi_{N_O}^D \end{bmatrix},$$

$$M_O = \mathcal{D} + \omega_O \mathcal{X}_D,$$

$$A_O = \rho_O \left\{ \mathcal{D}' + \omega_O \mathcal{X}_D' + \begin{bmatrix} 0 & \cdots & & 0 \\ \vdots & & & \vdots \\ 0 & \cdots & 0 & 0 \\ 0 & \cdots & 0 & -1 \end{bmatrix} \right\} - \mathcal{D}_\delta - \omega_O \mathcal{X}_\delta,$$

and

$$B_O(t) = \left[\frac{\rho_O}{k_{Fe}} Fe_{used}, 0, 0, \ldots, 0 \right]^T,$$

where

$$\begin{aligned}
\int \phi_i^D \phi_j^D \text{ means } & \int_0^{\psi_f} \phi_i^D(\psi)\phi_j^D(\psi)d\psi, \\
\int \phi_i^D \phi_j^{D'} \text{ means } & \int_0^{\psi_f} \phi_i^D(\psi)\chi_j^{D'}(\psi)d\psi, \\
\int \phi_i^D \chi_j^D \text{ means } & \int_0^{\psi_f} \phi_i^D(\psi)\chi_j^D(\psi)d\psi, \\
\int \phi_i^D \chi_j^{D'} \text{ means } & \int_0^{\psi_f} \phi_i^D(\psi)\chi_j^{D'}(\psi)d\psi, \\
\int \delta_O \phi_i^D \phi_j^D \text{ means } & \int_0^{\psi_f} \delta_O(\psi)\phi_i^D(\psi)\phi_j^D(\psi)d\psi, \text{ and} \\
\int \delta_O \phi_i^D \chi_j^D \text{ means } & \int_0^{\psi_f} \delta_O(\psi)\phi_i^D(\psi)\chi_j^D(\psi)d\psi.
\end{aligned}$$

Then (C.4) can be written as

$$M_O \dot{z}(t) = A_O z(t) + B_O(t).$$

Since the vector $B_O(t)$ depends on iron, we must solve this system simultaneously with the differential equation for iron, which we obtain from (2.12) by substituting (C.3) as below.

$$\begin{aligned}
\dot{Fe}(t) &= k_{Fe} \int_0^{\psi_f} \delta_O(\psi) O(t,\psi) d\psi + \dot{Fe}_{ex}(t) - \rho_{Fe\to O} - \rho_{Fe,loss} \\
&= k_{Fe} \int_0^{\psi_f} \delta_O(\psi) \sum_{i=1}^{N_O} d_i(t)\phi_i^D(\psi) d\psi + \dot{Fe}_{ex}(t) - \rho_{Fe\to O} - \rho_{Fe,loss} \\
&= \sum_{i=1}^{N_O} d_i(t) \left[k_{Fe} \int_0^{\psi_f} \delta_O(\psi)\phi_i^D(\psi) d\psi \right] + \dot{Fe}_{ex}(t) - \rho_{Fe\to O} - \rho_{Fe,loss}.
\end{aligned}$$

Appendix D

Code validation for class M

As in class P, we note that if we don't use upwinding, the error can propagate in time and overwhelm the solution, as demonstrated by comparing the numerical solutions for class M (using the forcing procedure described perviously) with and without upwinding, as in Figures D.1.1 and D.1.2.

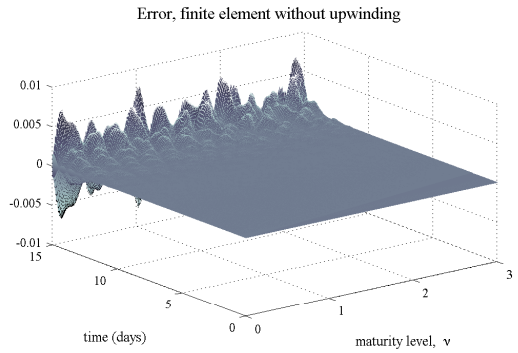

D.1.1: Error without using upwinding.

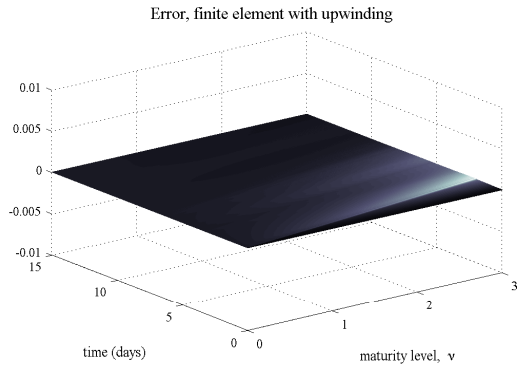

D.1.2: Error using upwinding.

Figure D.1: Code validation. We using a forcing function strategy to compare the numerical solution to a known exact solution. Exact solution is of the order 10^2.

In order to determine an appropriate value for the parameter ω_M, we fix the number of elements and compare the error using several values for the upwinding parameter.

We note that the error is of the same order for several values of the parameter and we choose to continue our simulations with $\omega_M = 2$ as the upwinding parameter for class

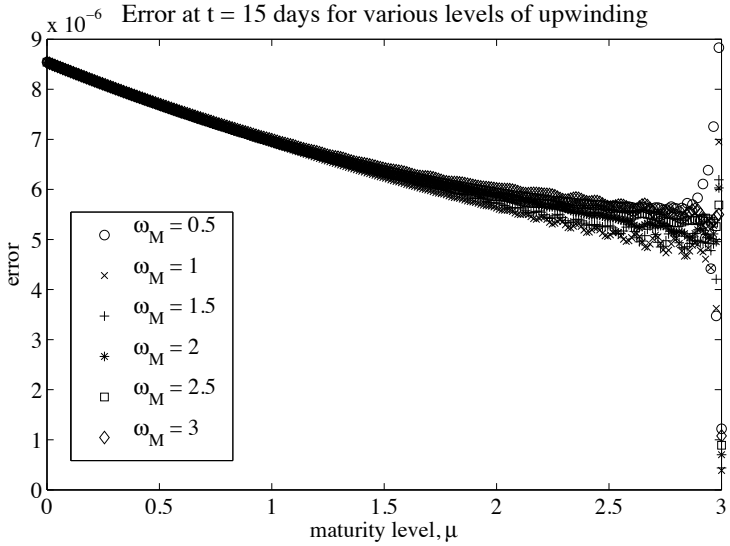

Figure D.2: Effect of varying ω_M on error between numerical and exact solution at $t = 15$ for $N = 256$ spatial elements. Exact solution is of the order 10^2.

M.

As before, we sequentially increase the number of splines elements by a factor of two to confirm that the numerical solution converges to the exact solution. The results appear in Table D.1.

Table D.1: Convergence of Solution–Maximum Error at $t = 15$ with $\omega_M = 2$ for an increasing number of splines. Exact solution is of the order 10^2.

N_M	Maximum error	(Max Error for N_M)/(Max Error for $2N_M$)
4	0.0614	5.4641
8	0.0112	4.5726
16	0.0025	4.2623
32	5.7693e-04	4.1259
64	1.3983e-04	4.0617
128	3.4427e-05	1.0000
256	3.4427e-05	16.1836
512	2.1273e-06	2.4047
1024	8.8464e-07	

Appendix E

Code validation for class O

Unlike classes P and M, at time $t = 15$ days, in Figure E.1 we are not able to immediately see the advantage of using upwinding using the same forcing function strategy we used in classes P and M, as the error is of the same order.

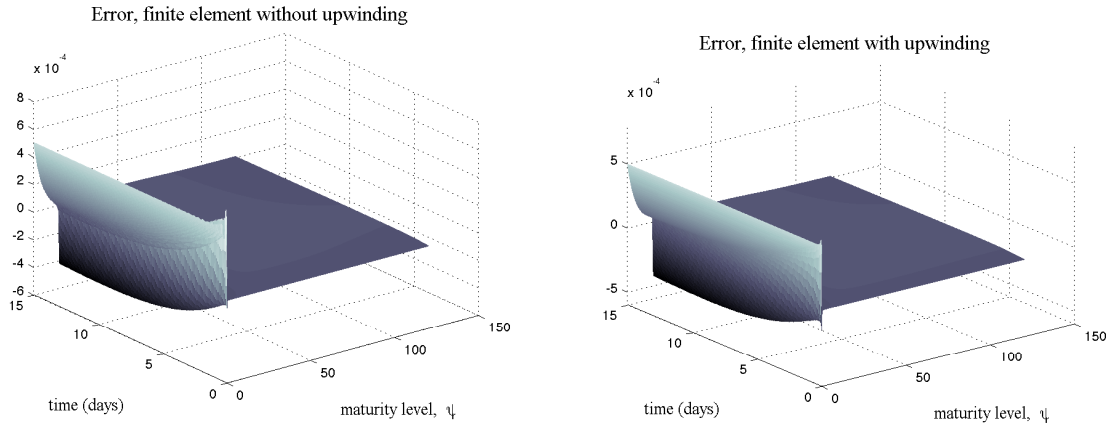

E.1.1: Error without using upwinding.

E.1.2: Error using upwinding.

Figure E.1: Code validation. We using a forcing function strategy to compare the numerical solution to a known exact solution. Exact solution is of the order 10^2.

We continue investigating by fixing the number of elements and comparing the error using several values of the upwinding parameter ω_O.

We note that the error is of the same order for several values of the parameter, including for no upwinding. We choose to continue our simulations with upwinding (for

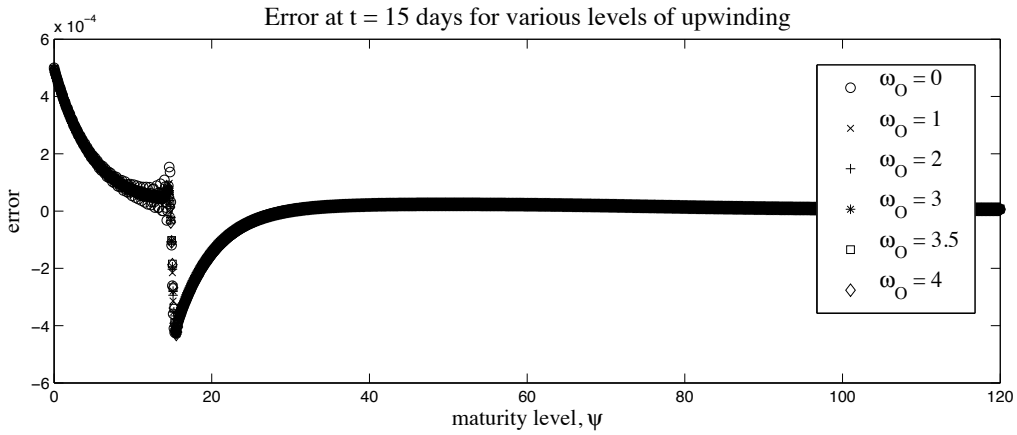

Figure E.2: Effect of varying ω_O on error between numerical and exact solution at $t = 15$ for $N = 1201$ spatial elements. Exact solution is of the order 10^2.

consistency with the other classes), using $\omega_O = 3.5$ as the upwinding parameter for class O.

As before, we sequentially increase the number of splines elements by a factor of two to confirm that the numerical solution converges to the exact solution. The results appear in Table E.1.

Table E.1: Convergence of Solution–Maximum Error at $t = 15$ with $\omega_O = 3.5$ for an increasing number of splines. Exact solution is of the order 10^2.

N_M	Maximum error	(Max Error for N_O)/(Max Error for $2N_O$)
8	4.6086	2.6825
16	1.7180	3.1906
32	0.5385	3.5164
64	0.1531	3.7385
128	0.0410	3.8632
256	0.0106	3.9299
512	0.0027	3.9645
1024	6.8052e-04	3.9821
2048	1.7089e-04	3.9911
4096	4.2819e-05	

Appendix F

Complete Simulation Results

F.1 ETD treatment, inflammation 0

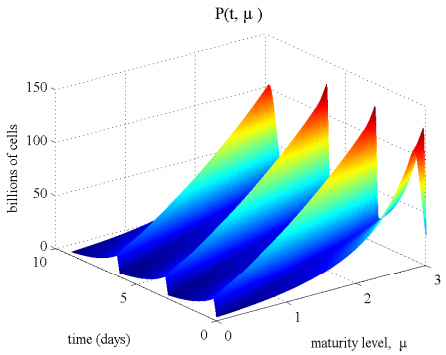

Figure F.1: Class P, ETD treatment, inflammation 0.

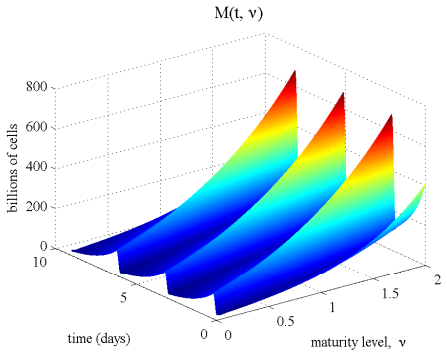

Figure F.2: Class M, ETD treatment, inflammation 0.

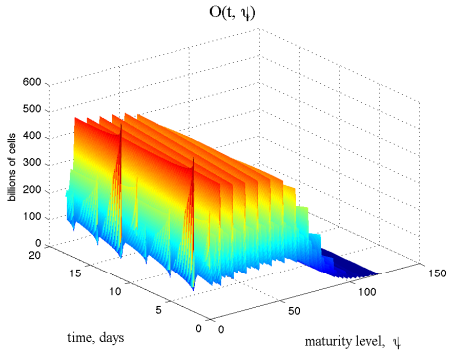

Figure F.3: Class O, ETD treatment, inflammation 0.

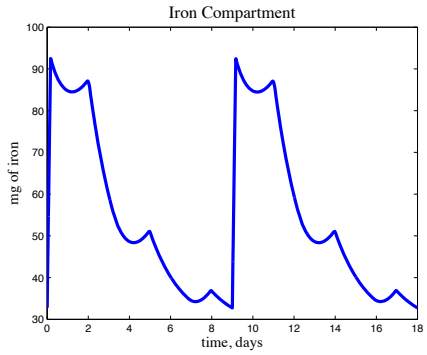

Figure F.4: Iron Compartment, ETD treatment, inflammation 0.

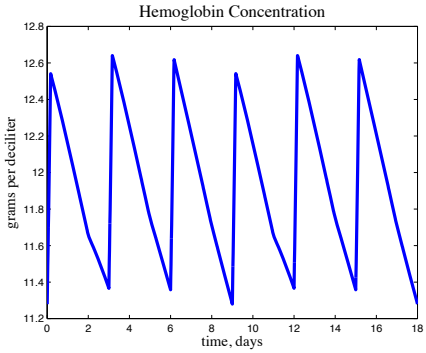

Figure F.5: Hemoglobin Concentration, ETD treatment, inflammation 0.

F.2 ETD treatment, inflammation 0.25

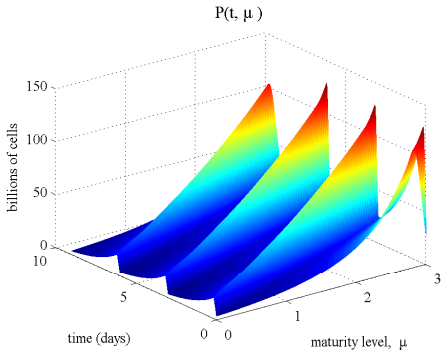

Figure F.6: Class P, ETD treatment, inflammation 0.25.

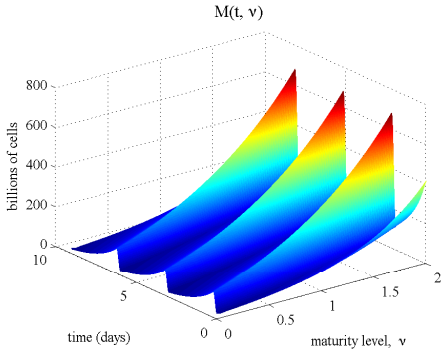

Figure F.7: Class M, ETD treatment, inflammation 0.25.

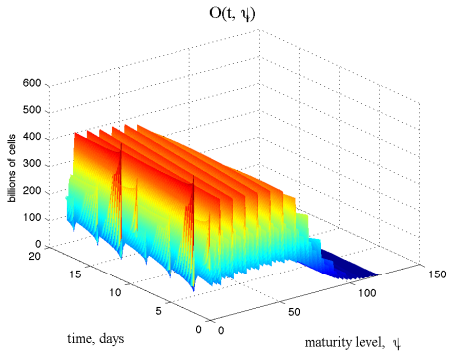

Figure F.8: Class O, ETD treatment, inflammation 0.25.

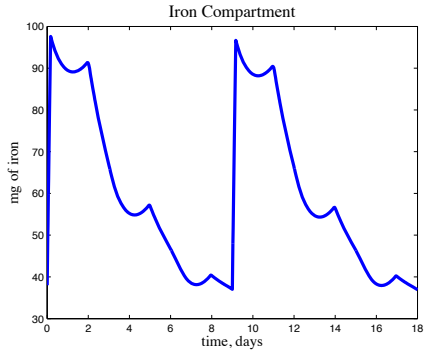

Figure F.9: Iron Compartment, ETD treatment, inflammation 0.25.

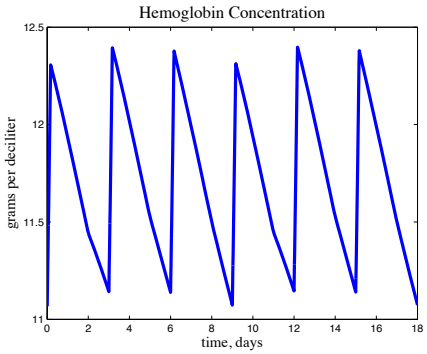

Figure F.10: Hemoglobin Concentration, ETD treatment, inflammation 0.25.

F.3 ETD treatment, inflammation 0.37

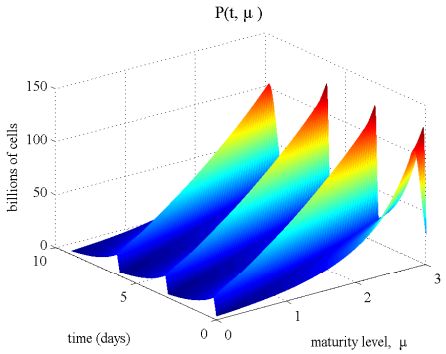

Figure F.11: Class P, ETD treatment, inflammation 0.37.

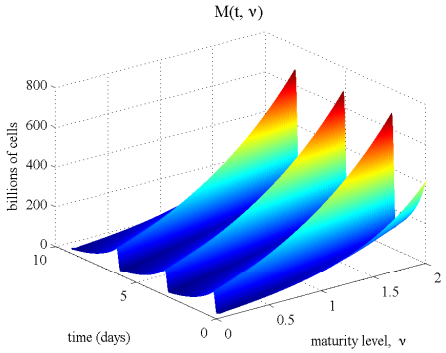

Figure F.12: Class M, ETD treatment, inflammation 0.37.

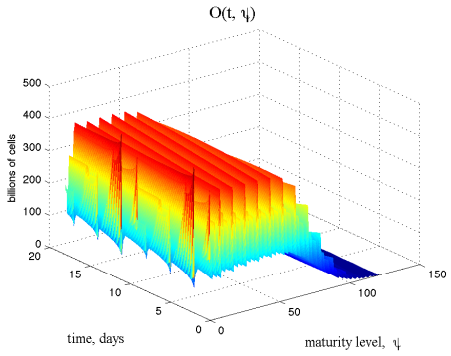

Figure F.13: Class O, ETD treatment, inflammation 0.37.

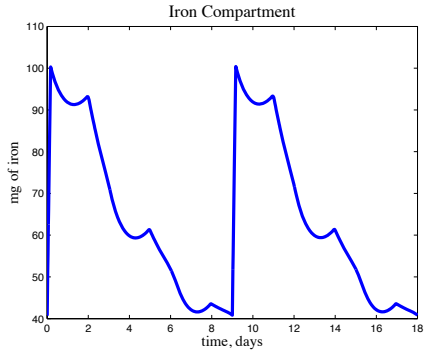

Figure F.14: Iron Compartment, ETD treatment, inflammation 0.37.

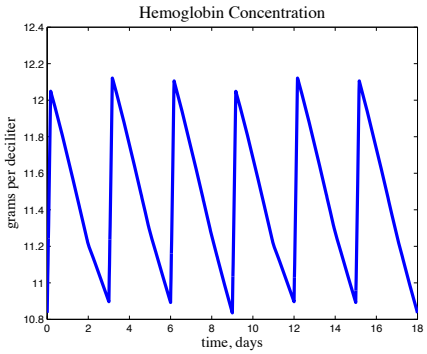

Figure F.15: Hemoglobin Concentration, ETD treatment, inflammation 0.37.

F.4 ETD treatment, inflammation 0.5

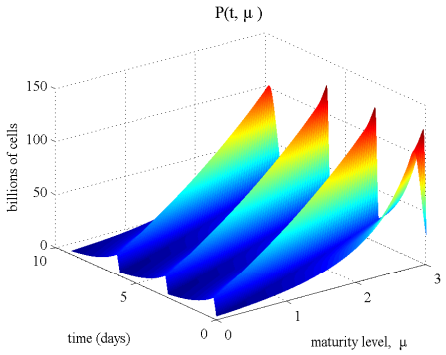

Figure F.16: Class P, ETD treatment, inflammation 0.5.

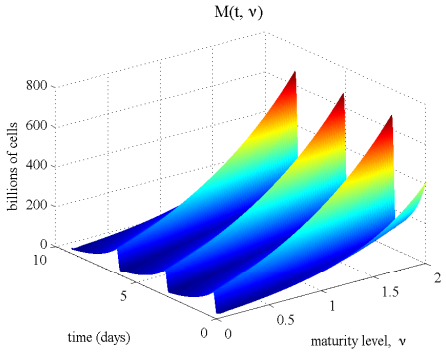

Figure F.17: Class M, ETD treatment, inflammation 0.5.

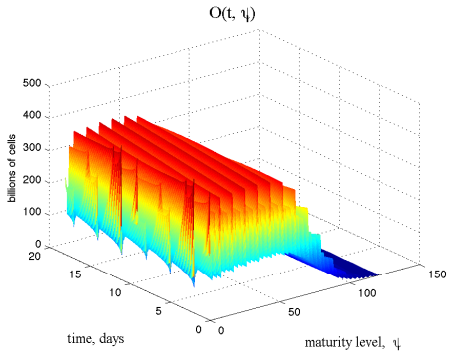

Figure F.18: Class O, ETD treatment, inflammation 0.5.

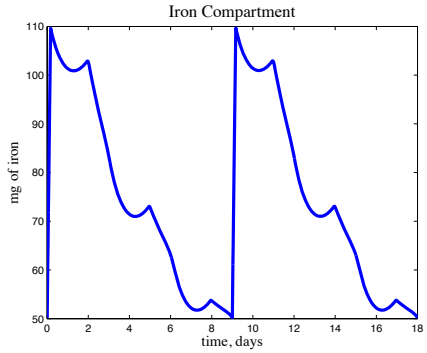

Figure F.19: Iron Compartment, ETD treatment, inflammation 0.5.

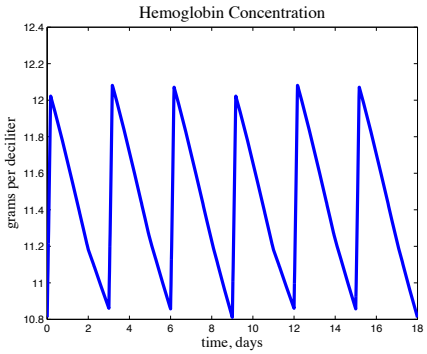

Figure F.20: Hemoglobin Concentration, ETD treatment, inflammation 0.5.

F.5 ETD treatment, inflammation 0.63

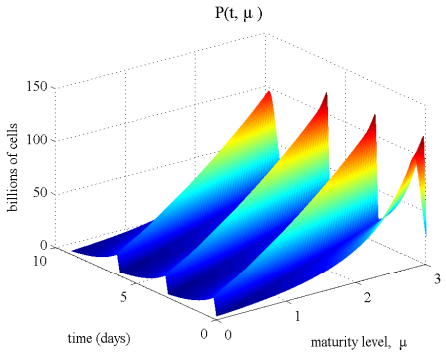

Figure F.21: Class P, ETD treatment, inflammation 0.63.

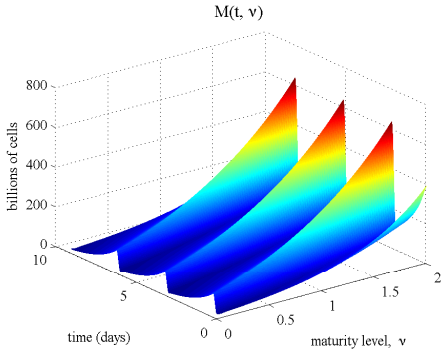

Figure F.22: Class M, ETD treatment, inflammation 0.63.

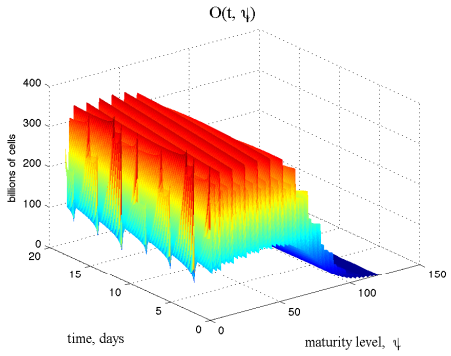

Figure F.23: Class O, ETD treatment, inflammation 0.63.

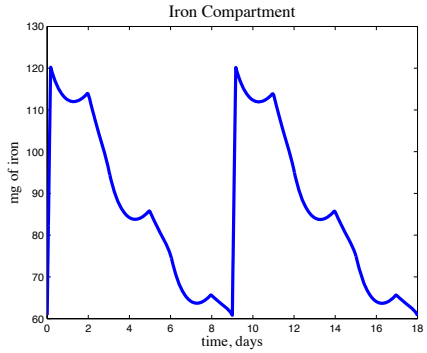

Figure F.24: Iron Compartment, ETD treatment, inflammation 0.63.

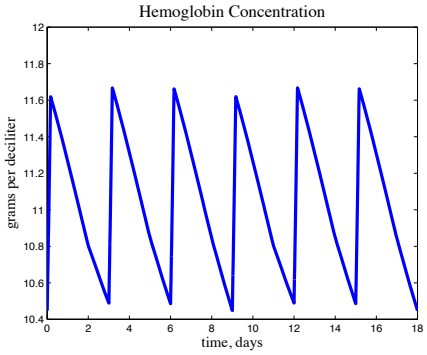

Figure F.25: Hemoglobin Concentration, ETD treatment, inflammation 0.63.

F.6 ETD treatment, inflammation 0.75

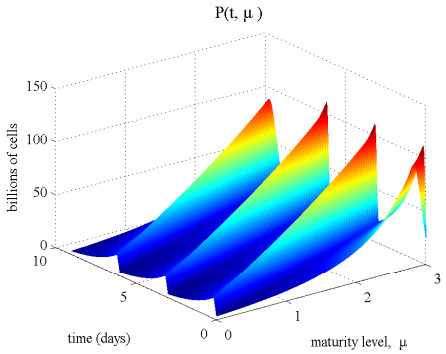

Figure F.26: Class P, ETD treatment, inflammation 0.75.

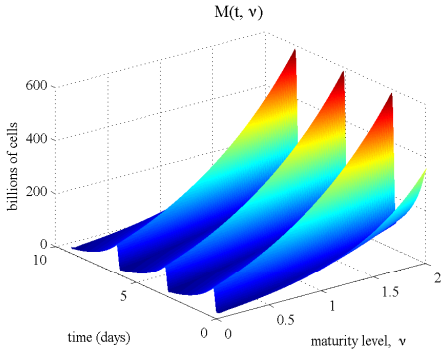

Figure F.27: Class M, ETD treatment, inflammation 0.75.

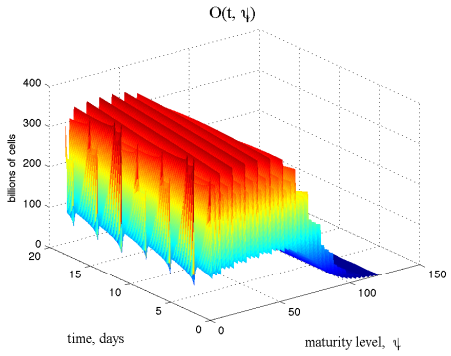

Figure F.28: Class O, ETD treatment, inflammation 0.75.

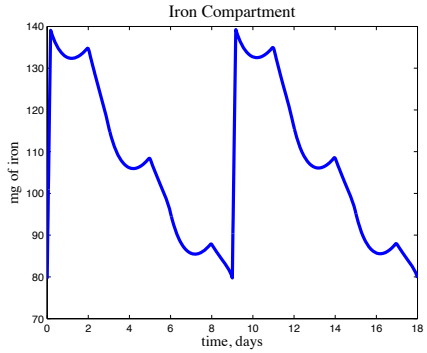

Figure F.29: Iron Compartment, ETD treatment, inflammation 0.75.

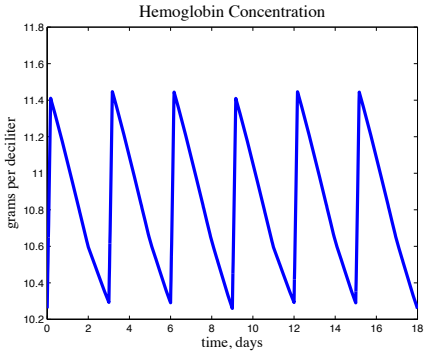

Figure F.30: Hemoglobin Concentration, ETD treatment, inflammation 0.75.

F.7 ETD treatment, inflammation 1

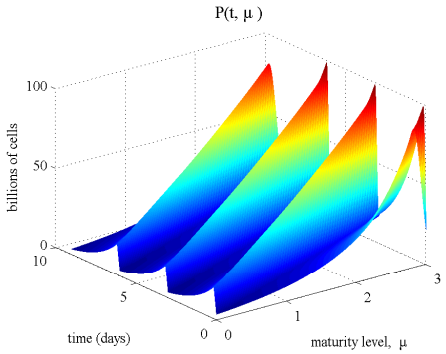

Figure F.31: Class P, ETD treatment, inflammation 1.

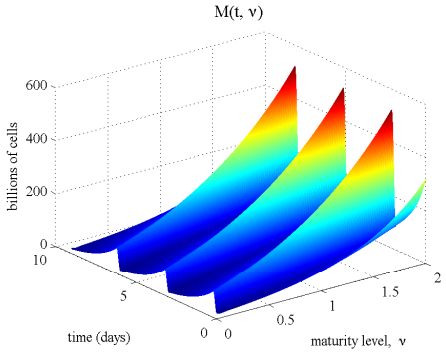

Figure F.32: Class M, ETD treatment, inflammation 1.

F.8 MWF treatment, inflammation 0

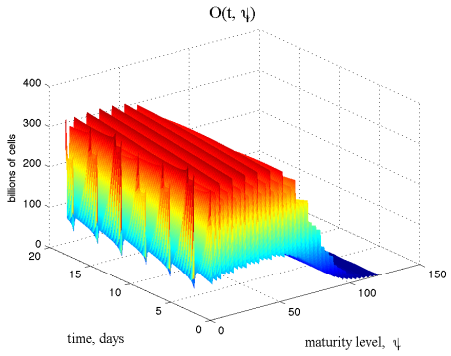

Figure F.33: Class O, ETD treatment, inflammation 1.

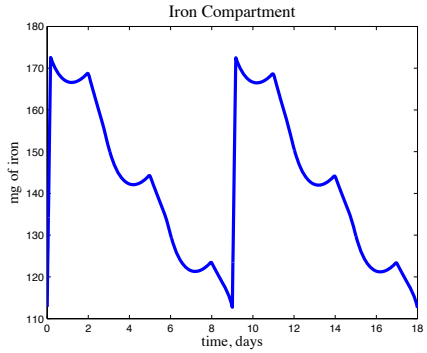

Figure F.34: Iron Compartment, ETD treatment, inflammation 1.

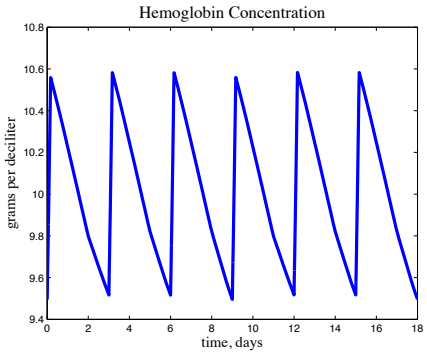

Figure F.35: Hemoglobin Concentration, ETD treatment, inflammation 1.

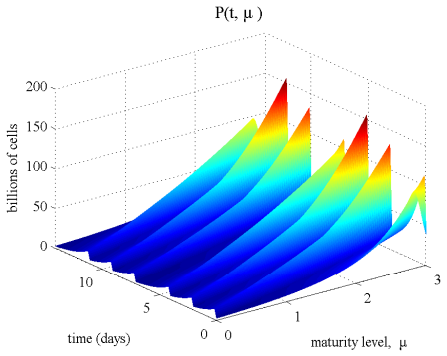

Figure F.36: Class P, MWF treatment, inflammation 0.

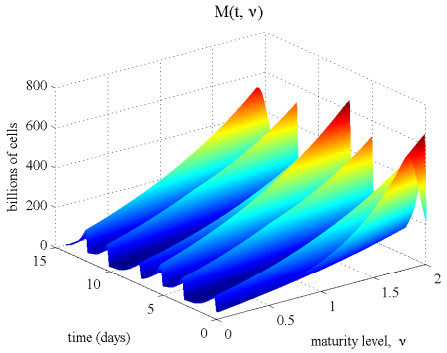

Figure F.37: Class M, MWF treatment, inflammation 0.

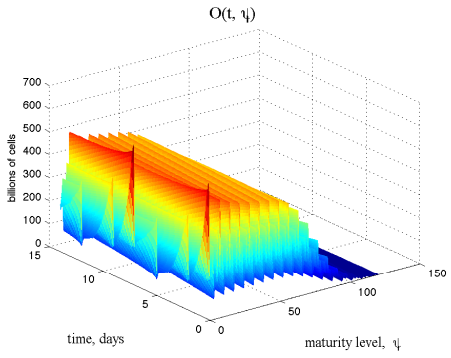

Figure F.38: Class O, MWF treatment, inflammation 0.

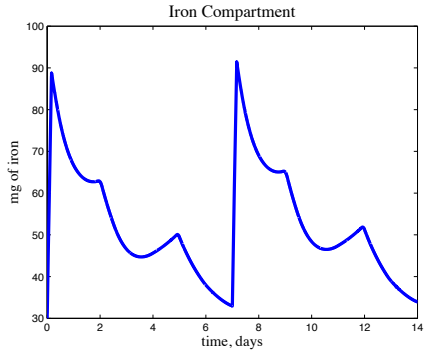

Figure F.39: Iron Compartment, MWF treatment, inflammation 0.

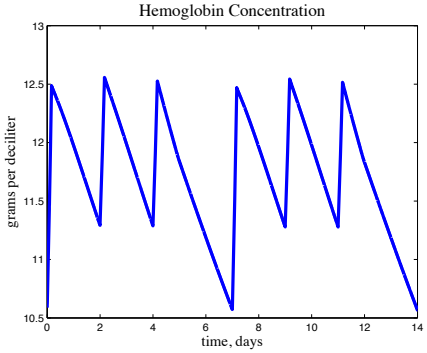

Figure F.40: Hemoglobin Concentration, MWF treatment, inflammation 0.

F.9 MWF treatment, inflammation 0.25

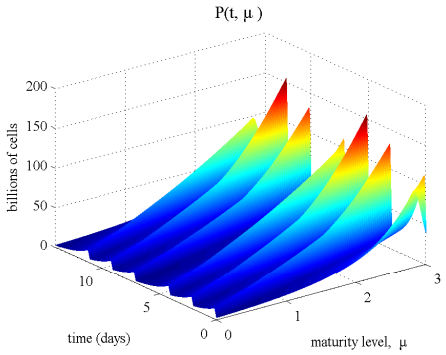

Figure F.41: Class P, MWF treatment, inflammation 0.25.

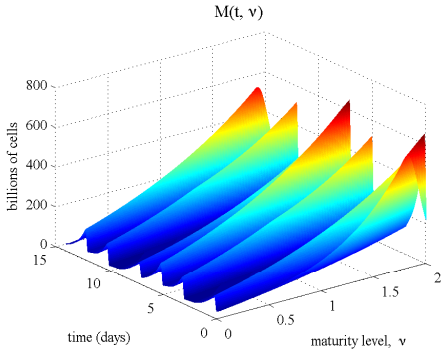

Figure F.42: Class M, MWF treatment, inflammation 0.25.

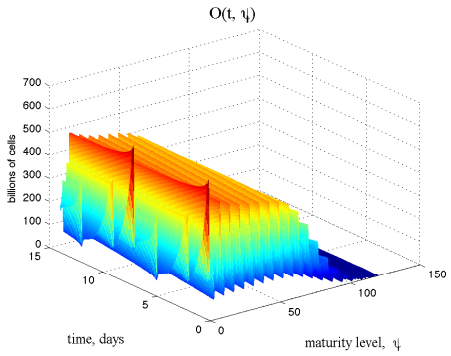

Figure F.43: Class O, MWF treatment, inflammation 0.25.

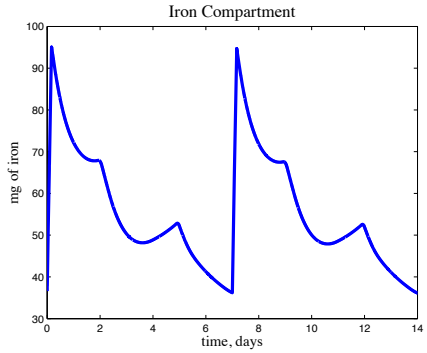

Figure F.44: Iron Compartment, MWF treatment, inflammation 0.25.

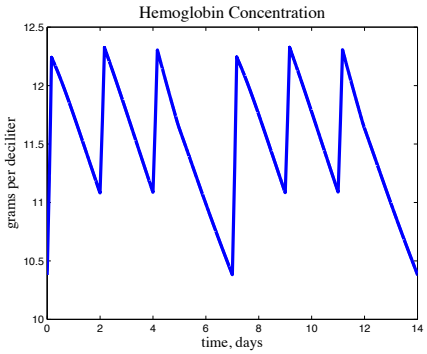

Figure F.45: Hemoglobin Concentration, MWF treatment, inflammation 0.25.

F.10 MWF treatment, inflammation 0.37

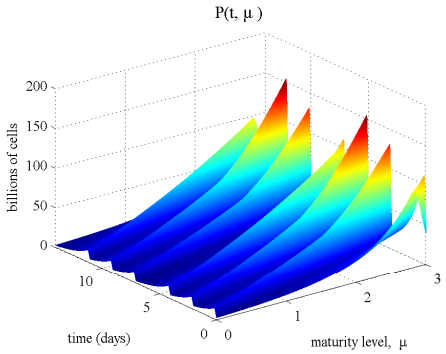

Figure F.46: Class P, MWF treatment, inflammation 0.37.

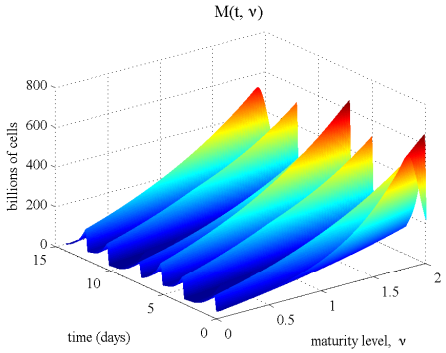

Figure F.47: Class M, MWF treatment, inflammation 0.37.

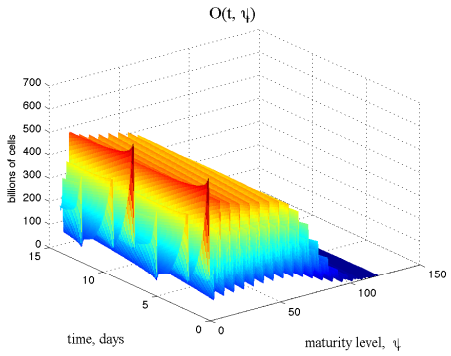

Figure F.48: Class O, MWF treatment, inflammation 0.37.

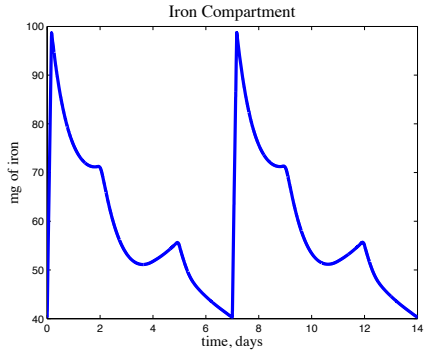

Figure F.49: Iron Compartment, MWF treatment, inflammation 0.37.

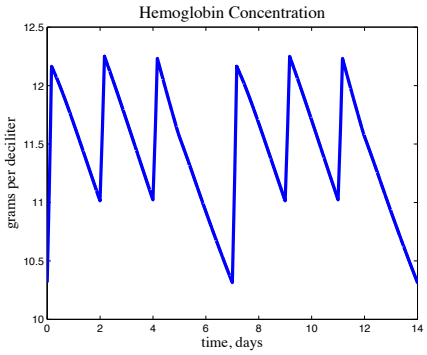

Figure F.50: Hemoglobin Concentration, MWF treatment, inflammation 0.37.

F.11 MWF treatment, inflammation 0.5

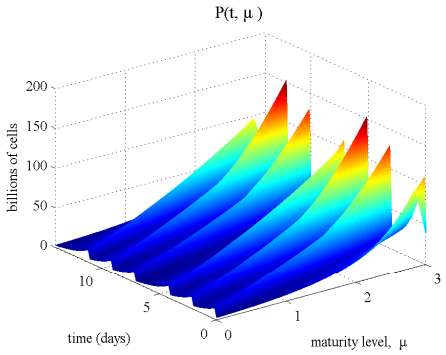

Figure F.51: Class P, MWF treatment, inflammation 0.5.

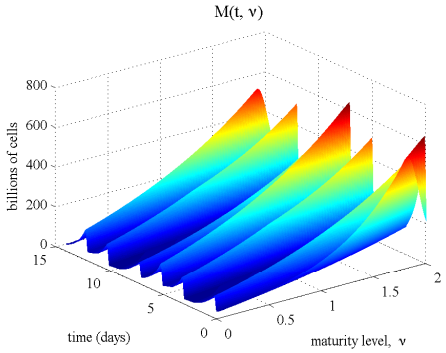

Figure F.52: Class M, MWF treatment, inflammation 0.5.

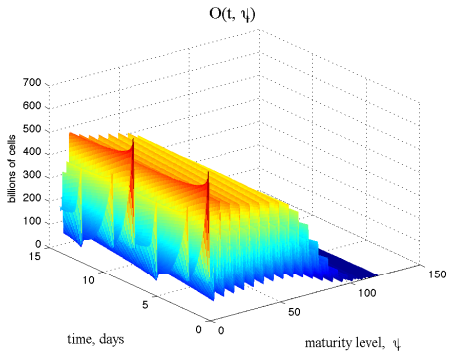

Figure F.53: Class O, MWF treatment, inflammation 0.5.

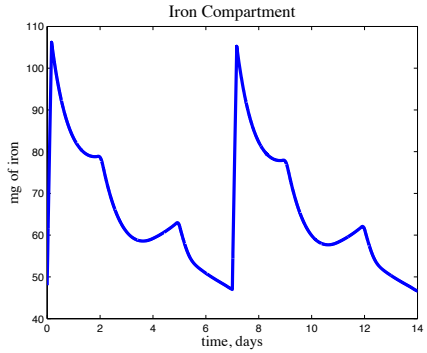

Figure F.54: Iron Compartment, MWF treatment, inflammation 0.5.

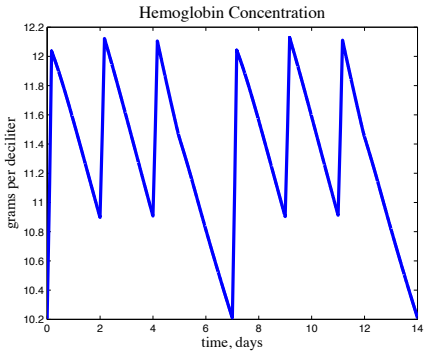

Figure F.55: Hemoglobin Concentration, MWF treatment, inflammation 0.5.

F.12 MWF treatment, inflammation 0.63

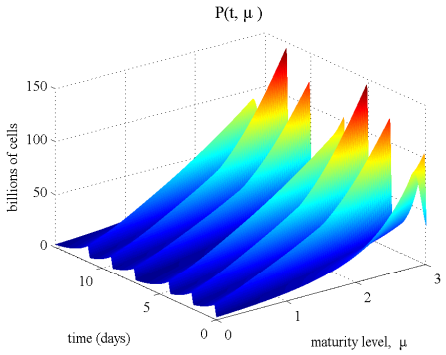

Figure F.56: Class P, MWF treatment, inflammation 0.63.

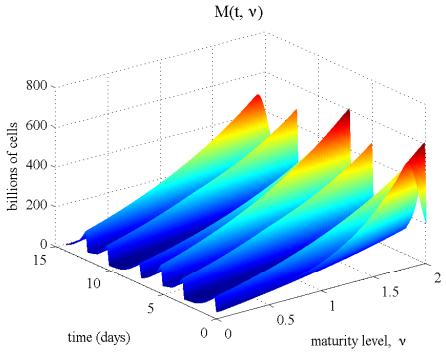

Figure F.57: Class M, MWF treatment, inflammation 0.63.

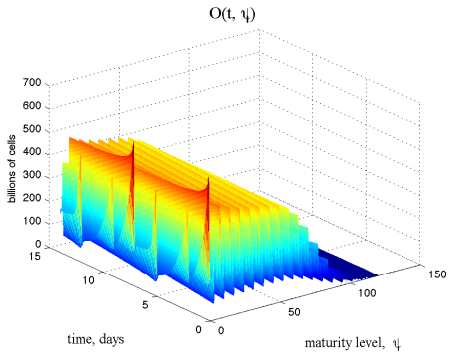

Figure F.58: Class O, MWF treatment, inflammation 0.63.

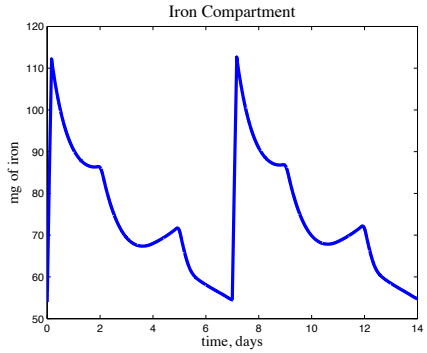

Figure F.59: Iron Compartment, MWF treatment, inflammation 0.63.

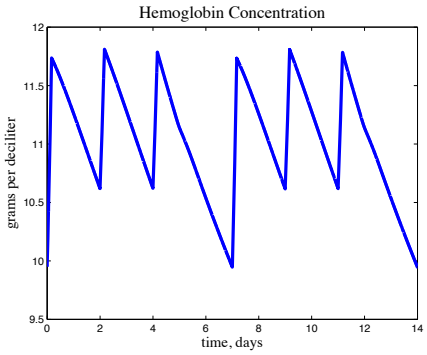

Figure F.60: Hemoglobin Concentration, MWF treatment, inflammation 0.63.

F.13 MWF treatment, inflammation 0.75

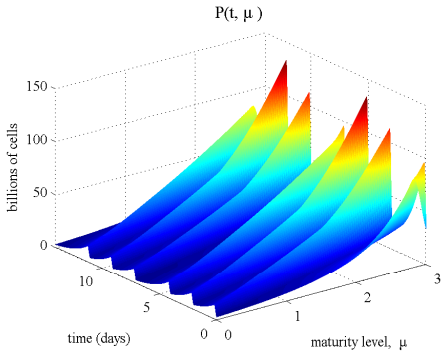

Figure F.61: Class P, MWF treatment, inflammation 0.75.

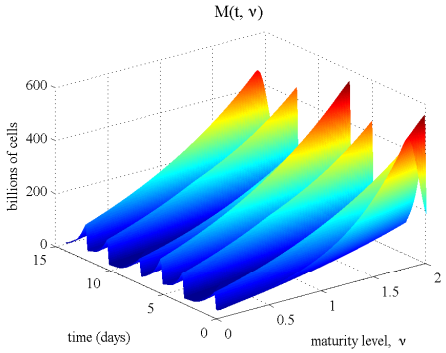

Figure F.62: Class M, MWF treatment, inflammation 0.75.

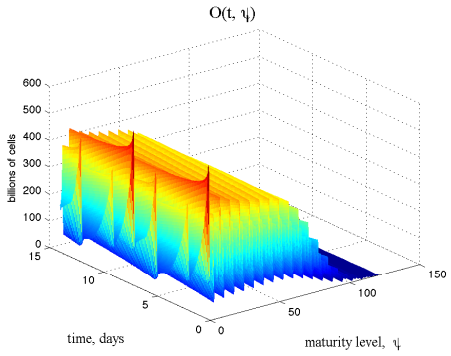

Figure F.63: Class O, MWF treatment, inflammation 0.75.

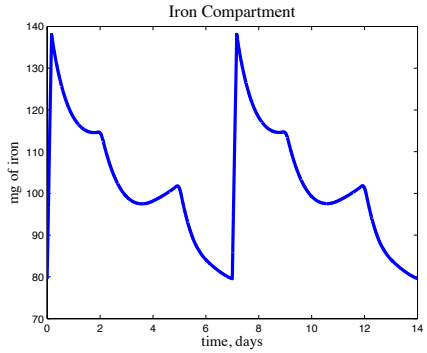

Figure F.64: Iron Compartment, MWF treatment, inflammation 0.75.

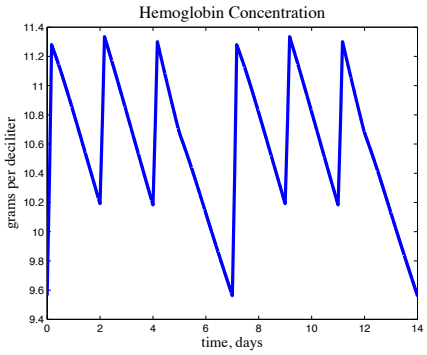

Figure F.65: Hemoglobin Concentration, MWF treatment, inflammation 0.75.

F.14 MWF treatment, inflammation 1

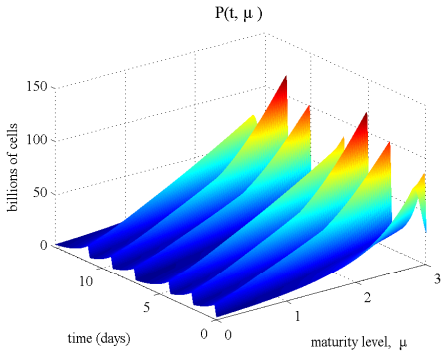

Figure F.66: Class P, MWF treatment, inflammation 1.

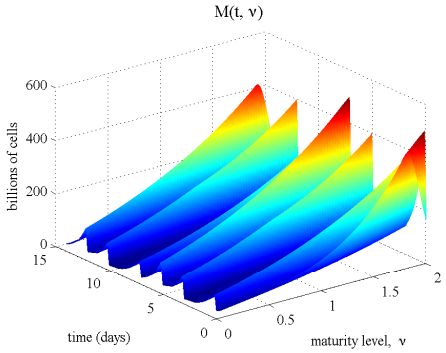

Figure F.67: Class M, MWF treatment, inflammation 1.

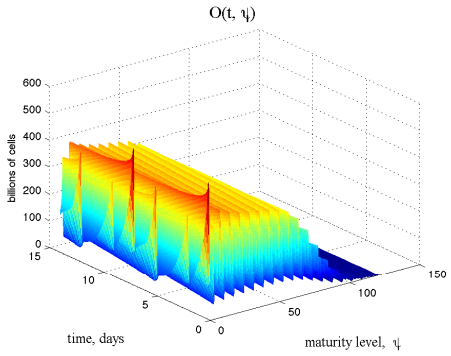

Figure F.68: Class O, MWF treatment, inflammation 1.

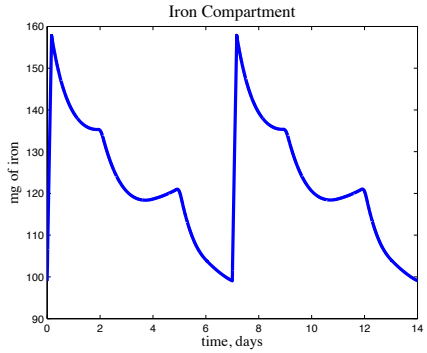

Figure F.69: Iron Compartment, MWF treatment, inflammation 1.

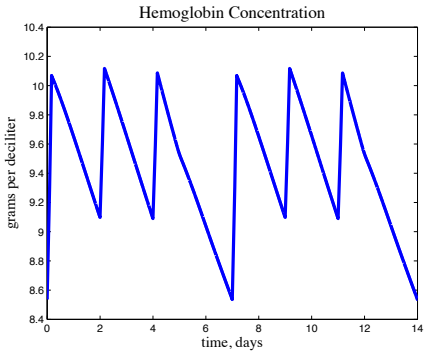

Figure F.70: Hemoglobin Concentration, MWF treatment, inflammation 1.